BSPE 00251-434-5

태평양 C-C지역 서부심해저 자생광물군의 광물 지화학적 특성 연구

Mineralogical and Geochemical Characters of Authigenic Deposits in the C-C Zones, NE Equatorial Pacific

1992. 4.

한국해양연구소

제 출 문

해양연구소장 귀하

본 보고서를 "태평양 C-C지역 서부심해저 자생광물군의 광물, 지화학적 특성 연구" 사업의 최종보고서로 제출합니다.

1991년 4월

한 국 해 양 연 구 소

연구책임자 : 정 갑 식

이 경 용

문 재 운

연 구 원 : 정 회 수

기 술 원 : 지 상 범

요 약 문

I. 제목

태평양 C-C지역 서부심해저 자생광물군의 광물, 지화학적 특성 연구

II. 연구내용 및 결과

Part I :

북동 태평양 C-C지역 서부에 위치한 KODOS지역에서 83년과 89년 두차례에 걸쳐 획득한 자료를 이용하여 망간단괴 및 퇴적특성을 연구하였다. 망간단괴의 여러가지 특성(부존량, Type, 그리고 성분)은 최상부층의 퇴적작용과 밀접한 관련이 있으며, 특히 부존량은 음파적으로 투명한 최상부층이 50m 이하의 두께일때 가장 높았다. 단괴 부존량이 높은 남부지역은 마이오세 중기 이후 생물생산성이 높은 지역에서 퇴적된 Clipperton 층의 분포와 일치한다. 반면에 북부지역의 단괴는 퇴적율이 극히 낮거나 침식된 에오세-올리고세 퇴적층의 발달, 혹은 화산재의 퇴적결과로 보인다.

표면이 거친 R-형 단괴는 주로 해저평원에서 산출되며 Todorokite, Mn, Ni 그리고 Cu가 고농도로 함유되어있다. 표면조직이 매끈한 S-형이나 R 및 S형 중간인 T-형 단괴들도 퇴적층의 두께가 일정치 않은 불규칙한 해저면이나 심해저, 즉 저층해류의 영향이 큰 지역에서 주로 산출된다. S-형 단괴는 Vernadite, Fe 및 Co의 함량이 높다. T-형 단괴는 이들 두 형의 단괴성분의 중간이다.

이들 단괴형들의 성분 차이는 주로 준액상의 최표층 퇴적층의 퇴적과 침식에 의

해 조절되는 것으로 보인다. 망간단괴들은 강한 저층해류의 반복된 침식작용으로 인해 Patch나 Pavement를 이루어 분포하며 저층해류가 약한 기간동안에는 저서동물에 의해 최표층 퇴적물상에 분포하게 된다.

Part II :

태평양 클라리온-클리퍼톤 균열대내 북서단에 위치해 있는 KODOS-89 지역에 분포하는 망간단괴의 물리·화학적 성질은 해저지형에 따라 상이하다. 해저평원 지역은 토도로카이트/버나다이트 및 Mn/Fe 비가 크며, 망간, 구리, 니켈, 아연의 함량이 높고, 철 및 코발트의 함량이 낮은 속성기원의 단괴가 지배적이며, 해저산 지역은 속성기원과 상반된 구성 광물 및 금속 함량을 갖는 수성기원의 단괴로 대표된다. 속성기원의 단괴는 결정질 산화광물의 침전이 퇴적물내에서 이루어지기 때문에 거칠은 표면조직(r-형)을 갖으며, 단괴의 크기가 증가함에 따라 구형, 타구형, 쟁반형의 외형으로 변모한다. 이에 비하여, 수성기원의 단괴는 해수로부터 미정질 산화광물이 흡착되므로 매끈한 표면조직(s-형)을 갖으며, 다단괴형 또는 불규칙형의 외형으로 특징된다. 망간단괴의 분포밀도는 해저산 지역이 평균 13.3 kg/m^2로 높으며, 해저평원 지역은 평균 3.9 kg/m^2로 낮지만 고위도 지역에 비해 저위도 지역이 높다. 이러한 망간단괴의 분포밀도 변화는 일차적으로는 씨앗효과에 의해, 이차적으로는 위도에 따른 퇴적물내 유기물 함량 차이에 의해 비롯되었다고 생각된다. 즉, 해저산 지역은 수성작용에 의한 단괴의 성장으로 기존의 단괴가 잘 쪼개지므로서 씨앗효과가 증대하여 분포밀도가 높다. 해저평원 지역중 남부지역은 주변에 해저산이 많이 분포되어 있어 핵물질의 공급이 용이하며, 이와 더불어 적도 고생산대로부터 원할한 유기물 공급으로 속성작용이 촉진되어 북부 지역에 비해 높은 분포밀도를 갖는다.

Summary

Part I :

In the Korea Deep Ocean Study (KODOS) area, west of the Clarion-Clipperton (C-C) fracture zones in the northeast equatorial Pacific, sedimentary characters of manganese nodule fiedl are analyzed using data obtained during two cruises in 1983 and 1989. It reveals that the nodule characters (abundance, type, and composition) are dependent on depositional processes of the topmost sediment layer in that abundant nodules occur in less-than-50 m thick topmost sediment layer which is acoustically transparent. Nodules are abundant in the southern part of the KODOS area, comprising the Clipperton Formation which was deposited under moderate sedimentation rate beneath northern margin of equatorial high productivity zone since middle Miocene. Nodules are scarce in the northern part of the area, probably due to extremely low or negative sedimentation rate of Oligocene to Eocene sequence and deposition of volcanic ashes. Rough-surface (R-type) nodules are dominant in the abyssal plain and are enriched in todorokite, Mn, Ni and Cu. Both smooth (S-type) and mixed surface (T-type) nodules occur generally on irregular sefloor with variable sediment thickness and seamounts where sediment accumulation has been enhanced or prohibited by bottom current. The S-type nodules are enriched in vernadite, Fe and Co. The T-type nodules are intermediate in composition between the two types. Nodule compositions

are also dependent on intermittent and prolonged deposition of boundary (peneliquid) layer during nodule growth. Intensified bottom current activities result in nodule patches or pavements on topographic highs by supplying large amounts of nodule-nucleating materials. Intensive bioturbation keeps nodules on the seafloor during rapid sediment accumulation.

Part II :

KODOS-89 area, the northwestern part of Clarion-Clipperton fracture zones in the Northeast Pacific, was surveyed in order to study the occurrence and distribution of manganese nodules. Variations in nodule characters are related mainly to seafloor topography. Nodules from abyssal plain have high Mn/Fe ratio and Mn, Cu, Ni and Zn concentrations, whereas those from seamount are characterized by low Mn/Fe ratio and high Fe and Co concentrations. These compositional characters are attributed to diagenetic and hydrogenetic accretionary process, respectively. Nodules of early diagenetic origin tend to accrete crystalline Mn-oxides uniformly within topmost sediments layer and maintain a regular spheroidal, ellipsoidal to discoidal shape with rough surface texture. On the other hand, those of hydrogenetic origin are characterized by polynucleation, irregualr shape, and smooth surface texture. Nodule abundance is high (avg. 13.4 kg/m^2) in seamount resulting from ample supply of nucleating materials by

autofragmentation of older nodules. Nodules are relatively poor (avg. 3.9 kg/m^2) in abyssal plain. However, the abundance in abyssal plain increases southward. This phenomenon is resulted from facilitation of taking seed materials from adjacent seamounts and enhancement of the early diagenesis by sufficent supply of organic materials. Nodule abundance is considered to be controlled primarily by seeding effects and secondly by supplies of organic materials.

CONTENTS

요약문 ..... (3)

SUMMARY ..... (5)

CONTENTS ..... (9)

Part I

LIST OF TABLES 3

LIST OF FIGURES 4

I. INTRODUCTION 9

II. GEOLOGICAL SETTING 10

1. Regional Setting 10

2. KODOS Area 13

III. MANGANESE NODULE OCCURRENCE 21

1. Nodule Types and Occurrence 21

2. Bottom Photograph 24

3. Mineralogical and Chemical Compositions 25

IV. DISCUSSION 28

V. CONCLUSIONS 33

VI. ACKNOWLEDGEMENTS 34

REFERENCES 35

Part II

LIST OF TABLES 77

LIST OF FIGURES 77

I. 서 론..... 79

II. 지질개요 81

III. 분석방법..... 84

IV. 결 과..... 86

1. 망간단괴의 물리적 특성..... 86

2. 망간단괴의 광물 및 금속함량..... 88

V. 토 의..... 90

1. 망간단괴의 형성기작..... 90

2. 망간단괴의 산출 특성..... 93

3. 망간단괴의 분포 특성..... 96

VI. 결 론..... 99

VII. 참고문헌..... 100

PART I :

KODOS 지역의 망간단괴 퇴적상

(Sedimentary Facies and Manganese Nodules of the Korea Deep Ocean Study (KODOS) area, Northeastern Equatorial Pacific between Clarion and Clipperton Fracture Zones)

List of Tables

Table 1. Manganese nodule charaters and geological environment in the KODOS area. ---- 49

Table 2a. Major minerals and elements in R-type nodules in the KODOS area.--- 52

Table 2b. Major minerals and elements in S-type nodules in the KODOS area.--- 53

Table 2c. Major minerals and elements in T-type nodules in the KODOS area.--- 53

Table 2d. Major minerals and elements in the KODOS area and the Marshall Islands.---- 54

Table 2e. Composition of surface and buried manganese nodules at site 8918.--54

Table 3. Geological factors of manganese nodule occurrence in the KODOS area. ---- 55

List of figures

Fig. 1. Seismic survey lines and sampling sites in the KODOS area. Thick lines represent both air-gun and 3.5 kHz high-resolution reflection profiling tracks whereas thin lines represent 3.5 kHz high-resolution reflection profiling tracks. Water depth is contoured at 200 m interval. After Heezen and Tharp (1978).--57

Fig. 2. Correlation of air-gun seismic stratigraphic units to lithologic compositions in DSDP site 163 core (seismic profile locates between sites 8904 and 8908 in figure 1). After van Andel et al. (1973).----------58

Fig. 3. Distribution of sedimentary sequence above acoustic basement, air-gun seismic profile.----------59

Fig. 4. Correlation of seismic units on 3.5 kHz high-resolution profile with the lithologic compositions. In northern and western parts of the KODOS area, acoustically transparent overlies diffusive or hyperbolic reflector (A and B). However, it is underlain by stratified Clipperton and lower transparent Marquesas formations in the southern part. Triangles represent Sonne cruise of Germany. After Piper et al. (1979) and von Stackelberg et al. (1987).----------60

Fig. 5. Various bedforms occurring in the KODOS area. a) sediment waves with various wavelengths and heights found generally on the abyssal plain area, b) upslope-migrating sediment waves on stratified but folded and faulted subbottom layer, c) superimposed hyperbolas implying closely-spaced sediment waves or furrows, d) uppermost transparent sediment layer overlying unconformably subbottom and turbidites filling troughs as flat layered sequence north of the Clarion fracture zone, e) sediment drift associated with small seafloor topographic reliefs and scoured stratified surface around a seamount in the south of the KODOS area, f) a large moat formed near the base of of a seamount. Often sediment mounds occur on eroded surface of subbottom layer within the moats. ---------- 61

Fig. 6. Photographs of sediment box cores. Sediment layer is divided into 2 or 3 units depending on sharp scoured surface, bioturbation, and color change. Highly-bioturbated cores retain more abundant nodules on the surface. ---------- 62

Fig. 7. Characters of nodules in box cores: R-type nodules occur near or half- buried within topmost sediment layer and various-shaped but S- and T-type nodules are generally polynucleated, exposed on the surface. ---------- 64

Fig. 8. X-radiograph showing buried nodules within sediment layer. The nodules in the upper are smooth-surfaced and polynucleated but that in the lower is rough-surfaced with outermost layer of numerous ascicules. On the surface, large abundant (20.0kg/m^2) T-type nodules occur. ---- 65

Fig. 9. Nodule size distribution showing an unimodal distribution pattern with dominance of 2 to 4 cm size class. ---- 66

Fig. 10. Macroscopic internal structures of nodules. Layers are delineated by thin clayey sediment and fractured irregular intersurfaces. Nuclei are various; fractured or fragmented older nodule (a) clay lump (b), weathered basalt fragments (c and d). Bar is 1 cm long. ---- 67

Fig. 11. Relationship between nodule abundance and water depth. R-type nodules occur mainly in 5100 to 5250 m water depth (abyssal plain). However, the nodules of other types occur in a wide range of water depth of various seafloor morphology. ---- 68

Fig. 12. Distribution of Mn-nodule abundance and type. Filled circle represents rough-surface (R-type) nodules, open circle for smooth-surface (S-type) nodules, and barred circle for transitional (T-type) or mixed (R- and S-type) nodules. ---- 69

Fig. 13. Relationship between nodule abundance (kg/m^2) and thickness of acoustically transparent layer (m) on 3.5 kHz seismic profiles. --- 70

Fig. 14. Distribution of nodule abundance on bottom photograph and 3.5kHz high-resolution seismic profiling tracks in seamount areas. Nodules are rare on thick transparent layer (a) but abundant on thin or eroded surface on which manganese crust and large amount of manganese crust fragments are shown (b). ---------- 71

Fig. 15. Bottom photograhs showing various activities of benthic animals, an ophiuroid feeding (?) on a nodule (b), a clam seems to disturb the seafloor (b), large worm (c), bioturbated sediment mound (d), coiling worm traces among nodules (e), and worm tubes (f). Photographs are not scaled. ---------- 72

Fig. 16. Relationship between ratios of todorokite / vernadite (peak intensity) and Mn/Fe depending on nodule types. ---------- 73

Fig. 17. Ternary diagram of chemical composition of nodules showing distinctive genetic processes of each nodule type (after Bonatti et al., 1972). For comparison, the chemical composition of Mn-crust from the Marshall Islands (sample number, 21) and the KODOS (sample number, 2) are also plotted. ---------- 74

I. INTRODUCTION

The sediment sequence in the northeast Pacific Ocean between Clarion and Clipperton (C-C) fracture zones comprises 3 acoustic layers delineated by distinct mid-reflectors (Ewing et al., 1968; Piper et al., 1979). These features are generally related to sediment types, sedimentation rates and bottom current and, in turn, control the distribution of maganese nodules and other characteristics (Calvert et al., 1978; Mizuno et al., 1980). Sediment types and sedimentation rates are generally considered important for the nodule abundance, and are mostly influenced by bottom current (Horn et al., 1973; Cronan, 1980). The relationship of sedimentary facies and stratigraphy, especially of the acoustically transparent uppermost sequence, to manganese nodule abundance was found earlier (Calvert et al., 1978; Mizuno et al., 1980; von Stackelberg, 1987). Usui et al. (1987) further report detailed studies of local variability of nodule abundance.

The Korea Ocean Research and Development Institute (KORDI) has carried out two cruises to the northeast Pacific: the first in November to December, 1983 aboard R/V Kana Keoki ; the second in October, 1989 aboard R/V Farnella (Figure 1). Both air-gun (40 in3, 28-130 Hz band path) and 3.5 kHz seismic profiles were obtained continuously along the survey lines. Manganese nodule and sediment samples were obtained by using box corer and free-fall grab at 33 sites. In this report, we summarize the results of detailed studies on acoustic stratigraphy, sedimentary facies, nodule abundance and types in the Korea Deep Ocean Study (KODOS) area.

II. GEOLOGICAL SETTING

1. Regional Setting

The northeastern equatorial Pacific seafloor is characterized by several NEE-SWW-trending fracture zones between the East Pacific Rise (EPR) and the Line Islands Ridge. These fracture zones resulted from transform faults during the movement of the Pacific plate since late Cretaceous (McKenzie and Morgan, 1969; Herron, 1972). This movement offsets the Pacific plate about 30° to the north during Cenozoic time (Francheteau et al., 1970). The Pacific plate has moved dominantly northwestward since middle Eocene after moving northward from the ancient EPR. The change of plate drifting direction is clearly evidenced by alignment of the Emperor and Hawaiian ridges (Morgan, 1972; Clague, 1981). A Deep Sea Drilling Project (DSDP) site 163 core (Figure 1) shows that the KODOS area was formed during the Campanion, about 78 Ma, in the southeast Pacific at about 12°S and 120°W (van Andel et al., 1976).

Morphologically the C-C zones are distinctive. The Clarion fracture zone forms a topographic low deeper than 5,600 m in the north, whereas the Clipperton forms a topographic high shallower than 4,700 m in the south (Heezen and Tharp, 1978). The seafloor between them is rather flat with some submarine volcanic seamounts, dissected by numerous faults. In a N-S

transverse, the fracture zones comprise large steps bounded by steep and high escarpments, deepening progressively to the north. A facture zone is delineated in the middle part along the zones (Sclater et al., 1971).

In the northeast Pacific, biogenic sedimentation along the Pacific equator formed a thick sedimentary bulge which is elongated parallel to the equator with a slight northwestward shift. The post-Eocene layer is thick , more than 500 m in the 140°W transect (Ewing et al., 1968; van Andel and Heath, 1973). Both DSDP cores and seismic profiles in the C-C zones show that the sedimentary sequence can be divided into three formations : the oldest is the Line Islands Formation, which is overlain by the Marquesas and Clipperton formations (Tracey et al., 1971; Cook, 1975). The DSDP site 163 core (Figure 2) shows that the sedimentary sequence in the KODOS area is composed of two formations, the Line Islands and an unnamed underlying formations (Tracey et al., 1971).

Surface sediments of the C-C zones comprise Eocene to Pliocene siliceous ooze and clay, forming a latitudinally intermediate zone between red clay and calcareous ooze (Horn et al., 1973; Ryan and Heezen, 1976; Rawson and Ryan, 1978). The C-C zones are located beneath the northern margin of the Pacific equatorial high bioproductivity zone (Koblentz-Mishke, 1977). Since late Oligocene, narrowed productive equatorial zone and enhanced bottom erosional processes limited the accumulation of biogenic products to just beneath the equatorial region (van Andel et al., 1976). It resulted in the

distribution of late Cenozoic siliceous ooze and clay at a low sedimentation rate below the carbonate compensation depth (CCD) which reaches 4400 to 4800 m water depth in the C-C zones (Horn et al., 1973; Berger et al., 1976).

Bottom current flow in the C-C zones is presently too weak to redistribute sediments (Hayes, 1979; Gardner et al., 1984). However, several investigations of bedforms on seismic profiles and direct observations of water properties show that the northward-flowing Antarctic Bottom Water (AABW) passes through several passages of the Line Islands (Edmond et al., 1971; Mantyla, 1975; Normark and Spiess, 1976 ; Andrews et al., 1984), formimg a clockwise gyre, into the C-C zones (Volat et al., 1980). The Clipperton fracture zone might have guided the AABW to flow eastward (Johnson, 1972).

2. KODOS Area

Morphology : The KODOS area is located in the western margin of the C-C zones near the Line Islands Ridge (Figure 1). The seafloor is deep, generally more than 5,200 m. It is rather smooth in the eastern part but is rugged with seamounts and knolls in the southwestern part. The seamounts are mostly steep-sloped and wide (5 to 30 km) and up to 1500 m high (Figure 2). They generally lack sediments on tops and slopes, but some are covered with a thick sediment layer. The seamounts trend northwestward following the distribution pattern of the Line Islands Ridge. Deep-penetration seismic reflection profiles show that the seamounts are associated with block faults. The basement is irregular with numerous faults and forms small and large subdued and uprised topography beneath the sedimentary layer in the abyssal plain area. Many studies revealed that the seamounts forming the Line Islands Ridge were formed through sporadic submarine volcanism since late Cretaceous (Sclater et al., 1971; Herron, 1972; Morgan, 1972; Clague, 1981).

Seismic Stratigraphy : Air-gun seismic profiles in the KODOS area render it possible to delineate sedimentary sequence into several acoustic units depending on prominent subbottom reflectors and acoustic properties (Figure 2). The acoustic units are then correlate with the results of DSDP site 163 core (van Andel and Heath, 1973; van Andel et al., 1976).

Topmost unit is acoustically transparent and is composed of middle Eocene to late Oligocene radiolarian ooze with minor amounts of clay (Figure 2). The lower units comprise two acoustic units IIA and IIB. The unit IIA is acoustically stratified (chert beds in radiolarian ooze of early Eocene) and transparent (ferrugenous zeolitic clay of Paleogene). The units I and IIA comprise the Line Islands Formation. The acoustically stratified unit IIB consists of late Cretaceous nannofossil chalk and dolomite (Tracey et al., 1971).

The sedimentary layers are discontinuous due to the irregularity of faulted acoustic basement (Figure 3). Entire sedimentary layer is thick, more than 400 m near the Line Islands Ridge and thins progressively northeastward to less than 150 m. The unit I is variable in thickness, about 100 m in the southwestern part and about 60 m in the northeastern part of the KODOS area. The unit IIA occurs only in the west of 149°W transect as delineated earlier by Ewing et al. (1968). The areal distribution of sedimentary units in the KODOS area corresponds to general biogenic sedimentation on moving Pacific plate as revealed by a compilation of seismic data (Ewing et al., 1968) and the results of DSDP Legs 16 and 17 (Berger and Winterer, 1974; van Andel et al., 1976).

Shallow (3.5 kHz) Seismic Stratigraphy : Topmost sediment layer is divided into 2 or 3 units on 3.5 kHz seismic profiles (Figure 4). The topmost unit is entirely transparent, but often shows superimposed

hyperbolas and indistinctive internal reflectors. The underlying unit is either acoustically opaque (Figure 4a), diffused (Figure 4b) or stratified (Figure 4c).

In the northern part of the KODOS area, the topmost unit is correlated to the late Eocene to Quaternary zeolitic clay and clayey radiolarian ooze (von Stackelberg et al.,1987). The diffused or opaque unit represents middle/late Eocene laminated cherts in radiolarian ooze (Figure 4a and b). These units comprise the Line Islands Formation (van Andel and Heath, 1973). In the southern part, the topmost unit comprises middle Miocene to Quaternary radioralian ooze and clay with minor amounts of calcareous components, and the lower stratified unit to late Oligocene to early Miocene radiolarian and nannofossil oozes (Piper et al., 1979; von Stackelberg et al., 1987). Both transparent and stratified units are classified as the Clipperton Formation, which is underlain by a transparent unit, late Eocene to middle Oligocene radiolarian-nannofossil ooze and chalk (Marquesas Formation). Both Clipperton and Marquesas formations overlie the Line Islands Formation (Cook, 1975).

The topmost unit is thin (less than 100 m) and irregular, distributed on topographic highs or in lows. It resulted from intermittent activities of bottom current after the Pacific plate left the equatorial high productive region (van Andel et al., 1976). In the western part of the KODOS area, the topmost unit is thick, due to redistribution of large amounts of sediments

from the Line Islands Ridge by the AABW (Lonsdale and Smith, 1980, Mammerickx, 1985). von Stackelberg et al. (1987) attributed the diffused and opaque reflection beneath the topmost unit to hiatuses caused by invasion of strong bottom current. They found a regional hiatus of middle Miocene to early Pliocene in the sediment cores. The indistinctive or hyperbolic internal relflectors in the topmost transparent layer may represent the hiatuses (Mizuno et al., 1980), which are ubiquitous in the Miocene sedimentary sequence in the Pacific (Keller and Barron, 1983).

Bedforms : In the KODOS area, the bedforms are similar in acoustic configuration and properties to those formed by the AABW flows in the Pacific Ocean (Lonsdale and Smith, 1980; Damuth et al., 1983). Bedforms are dominated by sediment waves with 1 to 7 km in wavelength and 3 to 50 m in height (Figure 5a). The sediment waves seem to occur in various shapes and dimensions in the passways of the AABW (Mammerickx, 1985). Along the E-W transects the sediment waves migrate eastward on sloped seafloor of irregular subbottom (Figure 5b), similar to those formed by the AABW in Marshall-Gilbert archipelago in the central Pacific (Lonsdale and Smith, 1980). On smooth seafloor, the surface is composed of superimposed hyperbolas (Figure 5c), reflected from small-scaled sediment waves and furrows (Damuth et al., 1983; Embley et al., 1980).

North of the KODOS area, both sediment waves and turbidites occur (Figure 5d). The latter are acoustically layered in the topographic lows whereas the former are transparent on topographic highs. The sediment waves may have formed under the influence of AABW of fine-grained sediments supplied by turbidity current (Kolla et al., 1980). On the submarine ridges, the sediment waves and turbidites are often found together, resulting from activities of both AABW and occasional turbidity current (Lonsdale and Smith, 1980; Orwig, 1981). The turbidites are composed of volcanic ashes derived from the Hawaiian Islands during late Pliocene to early Quaternary (Rhem and Halbach, 1982).

Sediment drifts are acoustically transparent and occur generally in the east side of small hills and large seamounts (Figure 5e). Lonsdale (1981) considered that the drifts are formed by differential deposition of fined-grained sediments resuspended in the passways of AABW in the Samoan Passage, south Pacific. The moats are associated generally at the bases of large seamounts (Figure 5f). Within the moats, sediment mounds with wavy surface are often found on scoured subbottom. The occurrence of the moats is attributed to the erosional processes of bottom current which are intensified locally around topographic highs (Johnson, 1972; Normark and Spiess, 1976). The intensification of AABW seems to have occurred several times in Miocene (Keller and Barron, 1983) and in the glacial stages of Pleistocene (Johnson, 1972).

Sediment Characters : Seventeen box, 3 piston and 2 gravity core sediments were collected during 1983 and 1989 cruises (Figure 1). The sediment cores were split into halves and described. Two-cm-thick slabs were made from box cores and X-radiographed. Granulometric analysis was performed by using Sedigraph 5000D and relative concentration of clay minerals by X-ray diffractometer. Biogenic components were identified on smear slides under a microscope. Geotechnical properties were also measured in selected intervals of box and long cores.

The sediment cores are divided into 2 or 3 units by distinct color change, bioturbation and lithologic boundary (Figure 6). The topmost unit 1 is dark yellowish or reddish brown (10YR3/4 to 5YR3/3, Munsell, 1975) and homogeneous due to intensive bioturbation, mostly to about 10 cm depth from the surface. The unit 2 is dark brown (10YR3/3 to 5YR 3/2) and highly mottled with simple and large haloed burrows. The third unit is dark gray or brown (5YR3/1 to 10YR4/2) and less bioturbated. The distinctive color change between the topmost and lower units is due to oxidation and reduction states of ferric and ferrous oxides in the sediments (Lyle, 1983). The oxidation-reduction boundary is deep less than about 1 m in the Pacific (Piper et al., 1979; Lyle, 1983). In the KODOS area, the boundary is 120 cm deep below the surface.

The unit 1 is characterized by high water content (more than 300 %) and low sediment shear strength (0 to 20 g/cm^2). Its characters are similar to

those of "peneliquid layer" of Halbach and Ozkara (1979). However, units 2 and 3 are highly cohesive. They correspond to "historic layer" of the Pacific pelagic sediment layer (Berger and Heath, 1968). Sometimes, the boundary between the units 1 and 2 forms sharp truncations of sediment layer and burrows. It may be an erosional surface (or hiatus) made by strengthened bottom current flows probably in the late Pleistocene (von Stackelberg, 1987).

The sediments comprise either zeolitic clay or siliceous ooze where radiolaria-bearing clay is dominant. Radiolarians are extensively corroded and fragmented with minor amounts of diatom, silicoflagellate and calcareous nannofossils. Trace amounts (less than 5%) of platy, opaque minerals and micronodules are encountered. The radiolarians and diatoms range from Quaternary to Eocene in age. The units 1 and 2 are assigned to Quaternary; the lowermost unit to Tertiary in age based on radiolarians and diatoms. The mixed ages in the KODOS area agree with those in many other nodule fields in the north equatorial Pacific (Theyer, 1977; Craig, 1979; Piper et al., 1979; von Stackelberg et al., 1987). It is attributed to redistributional processes of AABW that occurred in Miocene (Keller and Barron, 1983) and Pleistoncene times (Johnson, 1972; Craig, 1979). At seamounts (st. 8906 and 8918) shallower than 4900 m water depth, the sediments are composed of calcareous nannofossil ooze in pale brown (10YR6/3) and show zoophycos and planolite burrows. It may indicate that

the carbonate compensation depth (CCD) is about 4,900 m in the KODOS area, similar to that in the Deep Ocean Mining Environmental Studies (DOMES) site A (Piper et al., 1979).

Clay-sized sediments are, 70% to 98% of bulk sediments, composed mainly of smectite and illite with subsequent amounts of kaolinite, chlorite, quartz and plagioclase. Smectite comprises 27 to 91% at the expense of illite. At depth of more than 50 cm, smectite is dominant (more than 70%), and clinoptillolite and phillipsite occur also. They are authigenic minerals formed at sea water/sediment interface (Hein et al., 1979), whereas illite is of terrigenous origin in the north Pacific (Windom, 1969).

III. MANGANESE NODULE OCCURRENCE

1. Nodule Types and Ocurrence

Manganese nodules were collected at 34 sites by both free-fall grab and box core samplers (Figure 1, 68 free-fall grabs and 20 box cores). Two or five free-fall grab samplers were deployed simultaneously at each sampling site. Nodules were described in detail for shape, surface texture, size, abundance, and relative position to substrate sediment (Table 1) based on the criteria of Moritani et al. (1977). Nodules were classified into 3 types based on surface texture. S-type nodules show smooth and greasy surface whereas R-type nodules are irregular, rough and gritty with microbotryoids. The surface is often transitional from rough bottom to smooth top surface or rough partially on the entire surface (Mixed nodule, Maylan, 1974). The nodules with transitional surface are tentatively classified as T-type.

The R-type nodules are mostly mononucleated, discoidal, spheroidal or ellipsoidal, but S and T-type nodules are polynucleated and irregular in shape (Figure 7). In box cores, large R-type nodules occur half-buried but most of small R-type nodules, entirely embedded in thin topmost surface sediment layer (peneliquid layer, Halbach and Ozkara, 1979). The S and T-type nodules occur, exposed on the seafloor. Large ellipsoidal or

discoidal R-type nodules show equatorial rims (intermediate surface contacting to the sediment/water interface) that is irregular and bumpy with large knobs and small bortryoids. The more bioturbated thick Quaternary sediment cores yield abundant nodules mainly of S or T-types on the surface (Figure 6). On X-radiographs of core sediments, buried nodules are ubiquitous at depths (upto 210 cm, st. 8304) with a few mm to 4 cm in diameter (Figure 8). They are S or R-type nodules. Small (less than 1 cm in diameter) buried nodules are all R-type. The types and abundance of buried nodules are independent of those on the surface.

Nodule size is variable, from few mm to larger than 8 cm in diameter. The size distribution is unimodal with a dominance of 2-4 cm class (Figure 9). In the abyssal plain, the size becomes larger to the south. Some small nodules occur as rough-surface and irregular-shaped coatings entirely or partially on nuclei of various materials, indicating immature stage of nodule growth. The nuclei of large nodules are mostly older nodules or their fragments with some sharks' teeth, indurated clay lumps, and pumice (Figure 10). On the seamounts, weathered basalt fragments are dominant in nodules. The configuration and number of nuclei determine nodule shapes. Two or three macroscopic Mn-oxide layers are delineated by thin and discontinuous sediment layers or fractured irregular interfaces in the nodules. Entire Mn-oxide layer is generally 2 to 3 cm and the outermost is 2 to 3 mm thick. In some dredge samples, large (20 to 50 cm in diameter),

irregular, platy and rough-surfaced nodules were found together with R-type nodules on the seamounts (st. 8319 and 8325). These nodules might have grown on the crust fragments fractured from the adjacent rocky bottom (von Stackelberg et al.,1984).

The R-type nodules occur generally in the abyssal plain whereas S type are found on hills, mounds, and seamounts. The T-type nodules occur mostly either with R or S-type nodules. On rocky seamount and on eroded seafloor (st. 8310 and 8909), both S and R-type nodules occur together with Mn-crust. The S and T-type nodules occur in a wide range of water depth and R-type nodules are collected generally between 5000 m and 5250 m (Figure 11). Nodules are abundant (5.0 to 28.9 kg/m^2) in the south of 10° 30' N where the seafloor is relatively irregular by large seamounts (Figure 12). However, the northern part near the Clarion fracture zone, nodules are rare, generally less than 2 kg/m^2. At a single site, the abundance is variable (e.g., 2.4 to 20.0 kg/m^2 at st. 8910) as well as type and size (Table 1).

On 3.5 kHz seismic profiles, nodules are found on less-than-90 m thick topmost transparent layer (Figure 13). The nodule abundance increases inversely to about 50 m thickness. The S and T-type nodules are abundant often on thick sediment layer that forms topographic reliefs of mounds, hills and channels. Earlier studies reveal that nodule occurrence is limited to deep-sea floor where the topmost sediment layer is thin less than 100 m (Mizuno et al., 1980; Usui et al., 1987).

2. Bottom Photograph

For delineating a regional distribution pattern of manganese nodules, still and video photographs were obtained by towing a camera system at about 6 m above the seafloor at 6 stations. At the same time, 3.5 kHz seismic profiles were obtained. The nodule abundance was estimated from a formular: A (abundance) = 6.6 D*C/100, where D (cm) is mean value of long axes of nodules, C (%), nodule coverage (C, %), similar to Handa and Tsurusaki (1981). The coefficient (6.6) was obtained from the observation of nodules in box cores and free-fall grabs.

On photographs, nodules are poor, less than 2 kg/m^2 in thick (more than 80 m) topmost transparent layer (Figure 14a), whereas abundant, more than 15 kg/m^2, in thin layer and on eroded hills (Figure 14b) and seamounts. Here the nodules occur together with Manganese crust and fragments, indicative of nodule patches or pavements (Spiess et al., 1977; Hugget and Somers, 1988).

Photographs show various benthic fauna such as large worm, bivalve, ophiuroid, actinaria (anemones), holothurian (cucumbers) (Figure 15). It seems that an ophiuroid feeds on a nodule (Figure 15a) and a clam disturbs the seafloor (Figure 15a). Worm tubes are ubiquitous, sparse or clustered (Figure 15d). Worm traces are sinuous, coiling or anastosmosing among nodules (Figure 15e). At bases, on slopes of small mounds and in large ploughs, nodules occur veneered with sediment cover, suggesting that benthic animals are abundant and active. The animals may have contributed to keep nodules on the seafloor by feeding and dwelling (Piper and Fowler, 1980; Garnder et al., 1984).

3. Mineralogical and Chemical Compositions

Seventy-nine nodule samples of 33 stations were analyzed for mineralogical and chemical compositions (Table 2). Twenty-three Manganese crust samples from the seamounts of the KODOS area and the Marshall Islands were also analyzed for a comparison. The mineral composition was semi-quantified for 10A° manganate (todorokite), δ-MnO2 (vernadite), and aluminosilicate minerals by using XRD (Haynes et al., 1982). The chemical concentrations were determined by using flame atomic absorption spectrometer.

Todorokite and vernadite are major components with minor amounts of aluminosilicate minerals (Table 2). Todorokite is dominant as shown by the ratio of todorokite to vernadite in peak intensity (0.86 to 5.4). Mn and Fe comprise dominant metal constituents 10 to 28% (average, 24%) and 3.9 to 18.7% (average, 9.3%), respectively. Cu and Ni concentrations range from 0.11 to 1.36% (average, 1.20%), from 0.50 to 1.45%; average, 0.78%) Co ranges from 0.12 to 0.39% (average, 0.26%). The nodules of the KODOS area are enriched in Fe and Co compared to those in the C-C zones (McKelvey et al., 1979).

The R-type nodules are distinguished from the S-type nodules by higher ratios of todorokite/vernadite and Mn/Fe (Figure 16), similar to granular and smooth nodules in other areas (Halbach et al., 1981; Piper and Blueford, 1982). The former are enriched in Mn, Ni and Cu whereas the

latter are abundant in Fe and Co. In the nodule bottom, Mn, Ni and Cu are slightly higher than those in the top part of both R and S-type (Table 2). The T-type nodules are intermediate in composition between R and S-types. According to the classification based on chemical compositions (Figure 17), the R-type nodules are diagenetic whereas S-type nodules are hydrogenous in origin (Bonatti et al., 1972; Halbach et al., 1981). The T-type nodules are transitional in composition.

The chemical composition of R-type nodule is attributed to the early diagenesis of topmost surface sediment layer (Calvert and Piper, 1984; Halbach and Ozkara, 1979) as shown by their occurrence in half-buried or embedded within the layer (Figure 7a). Enrichment of todorokite, Mn, Ni and Cu in the R-type nodules results from preferential accretion of Mn oxides to nodules (Piper and Williamson, 1977; Halbach et al., 1981; Dymond et al., 1984). Formation of Fe-rich smectite fractionates Mn and Fe into nodule and the sediments, respectively, resulting in high Mn/Fe ratio in nodules (Hein et al., 1979). The sediment diagenesis occurs in a few or tens of cm thick surface sediment layer and is more facilitated by sediment mixing by bioturbation and bottom current (Piper and Bluford, 1982).

It is generally believed that the S-type nodules have grown by direct precipitation of colloidal Fe-oxihydoxides from the overlying bottom waters as Manganese crust forms on rocky seamounts where chemical conditions are more oxigenated by bottom current (Lyle et al., 1977; Halbach and Ozkara,

1979; Calvert and Piper, 1984). The Manganese crust is composed mostly of vernadite with trace amounts of todorokite (Table 2d). The S-type nodules, exposed on the sediment surface, might have rarely been influenced by diagenesis (Bonatti et al., 1972; Halbach et al., 1981) (Table 2b).

The transitional composition of T-type nodules represents either several changes from sediment diagenesis to hydrogenesis and vise versa, or different processes on nodule top and bottom during the growth (Halbach et al., 1981; Dymond et al., 1984). Hydrogenous composition is dominant in the nodule top whereas diagentic composition is abundant in the bottom (Table 2c). According to microscopic and chemical characters, sediment diagenesis appears to contribute more than hydrogenesis to T-type nodule growth (Halbach et al., 1981; Usui, 1984). The growth of todorokite results in granular (rough) surface by forming cuspate or dendritic microstructure whereas vernadite forms smooth surface by thin and compact layer (Margolis and Glassby, 1973; Sorem et al., 1979). Diagenetic nodule seems to have grown faster as much as 10 times than hygrogenetic nodule (Dymond et al., 1984).

The buried R and S-type nodules show the compositions similar to those on the surface (Table 2). The compositional characters and surface texture (Table 2e and Figure 8) suggest that these nodules are growing or at least not being dissolved within the sediment column (Heye et al.,1979).

IV. DISCUSSION

In the KODOS area, the sedimentary sequence can be divided into 3 acoustic units. The north- and northwest-ward movement of the Pacific plate passing the equatorial high productivity zone resulted in the latitudinal distribution of sedimentary sequence in the northeast Pacific (Cook, 1975; Ryan and Heezen, 1976; van Andel et al., 1976; Rawson and Ryan, 1978). The topmost unit formed on the hiatuses of late Eocene to middle Miocene in the KODOS area, by bottom current activities on reduced biogenic sedimentation (Piper et al., 1979; von Stackelberg et al., 1987). The sedimentation processes of the topmost sediment layer seem to control the nodule facies both in local and regional scales (Table 3).

Most nodules from the KODOS area show 2 to 3 cm thick Mn-oxide layers from nuclei (Figure 10), it can be postulated, from the averge growth rate of 2 to 3 mm/my (Ku and Broeker, 1969; Guichard et al., 1978), that the nodules have started to grow since the regional hiatus of middle Miocene, which promoted nodule growth in the northeast equatorial Pacific (Glasby et al., 1982; von Stackelberg, 1982). Unimodal distribution of nodule size confirms the initiation of nodule growth on a regional hiatus (Figure 8). If the growth were promoted by two hiatuses, the size distribution would be bimodal (Mangini, 1988). During a hiatus, intensified bottom current supplies coarse materials for metal oxides to accrete, and enhances the

sediment diagenesis by sediment redistribution (Horn et al., 1973; Piper et al., 1979; von Stackelberg et al., 1987). In the latest Miocene to early Pliocene time, the nodules might have grown faster due to maximum supply of metals in the Pacific sediments (Leinen and Stakes, 1979; Segl et al., 1989). Thin (2-3 mm) outermost layer has accreted since the latest hiatus, probably of Plio-Pleistocene time (Usui et al., 1987).

The surface sediments in the KODOS area are dominated by radiolarian-bearing clay and siliceous ooze, which is most prolific for manganese nodules in the northeastern Pacific (Horn et al., 1973; Skornyakova, 1979; Frazer and Fisk, 1981). Nodule-rich area corresponds to the middle Miocene sequence of the Clipperton Formation (Cook, 1975; Ryan and Heezen, 1976) in ther southern part of the KODOS area. In the northern margin of present equatorial high productivity zone, nodule growth is most favored by supply of large amounts of metals, resulting from large input and active dissolution of siliceous sediments beneath the CCD (Cronan, 1980; Stoffers et al., 1981; Glasby et al., 1982). This condition has been maintained by low sedimentation rate due to bottom current and narrowed equatorial high productivity zone at least since late Oligocene (van Andel et al., 1976; Glasby, 1978).

Nodule abundance and types in the KODOS area seem to be controlled by the average sedimentation rate, inferred from the thickness of topmost transparent sediment layer on 3.5 kHz seismic profiles (Figure 13). Most

nodules are confined to the seafloor of thin (less than 50 m) topmost transparent layer, as reported in the central Pacific (Mizuno et al., 1980; Usui et al., 1987). Thin sediment thickness represents low sedimentation rate since the onset regional hiatus. In general, nodules are rare or absent in the equatorial region where sedimentation rate is high (Stoffers et al., 1981; Andrews et al., 1984). Compared with the nodules in red clay area (Dymond et al., 1984; Usui, 1984), the poverty of nodules in the northern part of the KODOS area seems to result from extremely low sedimentation rate or erosion of sedimentary sequence and incorporation of volcanic ashes (von Stackelberg et al., 1987). Here Eocene to Oligocene sediments crop out the seafloor (van Andel and Heath, 1973; Ryan and Heezen, 1976). The ash beds are unfavorable for nodule growth because they are toxic to benthic animals and prevent sediment diagenesis by sealing the sediment layer (von Stackelberg, 1982).

In the KODOS area, R-type nodules are most dominant on the seafloor with less-than 40 m thick topmost transparent layer. The S and T-type nodules are generally found irregular seafloor with thick sediment layer or seamounts where sediment accumulation has been enhanced or prohibited by bottom current. It is believed that R-type nodules grow by sediment diagenesis at low to moderate sedimentation rate whereas S-type, by hydrogenetic process (Lyle et al., 1977; Calvert et al., 1978; Halbach et al., 1981). This relationship between nodule type and bulk sedimentation

rates is manifested by the occurrence of granular (R-type) nodules on thin Quaternary or on outcropped Tertiary sediments; smooth (S-type) nodules occur on thick Quaternary sediment layer or rocky seamounts (Piper and Blueford, 1982; Usui, 1984; von Stackelberg et al., 1987). Active feeding and dwelling activities of benthic animals (Figure 6) help nodules occur under rapid sediment deposition (Piper and Fowler, 1980; von Stackelberg et al., 1987).

Large variations in nodule abundance for short distances may represent nodule patch or pavement (Table 1 and Figure 14b). The nodules on eroded seafloor are lag deposits (Kennett and Watkins, 1975; Rogers, 1987) because nodule-incorporated pelagic clays are easily winnowed by weak bottom current (Lonsdale and Southard, 1974). Nodule patch and pavement are ubiquitous near and on eroded seafloor and seamount area due to easy introduction of coarse materials of nodule nuclei by bottom current (Horn et al., 1973; Glasby et al., 1982). In the KODOS area, the analysis of various data suggests that the nodule facies depend on various factors such as sedimentation rate, introduction of nucleating materials, which are in turn controlled by bottom current and benthic animal activities. Otherwise nodules would have been buried into the sedimentary strata following the burial probability within 1 million years or less (Heath, 1979).

A good agreement between nodule type and bulk composition suggests that nodule accretion processes are similar during short and long periods of

nodule growth (Figure 17). Some discrepencies between them are found because the surface texture represents the latest growth processes of a nodule (Halbach et al., 1981). Two or three boundaries between Mn-oxide layers (Figure 10) resulted from several changes of nodule position caused by rolling on indurated seafloor or burial within the topmost sediment layer by bottom current for rather long periods (Glassby, 1977). These changes lead to episodic growth causing the compositional variation in a sinlge nodule (Dymond et al., 1984; Segl et al., 1989), resulting from repeated erosion and deposition of the topmost surface sediment layer (Maylan, 1974; Halbach et al., 1981; Krishnaswami et al., 1982). The bulk composition of a nodule represents the average microscopic internal layer formed in less-than-10,000 years (Margolis and Glasby, 1973; Segl et al., 1989).

V. CONCLUSIONS

Sedimentation in the KODOS area has been dominated by pelagic settling of biogenic sediments on the Pacific plate which was drifted north- and northwest-ward beneath the equatorial region since late Cretaceous. Discontinuous topmost sediment layer results from the activities of AABW since late Eocene. The bedforms also reflect the effect of AABW, probably through several passages of the Line Islands Ridge.

The nodule characters suggest that local and regional sedimentation processes of AABW are responsible for the variations in nodule abundance, type and composition. Nodules are rich in the southern part of the KODOS area which comprises the post-early Miocene radiolarian ooze and clay (Clipperton Formation) and on the seamounts in the southern part of the KODOS area. Nodule growth may have initiated as the Clipperton Formation onset the middle Miocene hiatus.

Thin topmost sediment layer (less than 50 m) is generally favorable for nodule growth. Nodules are poor in the northern part where sediments are not deposited, composed of Oligocene and Eocene sequence. Here, it is also due to deposition of volcanic ashes.

The R-type nodules occur mainly on the abyssal plain whose bulk composition is characterized by high todorokite, Mn, Ni and Cu concentrations. The S-type nodules are abundant in vernadite, Fe and Co.

The T-type nodules are intermediate in composition between the two types. Both S- and T-type nodules occur mainly on seamounts and on the seafloor with various thickness of sediment layer where bottom currents are active. The nodule type and composition result from the change in depositional processes (erosion or deposition) of topmost surface sediment layer results during nodule growth. Locally-intensified bottom current activities and supply of large amounts of nodule-nucleating materials are attributed to form nodule patches or pavements around and on low and high topographic reliefs where bottom current is strong. Benthic animal activities seem to affect nodule occurrence on thick sediment layer.

VI. ACKNOWLEDGEMENTS

We would like to thank the captain and crew of R.V. Kana Keoki and Farnella for our successful cruise in the KODOS area. Scientiffic staff from USGS and Korea Ocean Research and Development Institute helped and analyzed manganese nodule and sediment samples.

REFERENCES

Andrews, J., G. Friedrich, G. Pautot, W. Pluger, V. Renard, M. Melguen, D. Cronan, J. Craig, M. Hoffert, P. Stoffers, S. Shearme, T. Thijssen, G. Glasby, N. LeNotre, and P. Saget, 1984, The Hawaii-Tahiti transect: the ocenographic environment of manganese nodule deposits in the central Pacific: Marine Geology, v.54, p.109-130.

Berger, W.H. and G.R. Heath, 1968, Vertical Mixing in pelagic sediments, Journal of Marine Research, v.26, p.134-143.

Berger W.H. and E.L. Winterer, 1974, Plate stratigraphy and the fluctuating carbonate line, in K.J. Hsu and H.C. Jenkynes, eds., Pelagic sediments: on land and under the sea: IAS. Blackwell Scientific Publication, London, p.11-48.

Berger, W.H., C.G. Adeleck, and L.A. Mayer, 1976, Distribution of carbonate in surface sediments of the Pacific Ocean, Journal of Geophysical Research, 81(15): 2617-2627.

Bonatti, E., T. Kraemer, and H. Rydell, 1972, Classification and genesis of submarine iron-manganese deposits, in D.R. Horn, ed., Ferromanganese deposits on the ocean floor: Washington D.C., p.149-166.&

Calvert, S.E., N.B. Price, G.R. Heath, and T.C. Moore, Jr., 1978. Relationship between ferromanganese nodule compositions and sedimentation in a small survey area of the equatorial Pacific: Journal of Marine Research, v.36(1), p.161-183.

Calvert, S.E. and D.Z. Piper, 1984, Geochemistry of manganese nodules from DOMES site A, northern equatorial Pacific: multiple diagenetic metal sources in the deep sea: Geochimica Cosmoshimica et Acta, v.48, p.1913-1928.

Clague, D., 1981, Linear island and seamount chains, aseismic ridges and intraplate volcanism: results from Deep Sea Drilling Project: SEPM Special Publication, No.32, p.7-22.

Cook, H.E., 1975, North american stratigraphic principles as applied to deep-sea sediments: AAPG Bulletin, v.59(5), p.817-837.

Craig, J.D., 1979, The relationship between bathymetry and ferromanganese deposits in the north equatorial Pacific: Marine Geology, v.29, p.165-186.&

Cronan, D.S., 1980, Underwater minerals: Academic Press, London, 362p.

Damuth, J.E., R.D. Jacobi, and D.E. Hayes, 1983, Sedimentation processes in the northwest Pacific basin revealed by echo-character mapping studies: GSA Bulletin, v.94, p.381-395.

Dymond, J., M. Lyle, B. Finney, D.Z. Piper, K. Murphy, R. Conard, and N. Pisias, 1984, Ferromanganese nodules from MANOP sites H, S, and R - control of mineralogical and chemical composition by multiple accretionary processes: Geochimica Cosmochimica Acta, v.48, p.931-949.

Edmond, J.M., Y.-C. Chung, and J.G. Sclater, 1971, Pacific bottom water: penetration east around Hawaii: Journal of Geophysical Research, v.76(33), p.8089-8097.

Embley, R.W., P.J. Hoose, P. Londale, L. Meyer, and B.E. Tuchokle, 1980, Furrowed mud waves on the western Bermuda Rise: GSA Bulletin, v.91, p.731-740.

Ewing J.I., M. Ewing, T. Aitken, and W.J. Ludwig, 1968, North Pacific sediment layers measured by seismic profiling, in L. Knopoff, ed., The crust and upper mantle of the Pacific area: American Geophysical Union Monograph, No.12, p.147-173.

Francheteau, J., C.G.A. Harrison, J.G. Sclater, and M.L. Richards, 1970, Magnetization of Pacific seamounts: A prliminary polar curve for the northeastern Pacific: Journal of Geophysical Research, v.75, p.2035-2061.

Frazer, J.Z., and M.B. Fisk, 1981, Geological factors related to characteristics of seafloor manganese nodule deposits: Deep-Sea Research, v. 28A (12), p.1533-1551.

Gardner, W.D., L.G. Sullivan, and E.M. Thorndike, 1984, Long-term photographic, current, and nephelometer observations of manganese nodule environments in the Pacific. Earth and Planetary Science Letters, v.70, p.95-109.

Glasby, G.P., 1978, Deep-sea manganese nodule in the stratigraphic record: evidence from DSDP cores: Marine Geology, v.28, p.51-64.

Glasby, G.P., P. Stoffers, A. Sioulas, T. Thijssen, G. Friedrich, 1982, Manganese nodule formation in the Pacific Ocean : a general theory: Geo-Marine Letters, v.2, p.47-53.

Guichard, F., J.L. Reyss, and Y. Yokoyama, 1978, Growth rate of manganese nodules measured with Be-10 and Al-26: Nature, v.272, p.155-156.

Halbach, P., and M. Ozkara, 1979, Morphological and geochemical classification of deep-sea ferromanganese nodules and its genetic interpretation, in Du Centre National De La Recgerche Scientifique, ed., La genese des nodules de manganese: Colloques Internationaux Du CNRS. Paris, no.289, p.77-88.

Halbach, P., C. Scherhag, U. Hebisch, and V. Marchig, 1981, Geochemical and mineralogical control of different genetic types of deep-sea nodules from the Pacific Ocean: Mineralium Deposita, v.16, p.59-84.

Handa, K. and K. Tsurusaki, 1981, Manganese nodules : relationship between coverage and abundance in northern part of central Pacific: Geological Survey of Japan Cruise Report, v.15, p.184-217

Hayes, S.P., 1979, Benthic current observations at DOMES sites A,B, and C in the tropical north Pacific Ocean, in J.L. Bischoff, and D.Z. Piper, eds., Marine geology and Oceanography of the Pacific manganese nodule province: Marine Science, v.9, Plenum Press, New York, p.83-112.

Haynes, B.W., S.L. Law, and D.C. Barron, 1982, Mineralogical and elemental description of Pacific manganese nodules: Bureu of Mines Information circular, IC8906, U.S. Deptartment of the Interior, 60p.

Heath, G.R., 1979, Burial rates, growth rates and size distribution of deep-sea manganese nodules: Science, v.205, p.903-904.

Heezen, B.C. and P.M. Tharp, 1978. Bathymetric map of the northeast equatorial Pacific Ocean, 1:5,000,000: Miscellaneous investigation series, Map 1-1095, USGS, Menlo Park.

Hein, J.R., H.-W. Yeh, E. Alexander, 1979, Origin of iron-rich montmorillonite from the manganese nodule belt of the north equatorial Pacific: Clays and Caly Minerals, v.27(3), p.185-194.

Herron, E.M., 1972, Sea-floor spreading and the Cenozoic history of the east-central Pacific: GSA Bulletin, v.83, p.1671-1692.

Heye, D., V. Marchig, and H. Mayer, 1979, The growth of buried nodules. Deep-Sea Research, v.26A, p.789-798.

Horn D.R., B.M. Horn and M.N. Delach, 1973, Copper and Nickel content of ocean ferromanganese deposits and their relation to properties of the substrate, in M. Morgenstein, ed., The origin and distribution of manganese nodules in the Pacific and prospects for exploration: Hawaii Institution of Geophysics, Honolulu, p.71-76.

Hugget, Q.J. and M.L. Somers, 1988, Possibilities of using GLORIA system for manganese nodule assessment: Marine Geophysical Research, v.9, p.255-264.

Johnson, D.A., 1972, Eastward-flowing bottom currents along the Clipperton fracture zone: Deep-Sea research, v.19, p.253-257.

Keller, G. and J.A. Barron, 1983, Paleoceanographic implications of Miocene deep-sea hiatuses: GSA Bulletin, v.94, p.590-613.

Kennett, J.P. and N.D. Watkins, 1975, Deep-sea erosion and manganese nodule development in the southeast Indian Ocean: Science, v.188, p.1011-1013.

Kolla, V., S. Eittreim, L. Sullivan, J.A. Kostecki, and L.H. Burckle, 1980, Current-controlled, abyssal microtophography and sedimentation in Mozambique Basin, southwest Indian Ocean: Marine Geology, v.34, p.171-206.

Koblentz-Mishke, O.J., 1977. Primary production, in Vinogradov, M.E., ed., Oceanology, Biology of the Production, v.1. p.62

Krishnaswami, S., A. Mangini, J.H. Thomas, P. Sharma, J.K. Cochran, K.K. Turekian, and P.D. Parker, 1982, 10-Be and Th-isotopes in Mn-nodules and adjacent sediments: nodule growth histories and nodule behaviour: Earth Planetary Science Letters, v.59, p.217-234.

Ku, T.L., and W.S. Broecker, 1969, Radiochemical studies on manganese nodules from deep-sea origin: Deep-Sea Research, v.16, p.625-637.

Leinen, M. and D. Stake, 1979, Metal accumulation rates in the central equatorial Pacific during Cenozoic time: GSA Bulletin, v.90, p.357-375.

Lonsdale, P. 1981, Drifts and ponds of reworked pelagic sediment in part of the southwest Pacific. Marine Geology, v.43, p.153-193.

Lonsdale, P., and J.B. Southard, 1974, Experimental erosion of north Pacific red clay: Marine Geology, v.17, p.M51-M60.

Lonsdale, P., and S.M. Smith, 1980, Lower insular rise hills shaped by a bottom boundary current in the mid-Pacific. Marine Geology, v.34, p.M19-M25.

Lyle, M., 1983, The brown-green transition in marine sediments: a marker of the Fe (III)-Fe (II) redox boundary: Limnology and Oceanography, v.28, p.1026-1033.

Lyle, M., J. Dymond, and G.R. Heath, 1977, Copper-nickel-enriched manganese nodules and associated crusts from the Bauer basin, northwest Nazca plate: Earth Planetary Science Letters, v.35, p.55-64.

Mammerickx, J., 1985, A deep-sea thermohaline flow path in the northwest Pacific: Marine Geology, v.65, p.1-19.

Mangini, A., 1988, Growth rates of manganese nodules and crusts: in P. Halbach, G. Friedrich and U. von Stackelberg, eds., The manganese nodule belt of the Pacific Ocean. -Geological environments, nodule formation and mining aspects: Ferdinand Enke Verlag Stuttgart, W.Germany, p. 142-159.

Mantyla, A.W., 1975, On the potential temperature in the abyssal Pacific Ocean: Journal of Marine Research, v.33, p.341-354.

Margolis, S.V., and G.P. Glasby, 1973, Microlaminations in marine manganese nodules as revealed by scanning electron microscopy, GSA Bulletin, v.84, p.3601-3610.

Maylan, M.A., 1974, Field description and classification of manganese nodules, Hawaii Institute of Geophysical Report (Honolulu), HIG-74-9, p.158-168.

McKelvey, V.E., N.A. Wright, and R.W. Rowland, 1979, Manganese nodule resources in the northeastern equatorial Pacific, in J.L. Bischoff, and D.Z. Piper, eds., Marine geology and Oceanography of the Pacific manganese nodule province: Marine Science, v.9, Plenum Press, New York, p.747-762.

McKenzie, D.P., and N.J. Morgan, 1969, Evolution of tripple junctions: Nature, v.224, p.125-133.

Mizuno, A., T. Miyazaki, A. Nishimura, K. Tamaki, and M. Tanahashi, 1980, Central Pacific manganese nodules, and their relation to sedimentary history: Offshore Technology Conference, v.3830, p.331-340.

Morgan W.J., 1972, Deep mantle convection plumes and plate motions. AAPG Bulletin, v.56, p.203-213.

Moritani, T., S. Maruyama, M. Nohara, K. Matsumoto, T. Ogitsu, and H. Moriwaki, 1977, Description, classification, and distribution of manganese nodules Geological Survey of Japan, Cruise report, v.8, p.136-158.

Munsell, 1975, Munsell Color. MacBeth division of Kolmorgen Corp. Baltimore, Maryland, U.S.A.

Normark, W.R. and F.N. Spiess, 1976, Erosion on the Line Island archipelagic apron: effect of small scale topographic relief: GSA Bulletin, v.87, p.286-296.

Orwig, T.L., 1981, Channeled turbidites in the eastern central Pacific basin: Marine Geology, v.39, p.33-57. Paul, A.Z., 1976, Deep-sea bottom photographs show that benthic organisms remove sediment cover from manganese nodules: Nature, v.263, p.50-51.

Piper, D.Z. and M.E. Williamson, 1977, Composition of Pacific Ocean ferromanganese nodule: Marine Geology, v.23, p.M285-M303.

Piper, D.Z. and B. Fowler,1980, New constraint on the maintenance of Mn nodules at the sediment surface: Nature, v.286, p.880-883.

Piper D.Z., J.V. Gardner and H.E. Cook, 1979, Lithic and acoustic stratigraphy of the equatorial north Pacific: DOMES sites A, B, and C. in J.L. Bischoff, and D.Z. Piper, eds., Marine geology and oceanography of the Pacific manganese nodule province: Marine Science, v.9, Plenum Press, New York, p. 309-348.

Piper, D.Z. and J.R. Blueford, 1982, Distribution, mineralogy, and texture of manganese nodules and their relation to sedimentation at DOMES site A in the equatorial north Pacific: Deep-Sea Research, v.29(8A), p.927-952.

Rawson, M.D. and W.B.F. Ryan, 1978, Oceanic floor sediment and polymetallic nodules, World oceanic floor panorama: Lamont-Doherty Geology Obs., Palisades(map).

Rehm E. and P. Halbach, 1982, Hawaiian-derived volcanic ash layers in equatorial northeastern Pacific sediments. Marine Geology, v.50, 25-40.

Rogers, J., 1987, Seismic, bathymetric and photographic evidence of widespread erosion and manganese-nodule pavement along the continental rise of the southeast Cape Basin: Marine Geology, v.78, p.57-76.

Ryan, W.B.F. and B.C. Heezen, 1976, Smothering of deepsea benthic communities from natural disasters: NOAA Technical Report Contribution No. 03-6-022-35120, 132p.

Sclater, J.G., R.N. Anderson, and M.L. Bell, 1971, Elevation of ridges and evolution of the central eastern Pacific: Journal of Geophysical Research v.76(32), p.7888-7915.

Segl, M., A. Mangini, J. Beer, G. Bonani, M. Suter, and W. Wolfli, 1989, Growth rate variations of manganese nodules and crusts induced by paleoceanographic events: Paleocenography, v.4, no.5, p.511-530.

Skornyakova, N.S., 1979, Zonal regularities in occurence, morphology and chemistry of manganese nodules of the Pacific Ocean, in J.L. Bischoff, and D.Z. Piper, eds., Marine geology and Oceanography of the Pacific manganese nodule province: Marine Science, v.9, Plenum Press, New York, p.699-727.

Sorem, R.K., R.H. Fewkes, W.D. McFarland, and W.R. Reinhart, 1979, Physical aspects of the growth environment of manganese nodules in the "Horn region", east equatorial Pacific Ocean, in Centre National de la Recherche Scientifique, ed., La genese des nodules de manganses: Colloques Internationaux du CNRS, No.289. Paris, p.61-76.

Spiess, F., P. Lonsdale, M. Bender, D. Kadko, J. Zampal, and I. Ford, 1977, MANOP cruise report, site survey areas M and H. R/V. Melvelle. indomed (leg I)- Sept.-Oct. 1977: Kingston, MANOP Office, University of Rhode Island, 31p.

Stoffers, P., Heidelberg, G.P., Glasby, et al., 1981, The geochemistry of coexisting manganese nodules, micronodules, sediments and porewaters from five areas in the equatorial and southwestern Pacific: Chemical Erde, v. 40, p.273-297.

Theyer, F., 1977, Micropaleontological dating of DOMES project box cores from test areas A and B, tropical Pacific, in D.Z. Piper ed., Deep ocean mining environmental study: geology and geochemistry of DOMES Sites A, B, and C, equatorial north Pacific: U.S.G.S. Open-File Report, 77-778. p. 179-194.

Tracey, J.I. et al., eds., 1971, Initial Report of the Deep Sea Drilling Project, v.8, U.S. Government Printing Office, 1037p.

Usui, A., 1984, Regional variation of manganese nodule facies on the Wake-Tahiti transect: morphological, chemical and mineralogical study: Marine Geology, v.54, p.27-51.

Usui, A., A. Nishimura, N. Tanahashi, and S. Terashima, 1987, Local variability of manganese nodule facies on small abyssal hills of the central Pacific basin: Marine Geology, v.74, p.237-275.

van Andel, Tj.H. and G.R. Heath, 1973, Geological results of Leg 16 : the central equatorial Pacific west of the East Pacific Rise, in Tj.H., van Andel and G.R. Heath et al., eds., Initial Report of the Deep Sea Drilling Project, v.16. U.S. Government Printing Office, p.937-947.

van Andel, Tj.H., G.R. Heath, and T.C. Moore Jr., 1976, Cenozoic history of the central equatorial Pacific: A thynthesis based on Deep Sea Drilling Project data, in G.H. Sutton, M.H. Manghnani, R. Moberly, and E.U. McAffee, eds., The geophysics of the Pacific Ocean Basin and its Margin: American Geophysical Union Monograph, No. 16, p.281-296.

Volat, J., L. Pastouret, and C. Vergnaud-Granzzini, 1980, Dissolution and carbonate fluctuations in Pleistocene deep-sea cores : A review: Marine Geology, v.34, p.1-28.

von Stackelberg, U., 1979, Sedimentation, hiatuses and development of manganese nodules: Valdivia site VA-13/2, northern central Pacific, in J.L. Bischoff, and D.Z. Piper, eds., Marine geology and Oceanography of the Pacific manganese nodule province (Marine Science v.9): Plenum Press, New York, p.559-586.

von Stackelberg, U., 1982, Influence of hiatuses and volcanic ash rains on the origin of manganese nodules of the equatorial North Pacific ("Valdivia" cruises VA-13/2 and VA-18): Marine Mining, v.3(3/4), p.297-314.

von Stackelberg, U., H. Kunzendorf, V. Marchig, and R. Gwozdz, R., 1984, Growth history of a large ferromanganese crust from the equatorial North Pacific nodule belt: Geology Jb., p.213-236.

von Stackelberg, U., H. Beirdorf, and V. Riech, 1987, Relationship between manganese nodule formation and sedimentary processes in the equatorial north Pacific Ocean - a synthesis based on the results of cruise S025 (1982) with R/V Sonne: Geology Jb., 377-403.

Windom, W.L., 1969, Atmospheric dust record in permanent snowfields: implications to marine sedimentation: GSA Bulletin, v.80, p.761-782.

Table 1. Manganese nodule characters and geological environment in the KODOS area

Sta. No.	Location (Latitude/Longitude)	Sample No.	Manganese Nodules			Seafloor Condition			
			Morphology /surface tex	Size(cm)	Abundance (kg/m²)	Water depth	Sediment type	Morphology	Thickness (m) and property of acoustically transparent layer
8302	11°59.73'N/148°58.33'W	FFG(1)	Ss	<1	2	5,465	Pelagic Clay	Hill top	50: reflective surface but downwardly indistinctively stratified
8303	11 58.38 /148 03.08	BC 1	PSs	<1	0.6	5,360	"	Hill top	69: reflective but discontinuous surface, weak internal reflectors on opaque subbottom
8310	10 00.03 /146 59.26	FFG(2)	DSs, DSr	2.5-8.5	12.5-16.5 (14.5)	5,450	"	Wavy seafloor	34: weak surface and internal reflectors on stratified subbottom
8311	10 00.01 /148 02.78	FFG(2)	DSr	2.5-10.0	13.0-15.0 (14.0)	5,225	"	Wavy seafloor	31: highly reflective surface but weak internal reflectors on stratified subbottom
8313	19 01.51 /150 59.79	FFG(5)	PSs	1.5-7.0	11.0-17.5 (14.2)	5,180	"	Eroded surface between large seamounts	0: weakly stratified but opaque bottom
8314	9 00.78 /151 03.46	DR-14 FFG(1)	Dr	2.0-10.0	6.0	4,890 5,100	"	Wavy seafloor	50: highly reflective surface, but weak internal reflectors on weakly stratified subbottom
8315	8 57.78 /149 00.74	FFG(1)	Ss	1.5-6.0	5.0	5,140	"	Wavy seafloor	28: highly reflective surface, but weak internal reflectors on stratified subbottom
8318	9 01.40 /145 57.69	FFG(2)	Sr	1.0-10.0	3.0-5.0 (4.0)	5,150	"	Wavy but some eroded surface	<6: reflective surface, hummocky but stratified subbottom
8321	7 57.72 /145 59.32	FFG(2)	Sr	2.0-5.0	1.0	5,150	"	Base of hill	28: weak surface and no internal reflector on stratified subbottom
8322	7 58.16 /146 59.10	FFG(1)	Sr	1.5-3.5	1.0	5,190	"	Hill slope	16: reflective surface,no internal reflector on stratified subbottom
8323	7 57.34 /147 59.21	FFG(1)	DSr	1.0-12.0	2.0	5,080	"	Wavy seafloor	25: reflective surface,no internal reflector on hummocky subbottom
8324	7 59.87 /149 01.87	DR-24 FFG(1)	ICr	2.0-10.0	9.0	4,850 4,870	"	Hill slope	0: opaquely stratified bottom
8325	8 04.35 /149 57.68	DR-25 FFG(1)	CDSr DSr	1.0-20.0	5.0	4,782 4,855	"	Seamount slope	22: indistinctive surface and internal reflectors on stratified subbottom
8326	8 14.97 /151 02.55	DR-26 FFG(3)	DSr	1.5-15.0	9.0-14.5 (12.0)	4,990 4,976	"	Seamount slope	<6: highly reflective surface on weakly stratified subbottom

Note : BC is box corer; FFG, free-fall grab; DR, Dredge; Number in parenthesis, number of free-fall grabs deployed.
Sediment type was determined by naked eye from the sediments associated on nodules in 1983 cruise.
Thickness and acoustic properties of transparent layer were examined by using 3.5 kHz high-resolution subbottom profiler.

Table 1. Continued.

Sta. No.	Location (Latitude/Longitude)	Sample No.	Manganese Nodules			Seafloor Condition				
			Morphology	Size(cm)	Abundance (kg/m²)	Water depth	Sediment Type	Bioturbation	Morphology	Thickness (m) and property of acoustically transparent layer
8901	12°00.00'N/152°59.80'W	BC 1	ISr	1.0-3.5	0.3	5225	radiolaria -bearing Clay	Intensive	Wavy seafloor near a hill	7: weak surface, strongly stratified subbottom
		FFG(2)	SEr	0.5-3.0	0.1-0.5 (0.3)	5225				
8902	12 00.10 /153 40.00	BC 2	SEDFIs	2.0-6.0	8.3	5095	"	"	Sediment mound	78: weak and hummocky stratified surface, no internal reflectors on strongly stratified subbottom
		FFG(2)	Ps	2.0-8.0	6.9-9.2 (8.1)	5095				
8903	11 20.20 /153 40.30	BC 3	Dr	4.0-6.0	1.0	5220	radiolaria -rich Clay	"	Wavy seafloor	52: weak surface, no internal reflectors on strongly stratified subbottom
		FFG(1)	SEIr	2.0-8.0	1.0	5220				
8904	11 20.00 /152 45.00	BC 4		-	-	5112	radiolaria -bearing Clay	Intermediate	Flat seafloor between hills	52: distinctive surface, an internal reflector at 20 m depth on strongly stratified subbottom
		FFG(2)	SIDr	2.0-4.0	0.0-0.1	5112				
8905	11 00.00 /153 00.00	BC 5		-	-	5150	"	Intensive	Wavy seafloor between hills	78: weak surface, and internal reflector at 8 m depth on strongly stratified subbottom
		FFG(2)	SEr	2.0-4.0	0.0-0.03	5148				
8907	10 40.00 /153 40.10	BC 7	Er	<2.0	0.03	5220	"	Weak	Wavy (hilly) seafloor	85: strong surface but weak internal reflector at 50 m depth on weakly stratified subbottom
		FFG(2)	EFr,EFDs.r+r	2.0-8.0	1.5	5205				
8908	10 40.00 /152 40.00	BC 8	EFDr	2-8	0.9	5225	"	"	Hill slope	42: discontinuous surface, no internal reflectors on hyperbolic subbottom
		FFG(1)	SEDFIr	<2-4	0.2	5225				
8909	10 19.90 /152 50.00	BC 9	Fr, Ir, Fs	<2-4	0.3	4923	—	Intensive	Seamount slope (rocky)	<4: distinctive surface on opaque subbottom, a sediment patch
		DR 9	Crust, Is	1-20	-	4880				
8910	10 20.00 /153 50.00	BC 10	Crust, Is	<2	0.13	4874	—	—	Seamount slope (rocky)	<4: same as above but on hummocky subbottom
		FFG(3)	Ditto	<2-8	2.4-20.0 (7.4)	4890				
8911	9 59.70 /153 40.60	BC 11	EDPIr	<2-8	5.7	5105	radiolaria -bearing Clay	Intensive	Wavy seafloor	20: distinctive surface with a weak internal reflector at 3 m on weakly stratified subbottom
		FFG(2)	SEDIPr	<2-6	8.7-11.2 (8.5)	5100				
8912	10 00.00 /153 20.10	BC 12	SEDPr	<2-6	6.1	5075	"	Intermediate	Flat seafloor	20: highly reflective surface and discontinuous internal reflectors on weakly stratified subbottom
		FFG(2)	SEDIPr	<2-6	5.2-6.6 (6.0)	5075				

Table 1. Continued.

Sta. No.	Location (Latitude/Longitude)	Sample No.	Manganese Nodules			Seafloor Condition				
			Morphology	Size(cm)	Abundance (kg/m^2)	Water depth	Sediment Type	Bioturbation	Morphology	Thickness (m) and property of acoustically transparent layer
8913	10 00.00 /152 40.00	BC 13	EDIPr.s+r	2-8	6.9	5280	"	–	Levee top of moat off small seamount	20: reflective but discontinuous surface and weak internal reflectors on stratified subbottom
		FFG(4)	Pr, Ps+r	2-8	7.0-8.9 (7.8)	5275				
8914	9 35.40 /152 40.20	BC 14	FISPs.s+r	<2-6	13.1	5000	"	Intensive	Sediment mound between low seamounts	20: reflective surface and ambigous internal reflector on strongly stratified subbottom
		FFG(3)	Ditto	<2-6	13.3-28.9 (19.2)	5000				
8915	9 20.00 /152 40.00	DR 15	Es+r, Ds+r	<2-6	-	5175	radiolaria -bearing Clay	Intensive (Gravity Core)	Wavy seafloor	55: reflective surface and internal reflectors at 7 and 17 m depths on stratified subbottom
		BC 15	Pr	4-6	0.6	5230				
8916	9 19.80 /153 14.00	BC 16	DEPr, DEPs+r	2-6	6.1	5146	"	Intensive	Wavy seafloor	36: weak surface and internal reflectors on indistinctively stratified subbottom
8917	9 20.20 /153 50.10	BC 17	SEDIPr	<2-6	5.3	5070	radiolaria -rich Clay	Intermediate	Wavy seafloor	10: reflective surface and no internal reflector on highly opaque subbottom
		FFG(5)	Ditto	<2-8	2.5-5.2 (4.2)	5070				
8918	9 40.00 /153 30.10	BC 18	Ps, Ps+r	2-6	20.0	4640	"	Intensive	Sediment mound on seamount	55: weak surface and internal reflectors on weakly straified subbottom
8919	9 40.30 /153 21.70	DR 19	I-Pr	<2-50	-	4800	–	–	Seamount slope	0: opaque and strong bottom
8920	9 40.40 /153 14.00	BC 20	PEDIr.s+r	2-6	10.7	5140	radiolaria -bearing Clay	Intensive	Channel-like between high seamounts	82: reflective surface, weak and discontinuous internal reflectors on weakly stratified subbottom
		FFG(3)	Ditto	2-6	8.0-13.8 (11.2)	5145				
8921	10 10.00 /153 29.90	BC 21	DEPISr	<2-8	5.8	5145	"	Intermediate	Wavy seafloor (sediment drift)	10: weak and discontinuous surface , and weak internal reflectors on weakly stratified subbottom
		DR 21	Ditto	2-8		5140				

Table 2a. Major minerals and elements in R-type nodules in the KODOS area

Sample	I10/I2.4	Feldspar	Quartz	Mn	Fe	Mn/Fe	Cu	Ni	Cu+Ni	Co
8310-U	4.67	1.00	1.00	23	5.1	4,6	0.90	1.23	2.13	0.22
L				25	4.4	4.8	0.98	1.29	2.27	0.21
11	3.33	2.00	2.00	23	6.0	3.8	0.78	1.04	1.82	0.21
14	3.50	2.00	2.00	22	5.5	3.9	0.92	0.99	2.01	0.18
15-U	4.67	4.00	2.00	23	4.4	5.3	0.98	1.05	2.03	0.16
L				25	4.2	5.9	1.03	1.13	2.16	0.16
18	5.00	1.00	1.00	21	3.9	5.4	1.05	1.15	2.20	0.14
22	4.20	7.00	3.00	22	5.0	4.3	0.63	0.71	1.34	0.09
23	3.20	14.00	3.00	23	5.4	4.2	0.64	0.65	1.29	0.12
25	4.00	4.00	3.00	24	5.7	4.2	0.96	0.85	1.81	0.18
26	3.67	2.00	1.00	22	5.9	3.8	1.09	1.08	2.17	0.18
8901-B-1	2.00	9.00	3.00	10	6.7	1.5	0.40	0.77	1.17	0.12
F-1	1.60	19.00	3.00	17	8.3	2.1	0.69	1.05	1.74	0.21
2-F-4	0.86	5.00	2.00	22	12.2	1.8	0.33	0.93	1.26	0.28
3-B-1	3.67	4.00	3.00	24	8.5	2.8	0.93	1.23	2.16	0.22
B-3	3.60	7.00	4.00	24	7.3	3.3	1.04	1.29	2.33	0.23
F-4	5.40	4.00	3.00	26	7.2	3.7	1.06	1.32	2.38	0.24
4-F-1	5.17	4.00	3.00	27	5.6	4.9	1.36	1.57	2.93	0.79
F-2	3.57	6.00	4.00	23	6.0	3.8	0.94	1.22	2.16	0.17
F-3	3.33	13.00	3.00	22	4.8	4.6	1.01	1.22	2.23	0.15
5-F-2	3.86	6.00	3.00	25	4.5	5.5	1.10	1.37	2.47	0.14
7-B-1	3.11	6.00	4.00	22	4.8	4.5	1.09	1.37	2.46	0.16
F-4	3.83	5.00	3.00	24	5.2	4.7	1.17	1.33	2.50	0.19
F-5	4.80	3.00	2.00	26	6.7	3.9	1.00	1.33	2.33	0.21
F-6	4.80	3.00	2.00	24	6.2	3.8	0.78	1.26	2.04	0.20
8-B-1	4.00	5.00	3.00	25	5.8	4.3	1.05	1.35	2.40	0.21
B-3	4.00	5.00	2.00	24	5.3	4.6	1.09	1.32	2.41	0.16
B-5	4.60	8.00	3.00	28	5.9	4.8	1.15	1.40	2.55	0.16
9-B-4	3.86	2.00	1.00	23	5.0	4.6	0.82	0.89	1.71	0.49
11-B-1	3.17	3.00	2.00	24	7.8	3.1	0.86	1.37	2.23	0.24
B-2	3.83	2.00	1.00	26	6.7	3.9	1.08	1.38	2.46	0.24
B-4	3.50	9.00	3.00	22	8.6	2.6	0.80	1.24	2.04	0.24
12-B-1	4.00	1.00	3.00	26	7.2	3.7	1.10	1.40	2.50	0.23
B-5	3.25	5.00	2.00	24	6.2	3.9	1.18	1.42	2.60	0.23
B-6	3.67	4.00	2.00	28	6.4	4.4	1.19	1.36	2.55	0.20
B-7	3.00	3.00	2.00	25	7.5	3.3	1.01	1.36	2.37	0.21
B-8	2.86	5.00	3.00	23	5.9	3.8	1.02	1.39	2.41	0.23
13-B-2	2.00	2.00	2.00	24	9.9	2.4	0.77	1.25	2.02	0.30
13-B-4	1.67	1.00	2.00	23	9.1	2.6	0.72	1.23	1.95	0.26
15-B-1	3.29	4.00	1.00	23	7.2	3.2	0.95	1.32	2.27	0.14
16-B-5	3.80	4.00	2.00	26	8.5	3.1	0.94	1.33	2.27	0.23
B-6	1.75	5.00	2.00	27	7.3	3.8	0.94	1.33	2.27	0.20
17-B-1	3.50	4.00	2.00	26	7.3	3.5	1.02	1.35	2.37	0.17
B-3	4.75	6.00	3.00	25	7.0	3.6	0.98	1.27	2.25	0.18
B-4	4.00	3.00	1.00	26	6.8	3.9	1.02	1.31	2.33	0.18
20-B-2	2.67	4.00	2.00	23	9.9	2.3	0.70	1.21	1.91	0.30
B-3	2.17	4.00	2.00	23	10.5	2.1	0.63	1.28	1.91	0.25
B-5	1.43	3.00	2.00	22	10.7	2.1	0.68	1.33	2.01	0.26
21-B-1	3.83	3.00	2.00	28	8.4	3.3	1.00	1.42	2.42	0.24
B-2	2.80	4.00	3.00	27	8.2	3.3	1.09	1.45	2.54	0.23
B-3	2.80	3.00	2.00	24	8.2	3.0	0.94	1.44	2.38	0.23
B-4	4.67	6.00	3.00	23	8.4	2.7	0.95	1.38	2.33	0.18
B-5	3.80	3.00	2.00	25	8.7	2.9	0.98	1.44	2.42	0.23

Table 2b. Major minerals and elements in S-type nodules in the KODOS area.

Sample	I10/I2.4	Feldspar	Quartz	Mn	Fe	Mn/Fe	Cu	Ni	Cu+Ni	Co
8313-U	1.40	2.00	1.00	17	9.6	1.8	0.38	0.60	0.98	0.25
L				17	8.6	1.9	0.41	0.60	1.01	0.24
24-U	2.00	8.00	1.00	16	9.2	1.7	0.41	0.62	1.03	0.20
L				20	8.9	2.2	0.54	0.77	1.31	0.23
8902-F-1	1.50	3.00	2.00	25	12.1	2.1	0.63	1.28	1.91	0.39
F-2	0.83	3.00	2.00	23	12.0	2.0	0.54	1.19	1.73	0.35
F-3	0.86	4.00	1.00	20	11.8	1.7	0.33	0.97	1.30	0.29
9-B-1	2.00	3.00	2.00	19	11.9	1.6	0.62	1.11	1.73	0.53
10-B-1	0.29	1.00	1.00	20	18.7	1.1	0.21	0.63	0.84	0.30
14-B-4	1.00	1.00	2.00	21	13.9	1.5	0.36	0.92	1.28	0.30
18-B-3	1.00	3.00	1.00	24	11.9	2.0	0.51	0.08	0.59	0.33
B-4	1.00	0.00	1.00	23	12.3	1.9	0.45	1.02	1.47	0.30
19-D-5	0.50	0.00	0.00	23	17.8	1.3	0.11	0.50	0.61	0.28
D-6	1.00	0.00	1.00	24	13.3	1.8	0.47	1.03	1.50	0.32

Table 2c. Major minerals and elements in T-type nodules in the KODOS area

Sample	I10/I2.4	Feldspar	Quartz	Mn	Fe	Mn/Fe	Cu	Ni	Cu+Ni	Co
8910-F-3	1.86	3.00	1.00	25	9.4	2.6	0.76	1.32	2.08	0.31
13-B-3	2.00	3.00	2.00	24	9.4	2.5	0.71	1.26	1.97	0.26
14-B-1	1.00	0.00	3.00	20	16.1	1.3	0.37	0.87	1.24	0.19
B-2	1.00	3.00	2.00	24	13.4	1.8	0.52	1.03	1.55	0.30
16-B-1	3.33	4.00	2.00	22	7.7	2.9	0.90	1.35	2.25	0.24
18-B-2	1.00	3.00	2.00	23	12.2	1.9	0.52	1.06	1.58	0.29
20-B-4	1.83	3.00	2.00	25	10.6	2.3	0.76	1.34	2.10	0.26
20-B-6	1.00	4.00	2.00	25	9.3	2.6	0.81	1.37	2.18	0.26

Table 2d. Major minerals and elements in Mn crusts in the KODOS area and the Marshall Islands.

Samples	I2.4	Feldspar	Quartz	Mn	Fe	Mn/Fe	Cu	Ni	Cu+Ni	Co
8325				19	10.4	1.8	0.37	0.71	1.08	0.30
26				17	12.4	1.3	0.29	0.40	0.69	0.27
89-D1-2	92.00	1.00	1.00	23	16.8	1.4	0.06	0.75	0.81	0.62
D3-1	93.00	3.00	1.00	24	16.0	1.5	0.11	0.82	0.93	0.54
D4-4	92.00	3.00	0.00	21	17.0	1.2	0.09	0.69	0.78	0.56
D8-1	98.00	0.00	2.00	27	16.9	1.6	0.06	0.86	0.92	0.86
D9-20	94.00	2.00	0.00	24	17.7	1.4	0.19	0.74	0.93	0.42
D10-2	93.00	0.00	1.00	23	18.4	1.2	0.20	0.69	0.89	0.45
D11-2	92.00	0.00	0.00	23	14.6	1.6	0.12	0.88	1.00	0.61
D12-2	97.00	0.00	0.00	24	18.2	1.3	0.12	0.79	0.91	0.57
D13-7	96.00	3.00	1.00	19	17.5	1.1	0.24	0.71	0.95	0.37
D14-2	97.00	2.00	1.00	22	17.7	1.3	0.08	0.66	0.74	0.60
D15-3	99.00	0.00	1.00	25	15.5	1.6	0.10	0.82	0.92	0.62
D16-8	99.00	0.00	1.00	28	14.6	1.9	0.09	0.00	0.09	0.95
D17-2	94.00	2.00	1.00	24	16.6	1.5	0.09	0.80	0.89	0.68
D18-10	91.00	0.00	0.00	21	14.6	1.4	0.10	0.70	0.80	0.66
D19-1	96.00	0.00	0.00	21	18.0	1.2	0.10	0.60	0.70	0.43
D20-6	57.00	26.00	2.00	10	11.6	0.9	0.01	0.28	0.29	0.34
D21-1	86.00	1.00	0.00	16	13.4	1.2	0.01	0.40	0.41	0.26
D22-2	77.00	1.00	1.00	23	11.0	2.1	0.04	0.84	0.88	0.45
D23-7	95.00	0.00	0.00	26	14.1	1.8	0.05	0.81	0.86	0.59
D26-1	92.00	0.00	0.00	22	14.5	1.5	0.08	0.71	0.79	0.56
D27-1	92.00	0.00	0.00	24	11.4	2.1	0.05	0.81	0.86	0.57

Table 2e. Composition of surface and buried manganese nodules at site 8918.

Depth	Mn	Fe	Cu	Ni	Co
0 cm	23	12	0.50	1.1	0.31
6 - 8	16	11	0.52	1.0	0.29
8 - 10	22	13	0.47	1.0	0.31
10 - 13	23	11	0.51	1.0	0.31
16 - 20	22	12	0.57	1.0	0.23
25 - 30	22	13	0.53	1.0	0.25
32	23	12	0.68	1.0	0.29

* Note : U, L, top and bottom parts of nodule, respectively;
F, free-fall grab sample; B, box core sample; D, dredge sample.
I10 and I2.4 is peak intensities of todorokite and vernadite, respectively.
Other minerals are in relative %.

Table 3. Geological factors of manganese nodule occurrence in the KODOS area.

Morphologic Environment	Sub-Environment	3.5 kHz Seismic Characters		Water Depth (m)	Bioturbation in Box Core		Nodule Occurrence	
		Transparent Layer Thickness (m)	Reflection Property		Strong	Weak	Abundance Range Mean	Type R S T
Abyssal Plain	Flat and Wavy Seafloor	Thin (0-50m)	Weak to highly reflective surface no and some internal reflectors on stratified or opaque subbottom	5070-5450	4 High Abundance	3 Low Abundance	0.3-14.5 6.5 (kg/m²)	12 1 1 Stations
		Thick (52-78m)	Weak to reflective surface and few continuous internal reflectors on well-stratified subbottom	5112-5230	2 Low	1 Low	0.0-1.0 0.4	4
	Sediment Mound	Thin (20m)	Reflective surface and indistinctive internal reflectors on well-stratified subbottom	5000		1 High	13.1-28.9 19.2	1
		Thick (78m)	Weak and hummocky surface, no internal reflector on well-stratified subbottom	5095	1 High		6.9-9.2 8.1	1
Seamount	Top and Slope	Thin (4-6m)	Highly reflective surface, no internal reflector on opaque or well-stratified subbottom	4890-4976	Not Cored		0.3-7.4 4.6 Crust	1 1 1
		Thick (22,55m)	Weak-reflective surface and intrenal reflectors on weakly-stratified subbottom	4640-4855	1 High		5.0-20.0 12.5	1 1
	Base	Thin (20m)	Reflective but discontinuous surface and weak internal reflectors on stratified subbottom	5280	Not Cored		6.9-8.9 7.8	1
		Thick (82m)	"	5180	1 High		8.0-13.8 11.2	1
Hill	Top and Slope	Thin (0,16m)	Prolonged or reflective surface and no internal reflectors on stratified subbottom	4870-5190	Not Cored		1.0-9.0 5.0	2
		Thick (28-85m)	Weak to reflective surface and weak internal reflectors on stratified or opaque subbottom	5150-5220	1 Low	1 Low	0.6-2.0 1.2	1 2 1

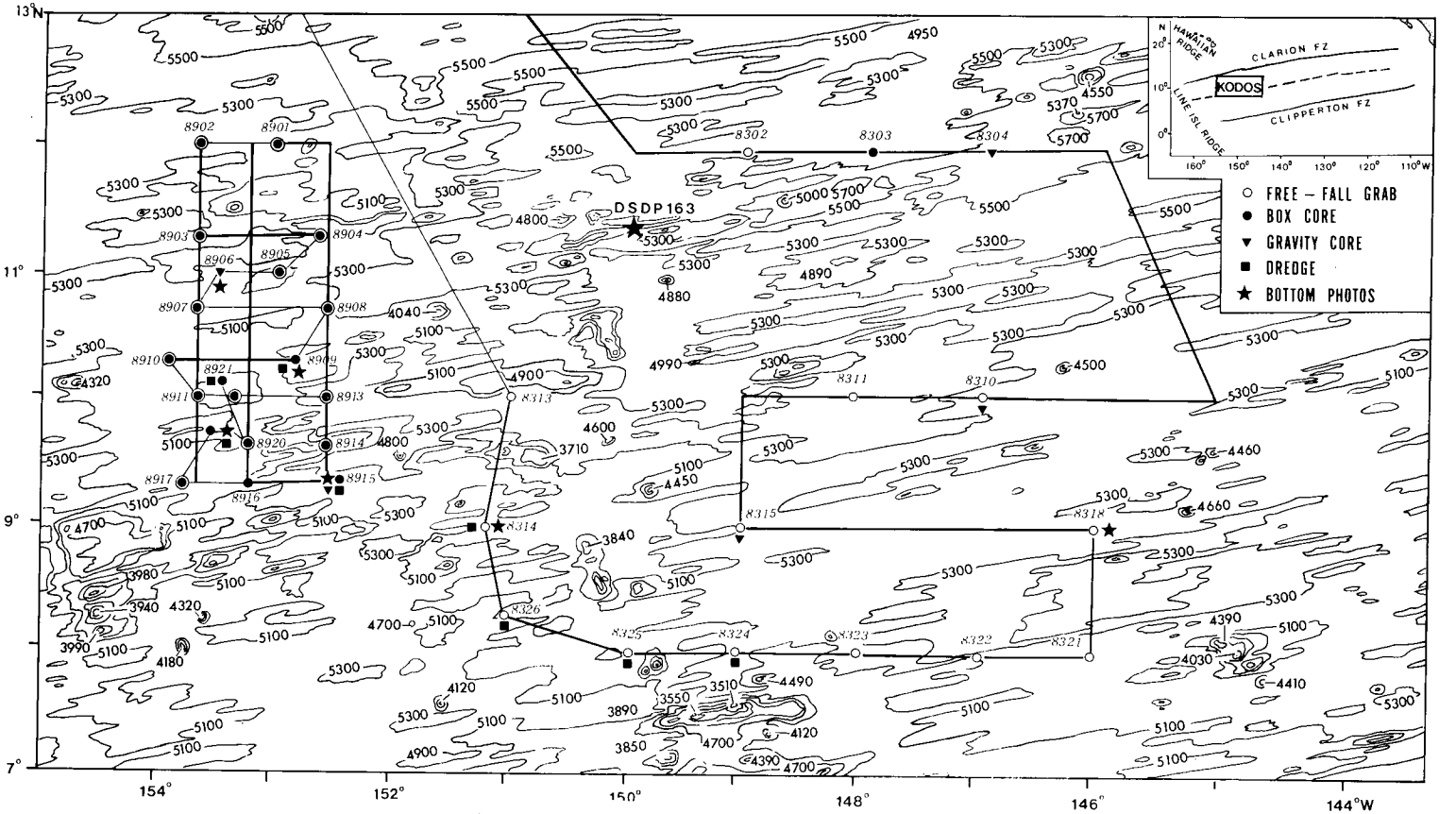
13°N
11°
9°
7°
154°
152°
150°
148°
146°
144°W
DSDP163
8902
8901
8903
8904
8906
8905
8907
8908
8910
8921
8909
8911
8913
8920
8914
8917
8916
8915
8313
8314
8302
8303
8304
8311
8310
8315
8318
8326
8325
8324
8323
8322
8321
FREE – FALL GRAB
BOX CORE
GRAVITY CORE
DREDGE
BOTTOM PHOTOS
HAWAIIAN RIDGE
CLARION FZ
KODOS
LINE ISL. RIDGE
CLIPPERTON FZ
20°
10°
0°
160°
150°
140°
130°
120°
110°W

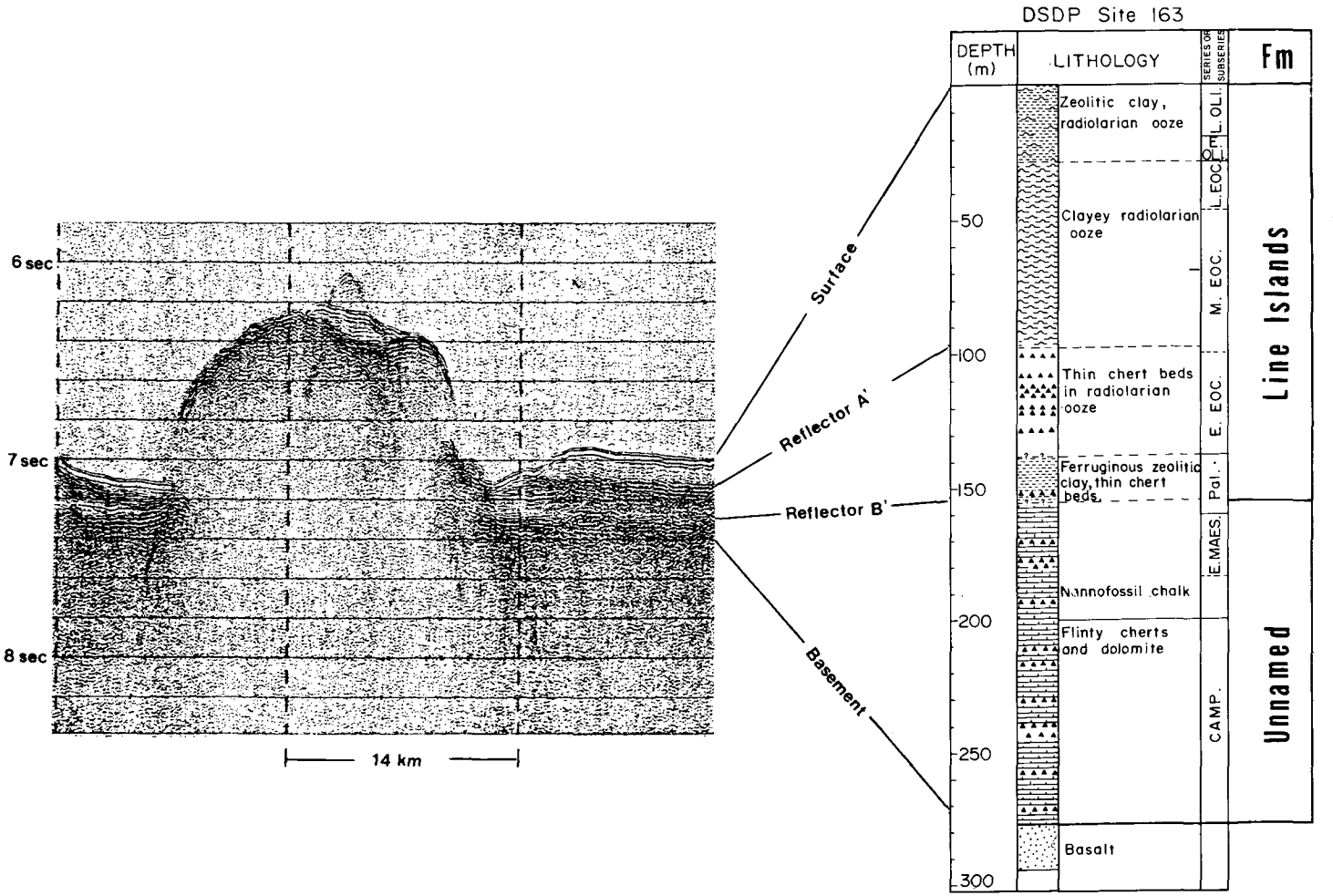
DSDP Site 163
DEPTH (m)
LITHOLOGY
SERIES OR SUBSERIES
Fm
Zeolitic clay, radiolarian ooze
Clayey radiolarian ooze
Thin chert beds in radiolarian ooze
Ferruginous zeolitic clay, thin chert beds
Nannofossil chalk
Flinty cherts and dolomite
Basalt
L. OLI.
L. EOC.
M. EOC.
E. EOC.
Pal.
E. MAES.
CAMP.
Line Islands
Unnamed
50
100
150
200
250
300
Surface
Reflector A'
Reflector B'
Basement
6 sec
7 sec
8 sec
14 km

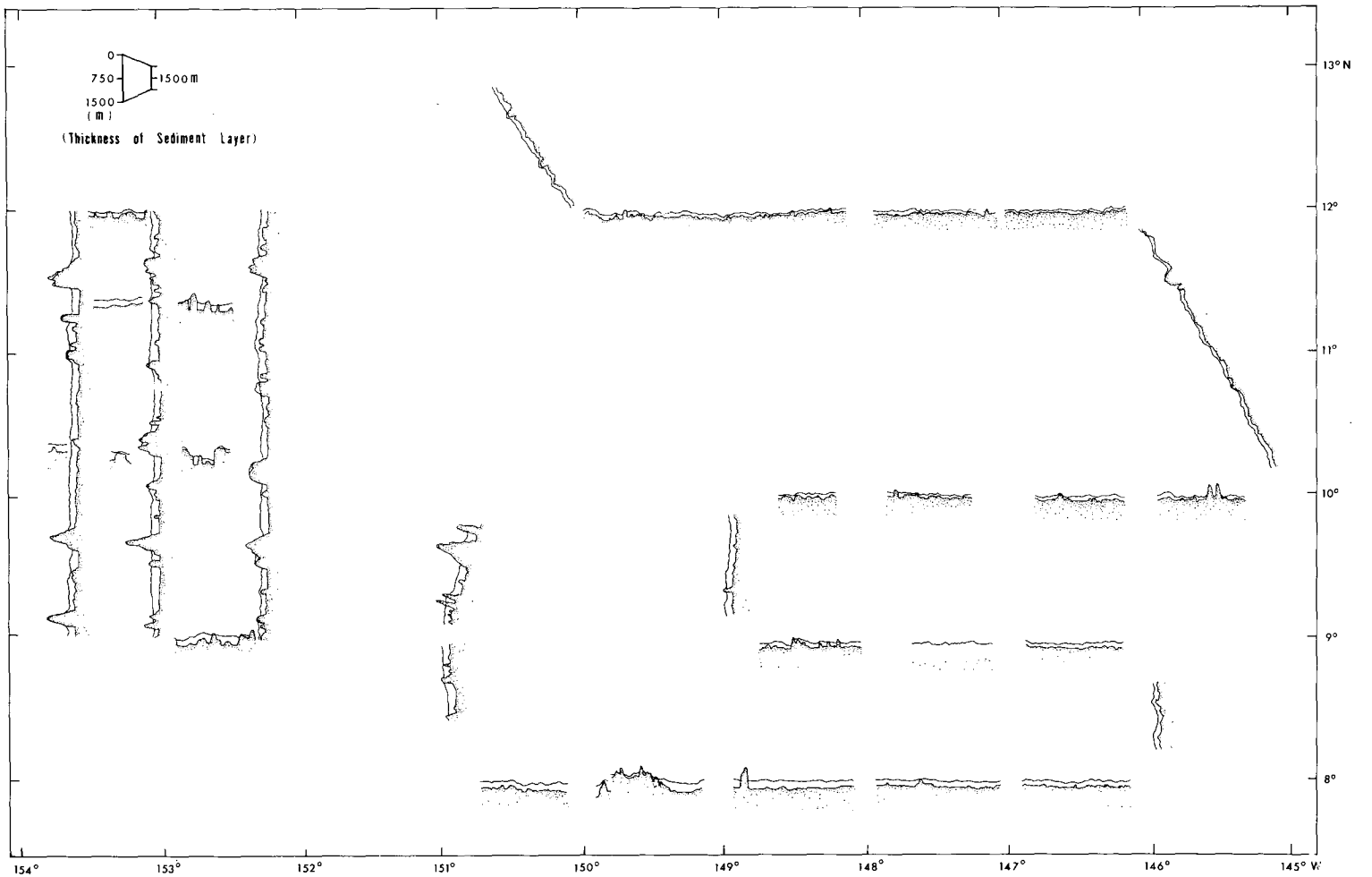
0
750
1500
(m)
1500m
(Thickness of Sediment Layer)
13° N
12°
11°
10°
9°
8°
154°
153°
152°
151°
150°
149°
148°
147°
146°
145° W

DSDP site 163	Lithologic Facies	3.5 kHz Seismic Facies
Line Is. Formation	Eocene to Quaternary zeolitic Clay and clayey radiolarian Ooze	Transparent, often hyperbolic or parallel internal reflectors occur
	Eocene radiolarian and closely laminated Cherts	Diffused due to hyperbolas, prolonged subbottom reflectors

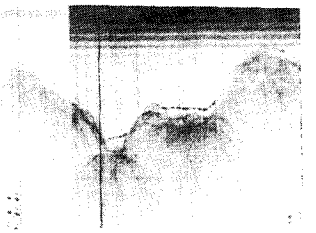

A

DSDP Site 163	Lithologic Facies	3.5 kHz Seismic Facies
Line Is. Formation	Eocene to Quaternary zeolitic Clay and clayey radiolarian Ooze	Transparent, often hyperbolic or parallel internal reflectors occur
	Eocene radiolarian and closely laminated Cherts	Diffused due to hyperbolas, prolonged subbottom reflectors

B

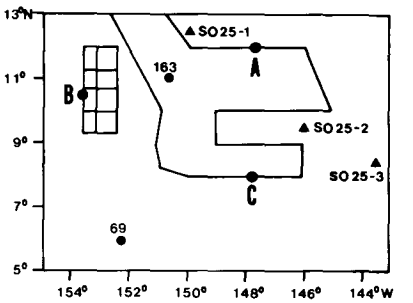

DSDP Site 69 and 70		Lithologic Facies	3.5 kHz Seismic Facies
Clipperton Formation	Radiolarian Ooze Unit	M. Miocene to Quaternary radiolarian and zeolitic Clay and Ooze, in place calcareous	Transparent, often parallel but indistinctive internal reflectors occur
	Cyclic Unit	Oligocene to E.Miocene alternating radiolarian and nannofossil ooze	Stratified
Marquesas Formation		?Eocene to Oligocene radiolarian-nannofossil Ooze to Chalk	Transparent

C

75 m

5 km

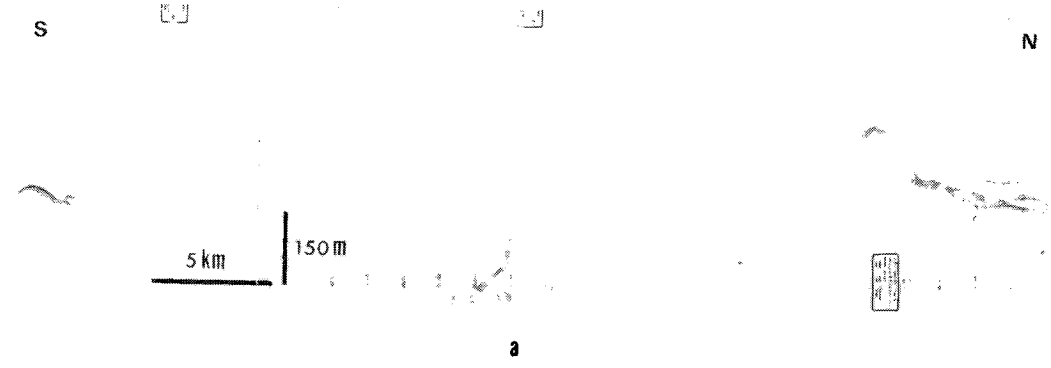

a

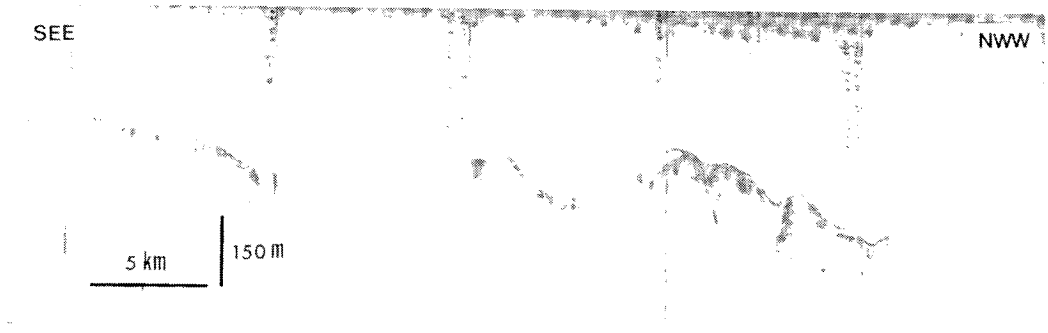

b

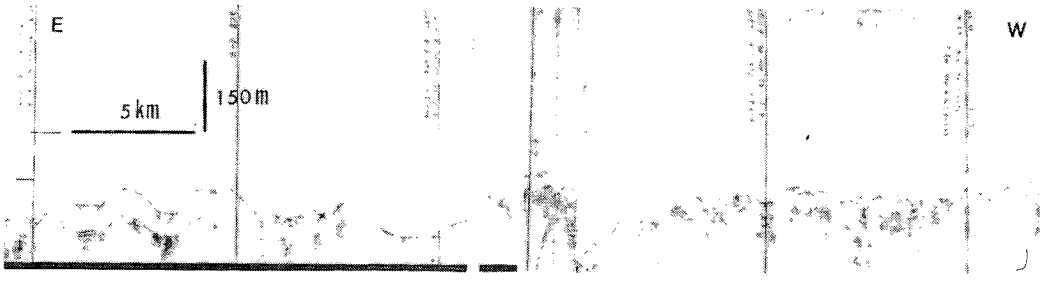

c

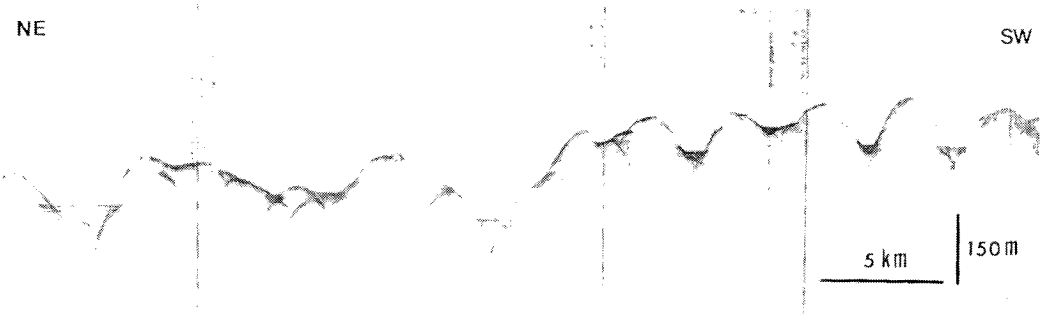

d

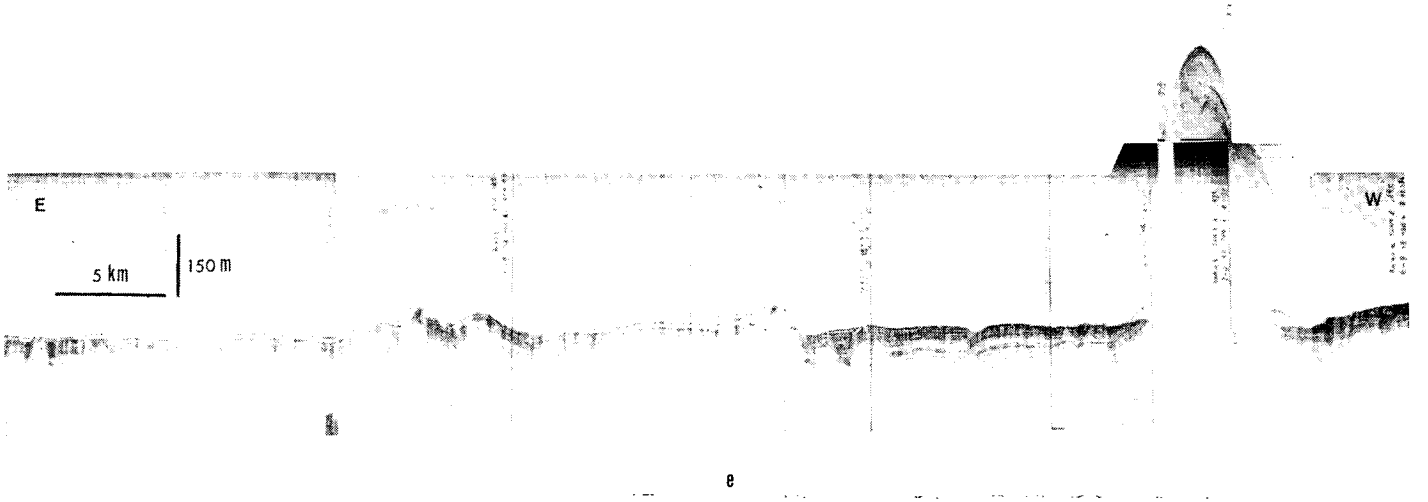
E
W
5 km
150 m

e

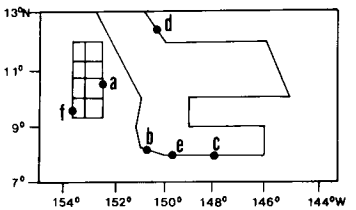
13°N
11°
9°
7°
154°
152°
150°
148°
146°
144°W
a
b
c
d
e
f

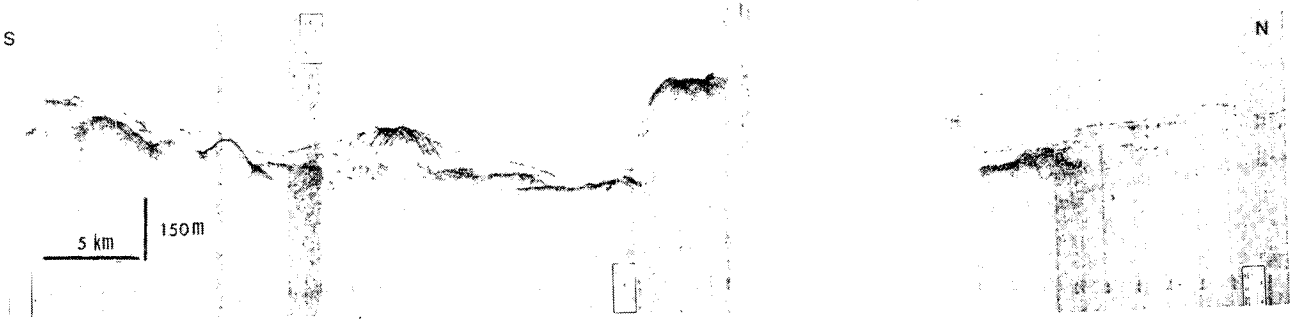
S
N
5 km
150 m

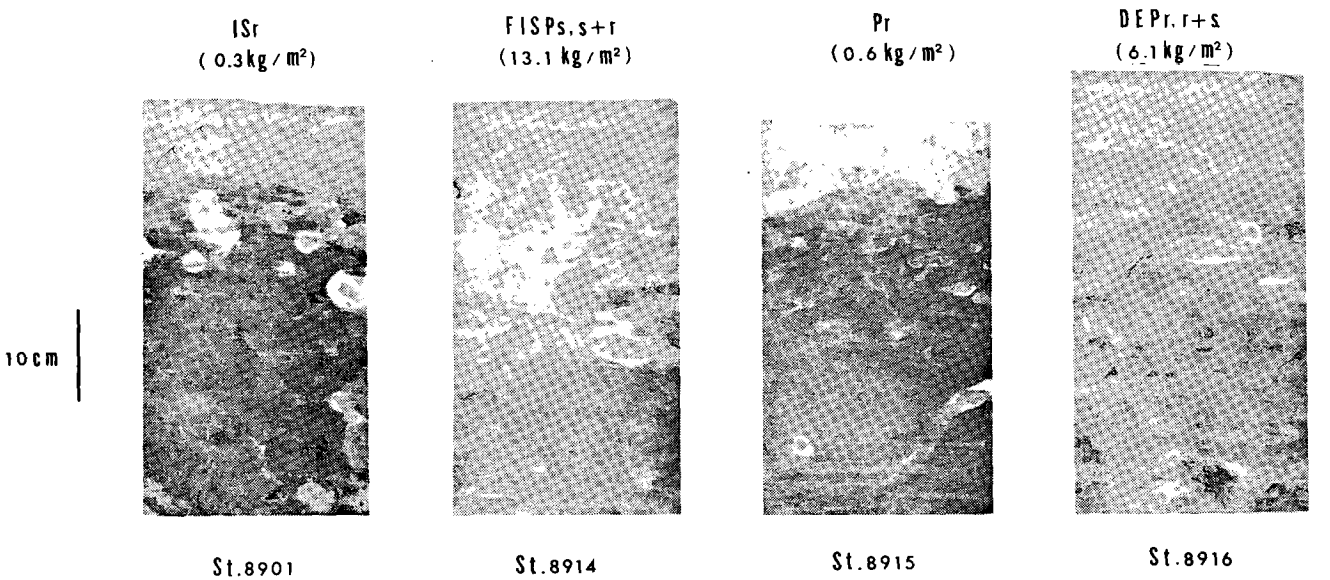
ISr
(0.3kg / m²)
FISPs, s+r
(13.1 kg / m²)
Pr
(0.6 kg / m²)
DEPr, r+s
(6.1 kg / m²)
10cm
St.8901
St.8914
St.8915
St.8916

DEPSr (6.1 kg/m²)

Ps, s+r (20.0 kg/m²)

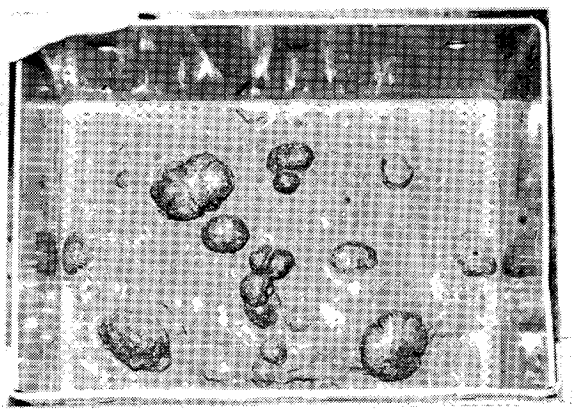

5 cm

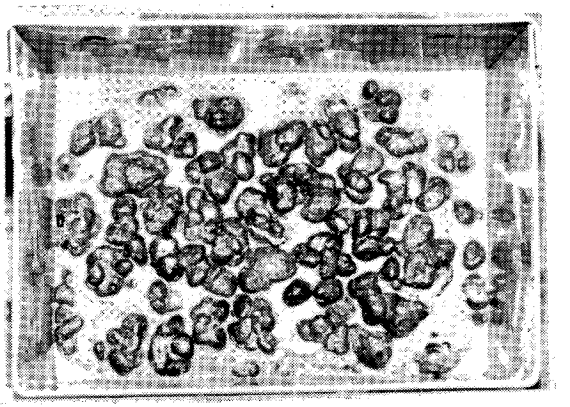

St. 8912

St. 8918

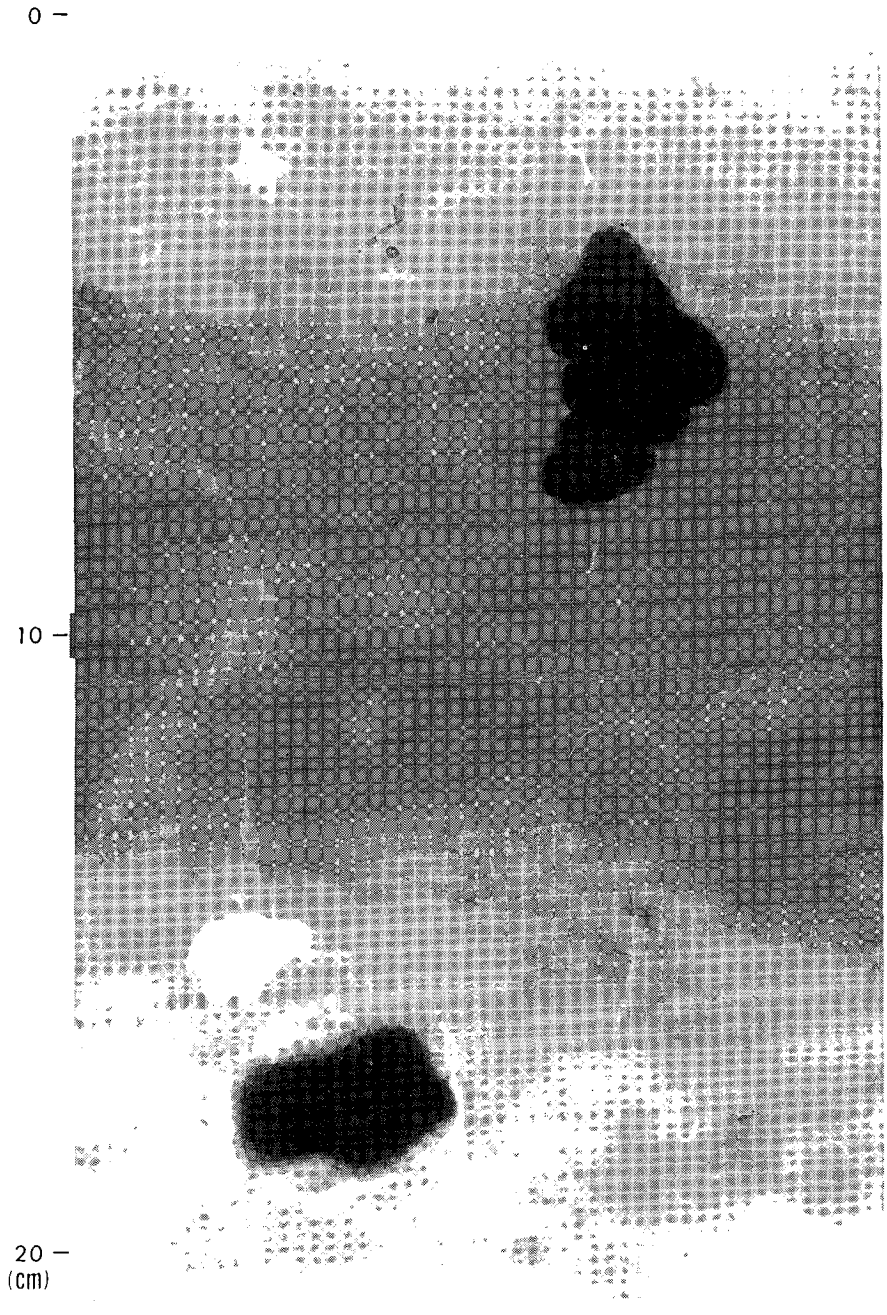
Pr,s+r (20.0 kg/m²)
0 —
10 —
20 —
(cm)

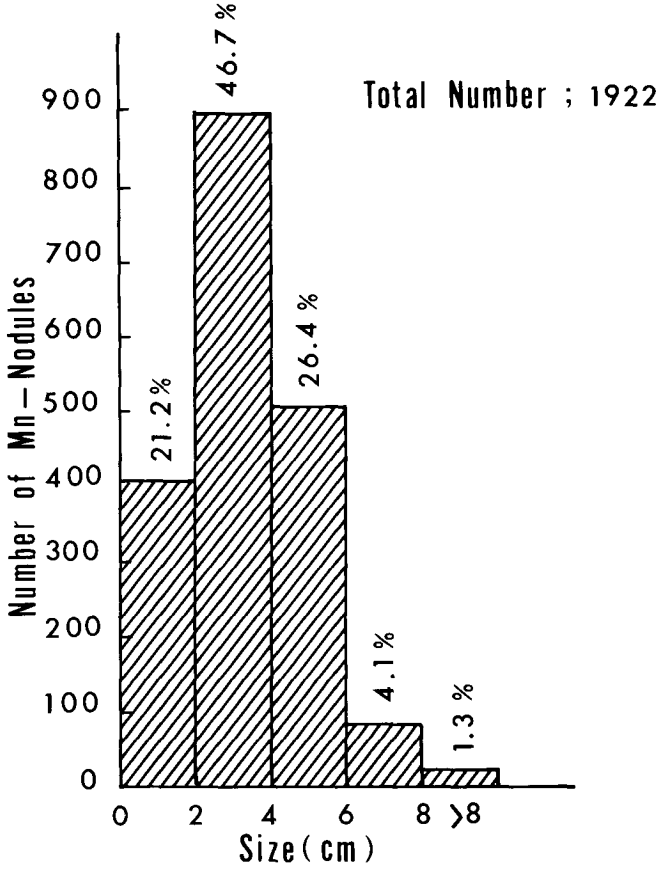
Total Number ; 1922
Number of Mn-Nodules
900
800
700
600
500
400
300
200
100
0
21.2%
46.7%
26.4%
4.1%
1.3%
0
2
4
6
8
>8
Size (cm)

Dr

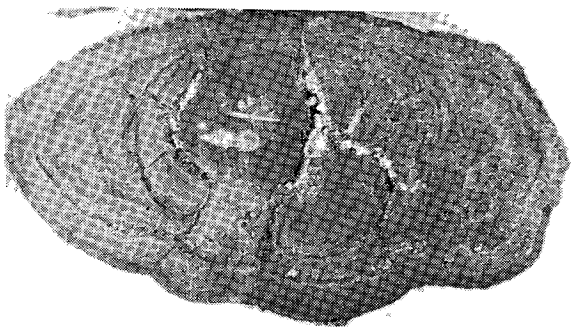

a

Is

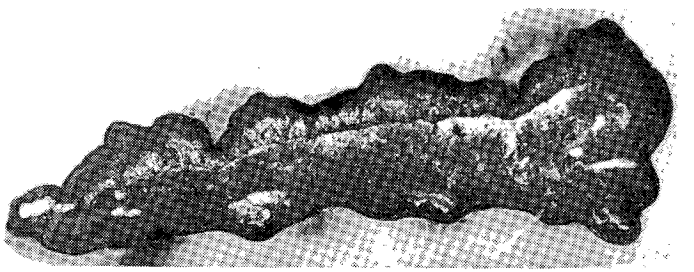

b

Dr+s

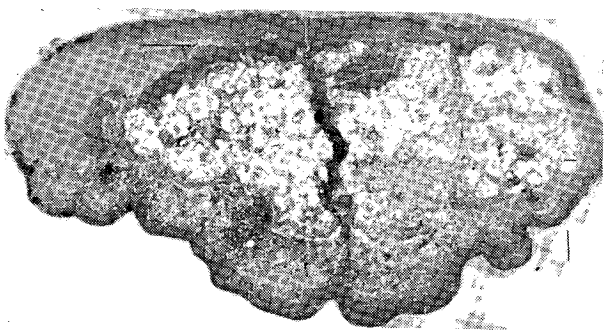

c

Dr

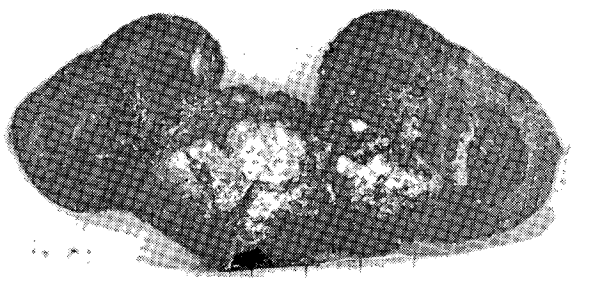

d

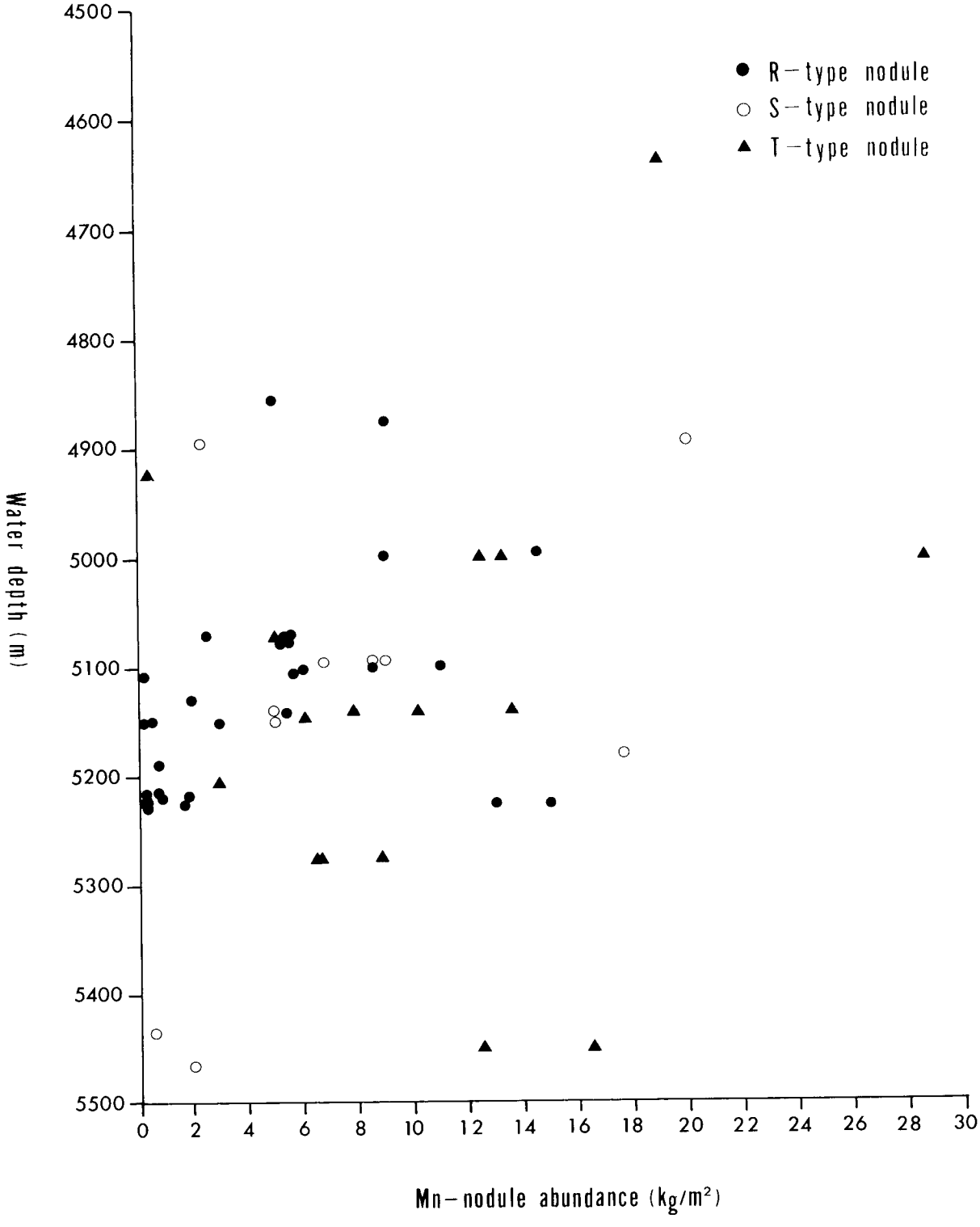
● R-type nodule
○ S-type nodule
▲ T-type nodule
Water depth (m)
4500
4600
4700
4800
4900
5000
5100
5200
5300
5400
5500
0
2
4
6
8
10
12
14
16
18
20
22
24
26
28
30
Mn-nodule abundance (kg/m²)

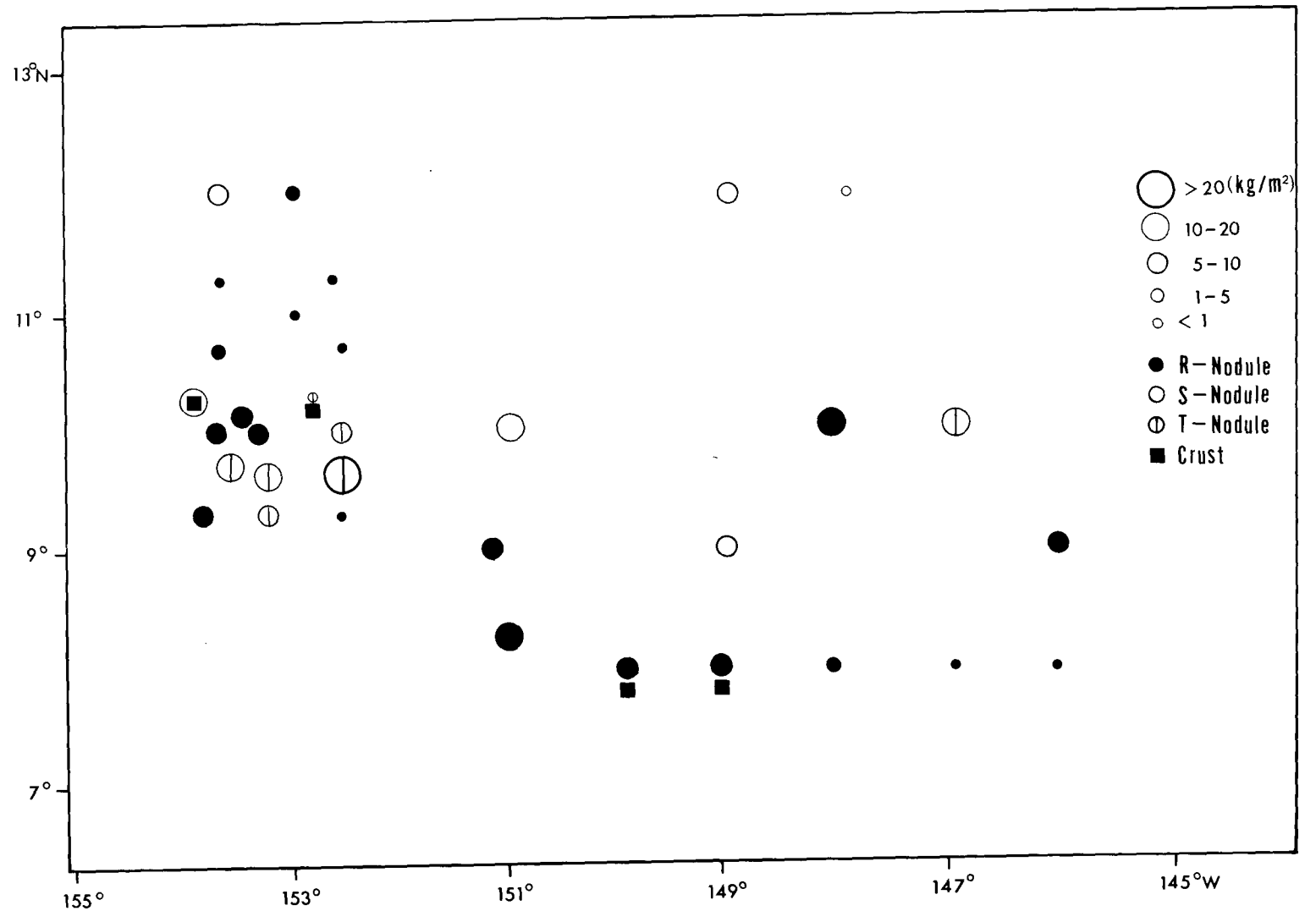
13°N
11°
9°
7°
155°
153°
151°
149°
147°
145°W
> 20(kg/m²)
10-20
5-10
1-5
< 1
R-Nodule
S-Nodule
T-Nodule
Crust

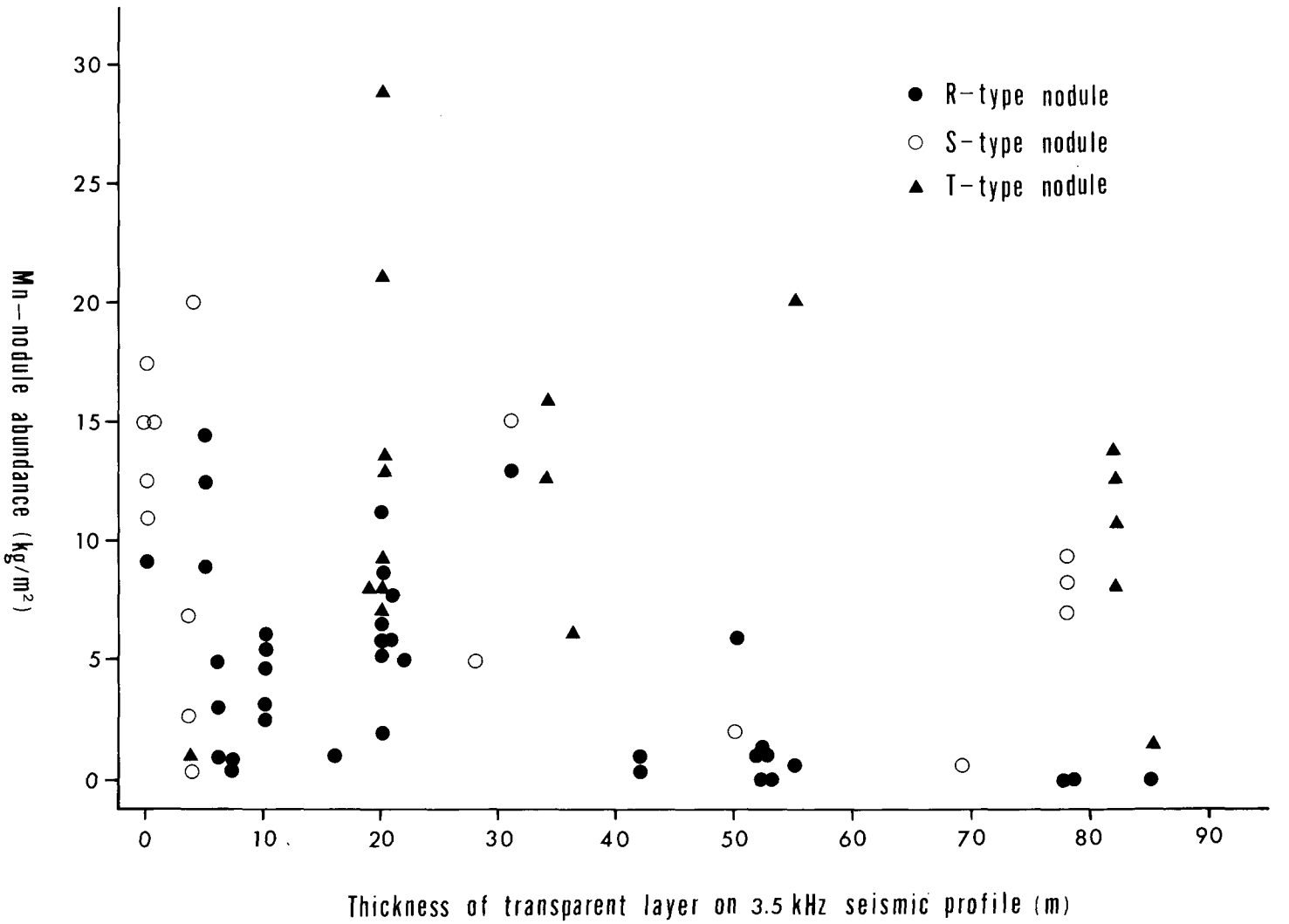
● R-type nodule
○ S-type nodule
▲ T-type nodule
Mn-nodule abundance (kg/m²)
Thickness of transparent layer on 3.5 kHz seismic profile (m)
0
5
10
15
20
25
30
0
10
20
30
40
50
60
70
80
90

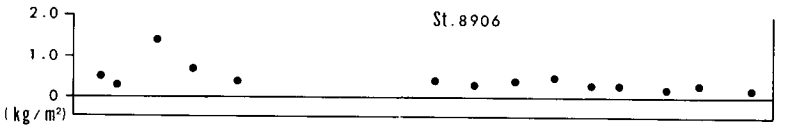
St.8906
2.0
1.0
0
(kg/m²)

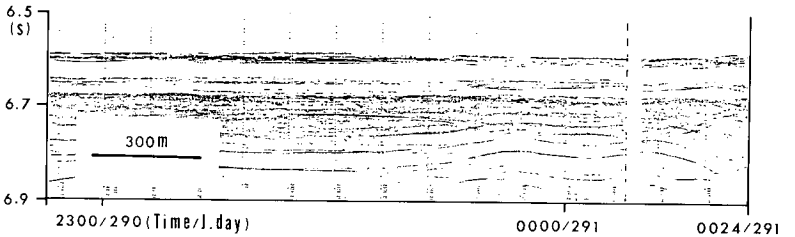
6.5
(s)
6.7
6.9
300m
2300/290(Time/J.day)
0000/291
0024/291

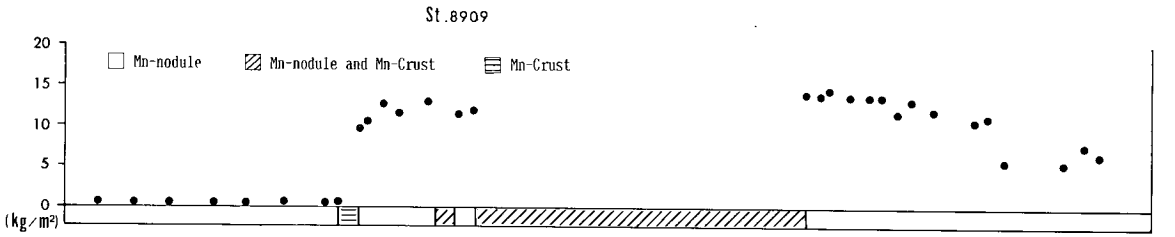
St.8909
Mn-nodule
Mn-nodule and Mn-Crust
Mn-Crust
20
15
10
5
0
(kg/m²)


6.3
(s)
6.5
6.7
300m
1206/292(Time/J.day)
1300/292
1400/292
1430/292

a

b

c

d

e

f

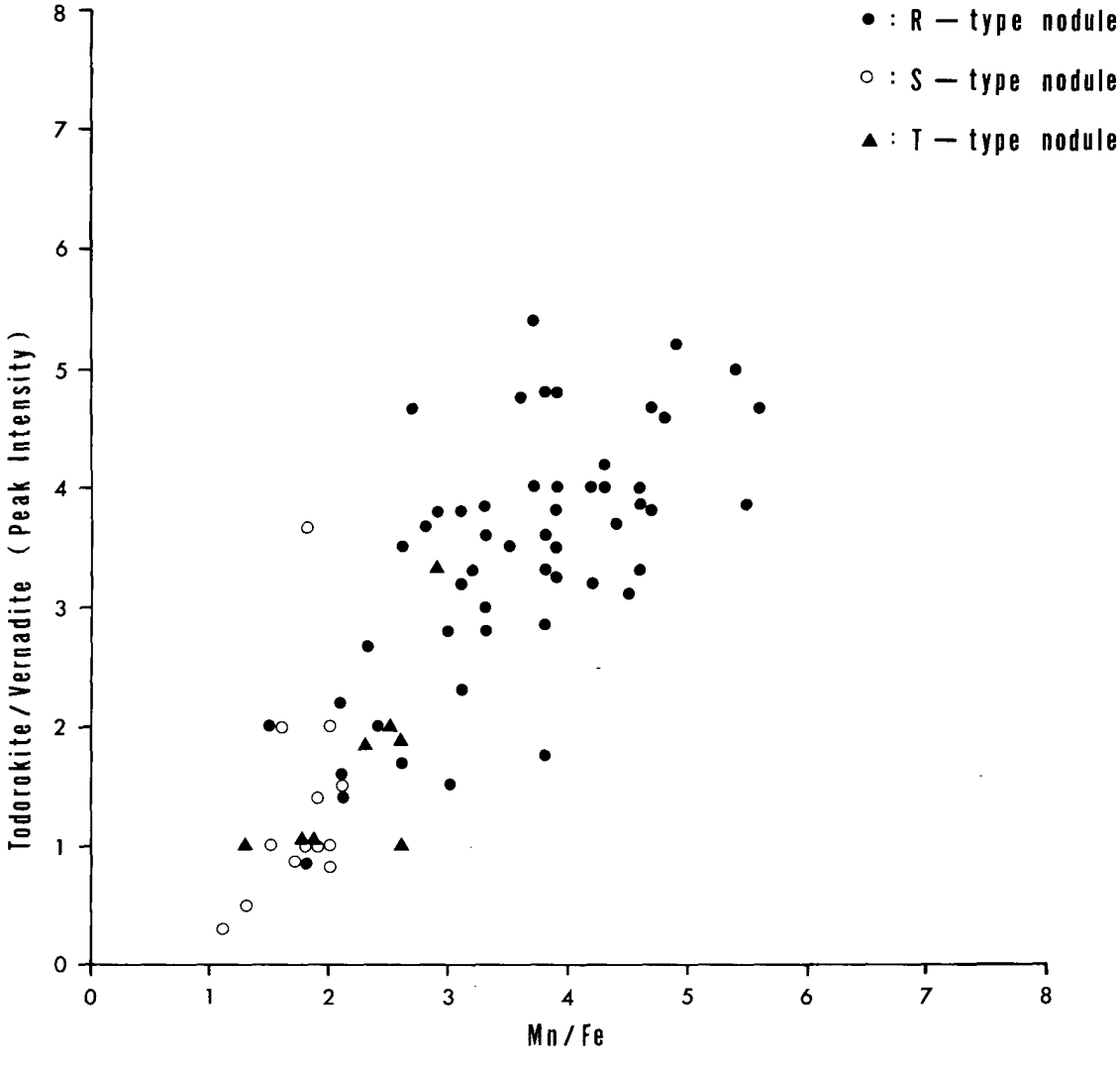
● : R — type nodule
○ : S — type nodule
▲ : T — type nodule
Todorokite / Vernadite (Peak Intensity)
Mn / Fe
0
1
2
3
4
5
6
7
8

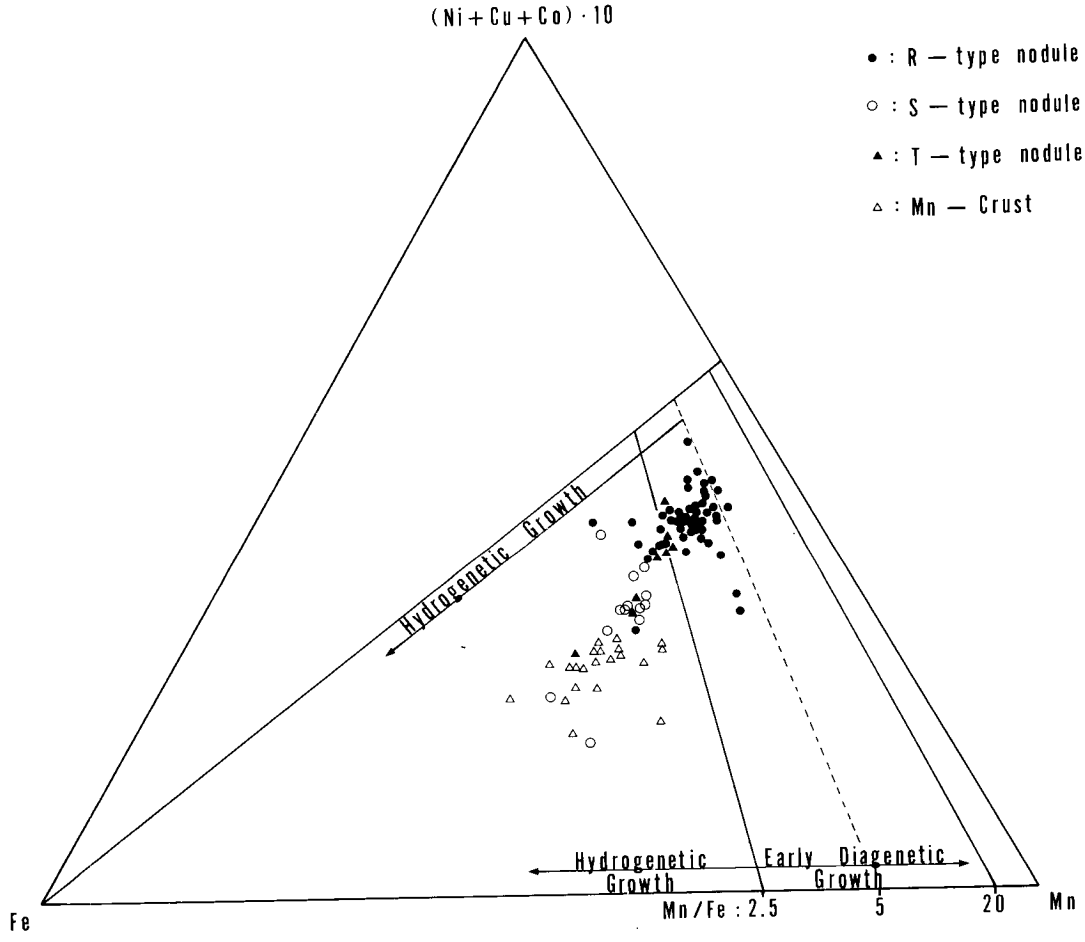
(Ni+Cu+Co)·10
● : R — type nodule
○ : S — type nodule
▲ : T — type nodule
△ : Mn — Crust
Hydrogenetic Growth
Hydrogenetic Growth
Early Diagenetic Growth
Fe
Mn/Fe : 2.5
5
20
Mn

PART II :

KODOS-89지역 망간단괴의 산상 및 분포 특성

(Occurrence and Distribution of Manganese Nodules in KODOS-89 Area, Northeast Pacific)

List of Tables

Table 1. Abundance and morphology of manganese nodules in KODOS-89 area.----109

Table 2. Mineral and metal content of manganese nodules in KODOS-89 area.----110

List of Figures

Fig. 1. Bathymetry and sample locations in KODOS-89 area.----------115

Fig. 2. Photographs showing occurrence of manganese nodules in KODOS-89 area.----------116

Fig. 3. Photographs showing internal texture of manganese nodules in KODOS-89 area.----------117

Fig. 4. Frequency distribution of external shape of manganese nodules in KODOS-89 area.----------118

Fig. 5. Frequency distribution of surface texture of manganese nodules in KODOS-89 area.----------119

Fig. 6. Relationship between latitude and size frequency of manganese nodules in KODOS-89 area.----------120

Fig. 7. Relationship between latitude and abundance of manganese nodules in KODOS-89 area.----------121

Fig. 8. Relationship between todorokite/vernadite and Mn/Fe ratios of manganese nodules in KODOS-89 area.----------122

Fig. 9. Relationship between todorokite/vernadite ratio and metal content of manganese nodules in KODOS-89 area.----------123

Fig. 10. Relationship between shape frequency(spheroidal+ellipsoidal+discoidal) and Mn/Fe ratio of manganese nodules in KODOS-89 area.---124

I. 서론

70 여종의 원소로 구성된 망간단괴는 전세계의 대양저 및 호수 등에 광범위하게 분포되어 있으며, 막대한 부존량과 니켈, 구리, 코발트, 망간 등과 같은 전략적 희유금속의 높은 함량으로 인해 광물자원으로 각광을 받고있다(Mero, 1965). 공식적 또는 비공식적으로 발표된 자료에 의하면, 현단계의 기술수준에서 상업적 가치를 갖는 망간단괴 광상은 심해 일부 지역에 국한하여 분포하고 있으며, 특히 북동태평양의 클라리온-클리퍼톤 균열대(Clarion-Clipperton Fracture Zones) 해역이 가까운 미래의 개발 후보지로 주목되고 있다(Mckelvey et al., 1983).

망간단괴는 콜로이드(colloid) 상태의 무기물, 미화석등의 유기물, 화산암편, 쇄설성광물 및 자생광물 등 다양한 물질로 구성되어 있으며, 크게 중심부의 핵과 이를 중심으로 동심원상으로 점차 성장한 철-망간산화광물층으로 대분된다(Sorem and Fewkes, 1979). 철-망간산화광물층은 매우 느린 속도로 성장하며(1-10 mm/my, Ku and Glasby, 1972; Ku et al., 1979), 철의 함량이 높은 비정질 또는 미정질 산화광물, 그리고 망간의 함량이 높은 결정질 또는 미정질 산화광물 등으로 구성되어 있다(Usui, 1984). 망간단괴의 특성은 산출 지역에 따라, 같은 지역 내에서도 단괴의 형태에 따라, 그리고 하나의 단괴에서도 각 부위에 따라 다양하다(Halbach et al., 1988). 이러한 다양성은 지역과 지질시대에 따른 해저환경을 반영하는 것으로, 형성기작에 의해 조절된다(Calvert and Price, 1977; Cronnan, 1980). 또한 해수 및 퇴적물의 공극수내에 용존된 원소들의 농도와 화학적 결합형태, 이들의 흡착성, 결정화학적 성질, 퇴적물의 산화도 등의 지화학적 조건은 망간단괴의 특성을 결정하는데 중요한 요인이 된다(Takematsu, 1989).

망간단괴의 산상 및 형성기작에 대한 지식이 축적될수록 보다 높은 분포밀도와 고품위의 망간단괴 광상을 예측·개발할 수 있을 것이다. 한국해양연구소는 1989년 10월 약 한달간 클라리온-클리퍼톤 균열대 북서단의 약 5만 km^2 지역에 대해 망간단괴 탐사를 수행한 바 있다(한국해양연구소, 1990). 본 연구는 상기 지역에서 산출되는 망간단괴의 물리·화학적 특성을 파악하고, 형성기작을 고찰하여, 산출 상태 및 분포 특성을 규명하고자 한다.

II. 지질개요

51,300 km^2 면적의 본 연구지역(9° 20'-12° 00' N, 151°-153° W)은 하와이 남동 방향의 북적도 태평양 클라리온-클리퍼톤 균열대 북서단에 위치하고 있으며, KODOS (Korea Deep Ocean Study)-89 지역으로 명명하였다(Fig. 1). 클라리온-클리퍼톤 지역은 프랑스, 일본, 소련, 중국, 미국 등 이미 여러나라가 단독개발광구를 확보하여 망간단괴 개발을 준비하고 있는 지역으로, 분포밀도는 최대 38 kg/m^2 (평균 10 kg/m^2)이며, 유가금속(니켈+구리+코발트) 함량은 2.5 %에 달한다(Mero, 1965).

기존의 연구보고(Sclater et al., 1971; Herron, 1972; Berger et al., 1976; Francheteau et al., 1979)에 의하면, 본 연구지역이 속한 클라리온-클리퍼톤 균열대 북서부 대양저 지각은 백악기말(약 8,000만년전)에 동태평양해령(11° S, 110° W)에서 생성된후, 해저확장에 의해 북 또는 북서 방향으로 이동되어 에오세 중기(약 5,000만년전)에는 표층해수의 생물 생산성이 높은 적도대(1.5° N, 126° W)에 위치하였으며, 해저면에는 유기질 퇴적물이 지배적인 퇴적층이 발달되었다. 적도 고생산대를 지난 이후에는 퇴적률이 급격히 감소하였고, 대양저 지각의 침강 작용이 수반되었다. 따라서 마이오세 초기(약 2,200만년전)에는 수심 약 4,800 m로 탄산염보상심도(Carbonate Compensation Depth, 약 4,600 m)보다 깊어져 탄산질 퇴적물은 용해되어 극히 낮은 퇴적속도(1-3 mm/천년)로 규질 퇴적물 및 육원성 점토의 퇴적층이 발달되었다(Theyer, 1977; Kennett, 1982). 이러한 대양저 지각의 지속적인 이동(현재 6-9 cm/년)으로 해저면에는 위도에 따른 특징적인 퇴적층서가 대상으로 분포한다. 연구지역 남쪽에는 마이오세 시기의, 북쪽에는 에오세

또는 올리고세의 규질 연니 및 규질 점토가 분포되어 있으며, 대부분이 적도 고생산대의 생물기원임을 나타낸다(Ryan and Heezen, 1976).

클라리온-클리퍼톤 지역에 유입되는 저층해류는 남극저층수(Antartic Bottom Water)에서 기원된 것으로, 남극저층수가 북상하여 Samoan Passage를 통과한후, 중앙태평양에서 동쪽으로 분지하여 Line Islands Ridge를 이루는 해저산 골들을 따라 가속되어 유입되는 것으로 보고되고 있다(Edmond et al., 1971; Mantyla, 1975; Volat et al.,1980). Deep Ocean Mining Environmental Study(DOMES) 및 Manganese Nodule Project(MANOP) 지역에서 관측한 저층해류 자료(Hayes, 1979; Gardner et al., 1984)에 의하면, 유속은 4-5 cm/sec로 미약하고 방향도 일정치 않지만, 주변지역의 음파탐사 기록 및 Deep Sea Drilling Project(DSDP) 코아 등의 자료(Keller and Barron, 1983)에 의하면, 과거 지질시대를 통하여 저층해류가 간헐적으로 활발히 작용하였음을 시사한다. 특히 마이오세-플라이오세 시기에는 저층해류의 영향력으로 퇴적물의 혼합과 퇴적층의 침식이 수반되어 여러 형태의 bedforms, sediment wave, moat, 그리고 퇴적결층을 형성하였다(Hayes et al., 1969; Johnson, 1972). 저층해류는 주변 해저산 또는 고화된 퇴적결층으로부터 단괴의 핵을 이루는 조립질 물질들을 공급하는데 중요한 역할을 한다(Glasby et al.,1982; von Stackelberg et al., 1987).

KODOS-89 지역은 수심 5,000 m 내외의 해저평원(abyssal plain) 지역으로 곳곳에 해저산(seamount) 및 해저능(abyssal hill) 등이 발달하여 다소 복잡한 지형적 특성을 갖는다(Fig. 1). 해저산들은 주로 남부에 분포되어 있으며, 너비 3,000 m, 높이 1,500 m에 달하는 큰 규모의 것도 존재한다. 이들 해저산들은 연구지역 서쪽에 위치한 Line Islands Ridge를 이루는 해저산 및 화산섬들과 마찬가지로 해저

화산활동에 의해 형성되었으며, 그 형성시기는 백악기말경으로 추론된다 (Sclater et al., 1971; Herron, 1972).

Air-gun 탄성파 자료에 의하면(한국해양연구소, 1990), 퇴적층의 두께는 대체적으로 400 m 정도이나 해저산 및 해저능의 발달과 단층 등의 영향으로 불규칙한 분포양상을 보여준다. 3.5 kHz 음파기록(한국해양연구소,1990)에 의하면, 퇴적층은 산란반사층에 의해 상부의 음파 투명층과 하부의 불투과층으로 구분되며, 투명층 내부에는 불연속적인 내부반사층(Internal Reflectors)이 발달하고 있어 저층해류에 의한 활발한 침식작용이 있었음을 암시한다. 해저면에는 여러 형태의 sediment wave들이 발달되어 있으며, 해저산 등의 주변에는 moat가 발달하여 있다. 이들의 방향성은 조사지역의 서쪽으로부터 저층해류의 유입이 있었음을 시사한다.

방산충과 규조류의 미고생물 연구자료에 의하면(한국해양연구소, 1990) 연구지역 퇴적층의 퇴적률은 약 0.2 mm/천년으로 매우 낮으며, 표층에서 10 cm 내외의 깊이를 경계로 상부는 제4기(Quaternary), 하부는 제3기(Tertiary) 퇴적물로 구분되는 특성을 보인다. 저서생물에 의해 심하게 교란된 이들 퇴적물은 주로 규질 연니의 용해로 이루어진 원양성 퇴적물로 구성되어 있으며, 일부 지역은 탄산질 연니 및 규질 연니가 국부적으로 분포하기도 하여, 퇴적물은 대부분이 적도 고생산대의 생물기원임을 추론케 한다.

III. 분석방법

조사지역의 총 21개 정점중 20개 정점에서 box core, free-fall grab 및 dredge 시료채취기를 이용하여 망간단괴를 회수하였으며, 4개 정점에서는 deep-sea camera system을 이용하여 각 4 km 구간의 정지 및 연속화면을 획득하였다. 회수된 망간단괴 및 사진자료에 근거하여 단위면적당 분포밀도(Abundance, kg/m^2)를 산출하였으며, 형태적 특성을 기재하였다.

망간단괴의 형태적 특성에 관한 분류는 구성 광물 및 화학적 조성과의 관계를 설명하기에 효과적이며, 산출상 및 분포밀도와 밀접한 관련을 가지므로(Halbach et al., 1975; Moritani et al., 1977; Usui, 1984), 크기, 외형, 표면조직의 특성에 따라 각각 분류하였다. 크기는 장경을 기준으로, 2 cm 미만, 2-4 cm, 4-6 cm, 6 cm 이상으로 구분하였고, 외형은 3축의 길이가 같은 구형(spheroidal), 1축은 길고 2축이 짧은 타구형(ellipsoidal), 2축은 길고 1축이 짧은 쟁반형(discoidal), 특정의 모양을 갖추지 않은 불규칙형(irregular), 그리고 몇 개의 작은 단괴들이 포도송이처럼 서로 붙어서 산출되는 다단괴형(polynodule) 등으로 분류하였다. 표면조직 특성은 조사선상에서 실시한 단괴의 육안 관찰과 촉감을 기준으로, 전표면이 세립의 오톨도톨한 돌기들로 피복되어 있어 거칠은 느낌을 주는 r-형, 돌기들이 발달되어 있지 않아 표면조직이 매끈매끈하며 비교적 단단한 느낌의 s-형, 그리고 전술한 두 가지 특성이 단괴의 상·하부에 따라 달리 나타나는 t-형으로 구분하였다.

망간단괴의 산출상 및 하부 퇴적물과의 관계가 잘 보존되어 있는 box core 시료채취기로 회수된 망간단괴를 대상으로, 각 정점을 대표하는 1-3개의 단괴는 광물

및 화학분석을 위한 전분석(bulk analysis)용 시료로 준비하였으며, 3-6 개는 반으로 절단하여 핵을 이루는 물질과 내부구조를 기술하였다. 준비된 시료들은 돌기들이 떨어지지 않도록 주의깊게 선상에서 해수로 세척하여 표면의 이물질을 제거한후 포장하여 실험실로 운송하였다. 이들 시료는 상온에서 1주일간 건조시켜 #200 비금속체를 통과하도록 미분말화한후, 균일하게 등분하여 X-선회절분석 및 원자흡광분석 등의 방법을 이용하여 동일 시료에 대해 광물 및 화학분석 결과를 얻고자 하였다.

광물분석은 X-선회절분석기기(X-ray diffractormeter, Model Philips PW 1710)를 이용하여 분석하였다. 이때 사용된 분석조건은, Target: Cu Kα, Filter: Ni, Scanning speed: 2°(2θ/min), Chart speed: 1 cm/min, Power: 30 kV, 25 mA 이다. X-선회절분석시 굴절피크의 세기는 구성광물의 함량과 밀접히 관련되므로 각 광물의 특징적 격자간 거리(d value)에서의 굴절피크 높이를 서로 비교하므로서 광물함량을 추론할 수 있다. 본 연구에서는 Hein et al.(1985)이 제시한 방법에 따라 각 광물의 상대적 함량비를 구하였다. 망간단괴내에는 비정질 광물이 상당량 함유되어 있고, 구성광물의 결정도도 매우 낮다(Burns and Burns, 1977). 따라서 본 연구에서 분석한 광물의 함량은 절대함량이 아니고, 단지 결정질 광물내에서의 상대함량만을 의미하는 것이다.

화학분석은 분석직전 분말시료를 120°C에서 24시간 동안 재건조시켰으며, 건조통 내에서 냉각시킨후 평량하여 테플론 비이커에 넣고 HF, HNO_3, HCl을 각각 5 ml씩 첨가하여 170°C 이하의 온도에서 반응시켰다. 반응이 끝난 시료는 0.1 N HNO_3로 30분간 용출시켜 희석한후, 불꽃원자흡광분석기(Atomic Absorption Spectrophoto- meter, Model IL 251)를 이용하여 금속함량(Mn, Fe, Cu, Ni, Co, Zn)을 분석했다 (Flanagan and Gottfried, 1980; Yamashige et al., 1989). 망간단괴의 분석시 미국립지질조사소(USGS) 표준 망간단괴 시료 P-1을 동시에 분석하여 자료의 정확도를 검증했다.

IV. 결 과

IV-1. 망간단괴의 물리적 특성

수회의 시료채취 및 해저면 사진촬영 자료에 의하면 본 연구지역의 망간단괴는 불규칙하게 해저면에 분포되어 있으며, 거의 대부분이 해저면의 퇴적물 표층(10 cm 이내)에서 산출된다. 일부지역에서는 퇴적물내 32 cm 심도까지 묻혀서 산출되기도 하지만, 그 이상의 깊이에서는 발견되지 않는다. 비록 퇴적물 표층의 한정된 공간에서 망간단괴가 산출되지만, 산출되는 지점을 해수와 퇴적물의 관점에서 보면 해저지형의 특성에 따라 상이한 양상을 나타낸다(Fig. 2). 해저평원 지역에서 산출되는 망간단괴는 대체적으로 단괴의 일부분 또는 전부가 퇴적물 표층에 살짝 묻혀서 산출되며, 단괴의 표면에 퇴적물이 상당량 부착되어 있다. 이에 비하여, 해저산 지역에서 산출되는 망간단괴는 많은 부분이 해수에 노출되어 있고 표면에 퇴적물이 거의 묻어 있지 않는 특성을 보인다. 그러나 해저산 지역 일지라도 기저부 및 봉우리 사이의 골에서 산출되는 단괴는 해저평원 지역의 경우와 같은 특성을 나타낸다. 해저능 지역은 상기 두 지역의 특성이 모두 나타난다.

망간단괴의 외형은 일반적으로 감자모양이라고 할 수 있으나, 세분하여 보면 구형, 타구형, 쟁반형, 불규칙형 및 다단괴형 등으로 분류할 수 있다(Table 1, Fig. 2). 단괴의 내부구조는 단순한 형태로 여러 종류의 핵을 중심으로 철-망간 산화물층이 동심원상으로 1 cm 내외의 두께로 발달되어 있다(Fig. 3). 단괴의 핵물질로는 기존의 단괴파편이 지배적이며, 상어 이빨 등의 유기물, palagonite, 이질의

퇴적암편 등이 소량 발견된다. 비록 한 지역에서 여러 유형의 외형을 갖는 망간단괴가 공존하지만, 산출되는 빈도값의 차이는 지역에 따라 상이하다(Fig. 4). 해저평원 지역에서는 단괴의 크기가 작은 경우 구형 또는 타구형, 큰 경우는 타구형 또는 쟁반형이 많이 산출되며, 해저산 지역에서는 다단괴형 및 불규칙형이 지배적이고, 해저능 지역은 두 지역의 중간 형태를 나타낸다.

표면조직 특성은 망간단괴의 전표면이 거칠은 r-형, 매끄러운 s-형 및 상·하부의 특성이 다른 t-형으로 분류된다(Table 1). 비록 t-형 단괴가 r-형 및 s-형 단괴와 동시에 산출되기도 하지만, 대체적으로 한 지역에서 산출되는 각 단괴의 표면조직 특성은 한 가지로 대표할 수 있으며, 해저지형의 특성에 따라 상이한 형태로 발달한다(Fig. 5). 해저평원 지역에서는 r-형이 지배적이며, 해저산 지역은 S-형 또는 t-형이 우세하지만 기저부 지역 및 봉우리 사이의 골 지역에서는 해저평원 지역과 같은 r-형의 특성을 갖는다. 해저능 지역은 r-형과 s-형이 지역에 따라 각각 발달한다. 따라서 망간단괴의 표면조직은 해저지형의 특성에 따라 상이하게 발달한다고 할 수 있으며, 이러한 현상은 성장환경을 반영하는 산출위치와 밀접한 관련을 갖는다. 즉, 단괴의 일부분 또는 전부가 퇴적물 표층에 살짝 묻혀서 산출되면 r-형, 퇴적물 표층위에 놓여져 많은 부분이 해수에 노출되어 있으면 s-형의 표면조직이 발달한다. t-형의 표면조직은 지역에 관계 없이 발달되나, 비대칭형의 비교적 큰(직경 6 cm 이상) 단괴에서 인지되며, 적은 양이 발견된다.

망간단괴의 크기는 해저지형과의 상관성은 인지되지 않으나, 한 지역의 평균적 크기는 위도의 영향을 받는다(Fig. 6). 비록 단괴의 크기가 2-4 cm 및 6 cm 이상 입도군의 산출빈도값은 위도에 따른 변화량이 인지되지 않으나, 2 cm 미만 및 4-6 cm 입도군의 경우는 북쪽에서 남쪽으로 갈수록 각각 감소하며 증가하는 경향을 나

타낸다. 따라서 망간단괴는 저위도 지역이 고위도 지역에 비해 크게 성장한다고 할 수 있으며, 이러한 현상은 특히 해저평원 지역에서 잘 관찰된다.

동일 조사정점에서 채취된 box core 및 다수의 free-fall grab 시료와 해저면 사진 분석자료에 의하면 망간단괴의 분포밀도는 좁은 지역내에서도 변화가 크다 (Table 1). 특히, 해저산 지역에서의 변화가 크며, 최대 19.9 kg/m^{2}의 분포밀도 차이를 보이고 있다. 좁은 지역내에서도 분포밀도의 변화량이 쉽게 인지되지만, 해저지형에 따라 차이가 있다. 해저평원 지역은 평균 3.9 kg/m^{2}로 비교적 낮고, 해저산 지역은 평균 13.3 kg/m^{2}로 높으며, 해저능 지역은 두 지역의 중간값인 평균 7.2 kg/m^{2}이다. 분포밀도의 변화는 해저지형뿐만 아니라 위도에 따라서도 변화한다(Fig. 7). 이러한 변화는 특히 해저평원 지역에서 뚜렷이 인지되는 것으로 저위도 지역일수록 분포밀도가 증가한다.

IV-2. 망간단괴의 광물 및 금속함량

망간단괴의 외형, 표면조직 및 크기 등을 고려하여 광물의 상대함량 및 금속의 절대함량을 구하였다(Table 2). 연구지역에 분포하는 망간단괴의 광물조성은 버나다이트(vernadite, 또는 δ-MnO_2), 토도로카이트(todorokite), 석영, 장석 및 필립사이트(phillipsite) 등이 인지된다. 이러한 결과는 태평양 지역 특히 클라리온-클리퍼톤 균열대 지역에서 채취되어 보고된 망간단괴의 구성광물 성분과 일치한다(Piper and Blueford, 1982). 화학분석 결과 철이 약 5-18 %(평균 약 9 %) 함유되어 있으나, 철수산화광물이 인지되지 않음은 이들 광물이 비정질로 산출됨

을 의미한다. 석영, 장석 및 필립사이트 등은 비교적 소량 산출되는데 이는 망간단괴 성장시 쇄설성 파편 또는 핵물질 기원에서 유래된 것으로 생각된다.

망간단괴의 주구성광물인 토도로카이트/버나다이트 비와 주구성원소인 Mn/Fe 비는 정의 상관관계를 보이며, 표면조직과 해저지형에 따라 상이한 특성을 갖는다(Fig. 8). 이들의 값은 해저평원 지역에서는 각각 0.2-0.7(평균 0.4), 1.5-5.5(평균 3.4)로 높고, 해저산 지역은 0.1-0.5(평균 0.2), 1.1-4.6(평균 2.1)로 낮다. 해저능 지역은 0.1-0.6(평균 0.2), 1.3-4.8(평균 3.0)로 두 지역의 중간값을 갖는다. 표면조직에 따른 이들 비의 변화량은 보다 뚜렷하여 r-형은 0.2-0.7(평균 0.5), 1.5-5.5(평균 3.5)이고, s-형은 0.1-0.3(평균 0.1), 1.1-2.1(평균 1.7)이며, t-형은 0.1-0.5(평균 0.2), 1.3-2.9(평균 2.3)이다. 또한 표면조직 특성은 다른 금속원소의 함량과도 밀접한 관련을 갖는다(Fig. 9). r-형 단괴는 망간, 구리, 니켈, 아연 등의 함량이 높은 반면에, s-형 단괴는 철 및 코발트의 함량이 높다. t-형 단괴는 r-형과 s-형의 중간값을 보여주나, 같이 산출되는 형과 유사한 값을 갖는다.

망간단괴를 구성하는 광물 및 금속함량들 사이에 상관관계가 인지된다(Fig. 9). 토도로카이트/버나다이트 비와 망간, 구리, 니켈 및 아연과는 정의 상관관계를, 철 및 코발트와는 역의 상관관계를 갖는다. 토도로카이트/버나다이트 비가 증가함에 따라 망간 및 코발트 함량은 뚜렷하지는 않지만 완만하게 변화하며(Fig. 9a, d), 철, 구리 및 아연 함량은 비교적 일정한 비율로 변화하고(Fig. 9b, c, f), 니켈의 경우는 다소 급하게 증가한후 거의 일정한 값을 유지한다(Fig. 9d).

V. 토 의

V-1. 망간단괴의 형성기작

일반적으로 망간단괴는 금속원소의 기원을 토대로 수성기원, 속성기원 및 열수기원으로 구분하여 설명되고 있다(Cronan, 1980). 수성기원은 금속의 공급이 주로 해수로부터 이루어져 다른 기원의 단괴에 비해 철, 코발트 등의 함량이 높고, 속성기원은 퇴적물내의 공극수로부터 금속을 공급받아 망간, 구리, 니켈, 아연 등의 함량이 높다. 열수기원은 해저열수작용이 활발한 지역에서 형성되므로 망간의 함량은 극히 높은 반면에, 철 및 다른 미량 금속의 함량은 낮으며, 성장속도가 빠르다(Usui et al., 1986). 본 연구지역에서 산출되는 망간단괴의 금속함량은 열수기원의 것과는 전혀 다른 양상을 보이며, 열수기원을 추론할만한 유화물의 존재 및 빠른 성장구조도 발견되지 않아 수성기원 및 속성기원의 두 가지 측면을 고려하여 설명하고자 한다.

망간단괴의 산출 위치는 성장환경을 반영하며(Usui, 1979), 산출 위치에 따라 표면조직의 특성이 결정된다(Raab and Meylan, 1977; Sorem et al., 1979). 즉, s-형의 표면조직은 단괴가 해수에 노출되어 산출되므로 해수로부터 금속원소가 콜로이드 상태로 침전되는 수성작용(hydrogenetic accumulation)에 의해 성장한 단괴에서 인지되며, r-형의 표면조직 특성은 퇴적물에 묻혀서 산출되므로 퇴적물의 공극수에 용존된 금속원소가 침전되는 속성작용(diagenetic accumulation)에 의해 성장한 단괴에서 잘 발달한다(Halbach et al., 1981). 해저산 지역은 표층의 준액

상퇴적층(peneliquid layer, Halbach and Ozkara, 1979)의 발달이 미약하여 저층 해류가 단괴의 성장을 촉진시키는 수성작용에 의해 성장한 단괴가 지배적이며, 해저평원 지역은 5-25 cm 두께의 준액상퇴적층이 발달되어 있어 속성작용에 의한 단괴의 성장이 활발하다(Halbach et al., 1988).

망간은 철에 비해 이동성이 크고, 산화준위가 높으며, 농도가 높기 때문에 망간단괴로 침전되는 양은 망간이 월등하며, 그 비율 또한 높다(Klinkhammer et al., 1982). 망간과 철의 선택적 침전은 해수에서보다 퇴적물내에서 활발하여 망간단괴의 Mn/Fe 비는 금속의 기원을 시사하는 좋은 지시자로, 2.5를 기준으로 높으면 속성기원, 낮으면 수성기원으로 분류한다(Halbach and Ozkara, 1979). 퇴적물내의 공극수에는 유기물의 분해에 기인하여 구리, 니켈, 아연 등의 함량이 해수에 비해 높고, 또한 유기물 분해로 산화도가 낮다(Halbach et al., 1981; Dymond et al., 1984). 따라서 속성작용에 의해 형성된 망간단괴는 대체적으로 구리, 니켈, 아연, 및 망간의 함량은 높고, 철 및 코발트의 함량이 낮으며, 수성작용에 의해 형성된 망간단괴는 속성작용의 경우와 상반된 특성을 갖는다 (Haynes et al., 1982). 퇴적물에서 공급되는 금속함량이 해수에서 공급되는 양에 비해 훨씬 많기 때문에 속성작용의 성장속도는 수성작용보다 3-30배 정도 빠르다 (Raab, 1972; Heye and Marchig, 1977; Bender, 1983).

또한 속성기원의 망간단괴는 결정질 망간산화광물인 토도로카이트 함량이 높고, 수성기원의 망간단괴는 비정질 내지 결정도가 낮은 버나다이트와 철수산화광물의 혼합상이 지배적이다(Usui, 1984). 망간단괴를 구성하는 망간산화광물중 결정도는 토도로카이트가 높고, 버나다이트는 낮으며(Glover, 1977), 산화도는 버나다이트가 높고, 토도로카이트는 낮다(Burns and Burns, 1977). 토도로카이트의 결정구조

는 모서리를 공유하는 〔MnO_6〕 8면체를 연결하는 사슬구조 형태로 공극이 발달되어 있으며, 다량의 Mn^{+2}를 함유하고 있다. Ni^{+2}, Cu^{+2}, Zn^{+2} 등은 Mn^{+2}와 이온반경이 비슷하여 서로 치환 또는 교환이 쉽게 일어난다(Burns and Burns, 1977). 버나다이트는 산화도가 높아 코발트의 함량을 높게 유도하며, 비정질 또는 낮은 결정도의 광물상으로 산출된다(Burns, 1976; Murray and Dillard, 1979).

본 연구지역은 크게 해저평원, 해저산 및 해저능 지역으로 구분되며, 각각의 지역에서 산출되는 망간단괴의 특성은 상이하다. 해저평원 지역은 퇴적물 표층에 묻혀서 망간단괴가 산출되는 경우가 많으며 r-형의 표면조직 특성을 갖는데 비해, 해저산 지역은 해수에 노출되어 단괴가 산출되며 s-형의 표면조직 특성으로 대표된다(Fig. 2, 5). 또한 r-형의 망간단괴는 망간, 구리, 니켈, 아연의 함량이 높고, 토도로카이트/버나다이트 및 Mn/Fe 비가 크며, 철 및 코발트의 함량이 낮다. 이에 비하여 s-형은 r-형과 역의 관계를 나타낸다(Fig. 8, 9). 따라서 해저평원 지역에서 산출되는 r-형의 망간단괴는 속성작용에 의해, 해저산 지역에서 산출되는 s-형의 망간단괴는 수성작용에 의해 각각 형성된 것을 지시한다. 비대칭형의 비교적 큰(직경 6 cm 이상) 단괴에서 인지되는 t-형은 상부에 비해 하부가 보다 더 발달된 양상으로 반구상의 모양을 나타내기도 한다(Fig. 3). 이는 단괴의 형성기작이 상·하부에 따라 다르며, 성장률의 차이가 있음을 시사한다. Moore et al.(1981)은 t-형 단괴에서 거칠은 하부가 매끈한 상부보다 성장속도가 3배나 높다고 보고하였다. 따라서 t-형 단괴는 상·하부에 따라 형성기작이 상이하게 작용하여 형성된 것으로 상부는 수성작용, 하부는 속성작용에 의해 발달된 것으로 생각된다.

해저평원 지역은 속성작용의 결과인 r-형의 표면조직을 갖는 단괴가 대부분이

며, t-형 단괴는 드물게 산출되고, 수성작용에 의한 s-형 단괴는 산출되지 않는다 (Table 1). 이에 비하여 해저산 지역은 s-형 단괴가 주종을 이루지만, t-형의 단괴도 상당량 있으며, 지역에 따라서는 r-형의 단괴도 산출된다. 이는 망간단괴의 형성기작이 같은 지역내에서도 복합적으로 작용됨을 시사하는 것이며, 특히 해저산 지역에서 잘 인지된다. 또한 망간단괴는 이동되면서 역전하기도 하며, 해저환경의 변화에 따라 다른 형성기작에 의해 성장하기도 한다(Sorem and Fewkes, 1979). 그러나 한 지역에서 같이 산출되는 단괴들은 표면조직의 특성은 다를지라도 전분석에 의한 광물 및 금속함량은 별 차이가 없다(Table 2). 표면조직 특성은 현재 또는 최근의 환경만을 지시하지 과거의 역사를 반영하지는 못한다. 따라서 망간단괴의 형성기작이 시기에 따라 다르게 또는 복합적으로 작용하여도 전체적으로는 과거 지질시대를 통해 한 지역내에서의 환경변화가 크지 않았으며, 한 가지의 형성기작에 의해 대표된다고 생각된다. 즉, 해저평원 지역은 속성작용이 지배적이며, 해저산 지역은 전체적으로 수성작용이 우세하지만, 속성작용의 효과도 무시할 수 없다. 해저능 지역은 상기 두 지역의 중간적 형태로 지역에 따라 다르다.

V-2. 망간단괴의 산출 특성

본 연구지역의 망간단괴는 불규칙하게 해저면에 분포되어 있으며, 거의 대부분이 해저면의 퇴적물 표층(10 cm 이내)에서 산출된다. 망간단괴의 평균 성장률인 1-10 mm/백만년(Ku and Glasby, 1972; Ku et al., 1979)에 비해 연구지역 퇴적물의 평균 퇴적속도는 0.2 mm/천년으로 훨씬 빠르다. 망간단괴의 성장률에 비해 퇴

적물의 퇴적속도가 빠름에도 불구하고 망간단괴가 이와 같이 퇴적물에 깊이 묻히지 않는 것은 저층해류의 작용 또는 저서성 생물들의 활동으로 설명되고 있다 (Moore and Heath, 1967; Glasby, 1977; Piper and Fowler, 1980). 즉, 단괴와 퇴적물의 입도 차이에 따른 선택적 이동으로 서로 분리되어 입도가 작은 퇴적물은 하부로, 입도가 큰 단괴는 상부로 이동하여 퇴적물 표층에 국한하여 밀집·분포되는 것으로 생각된다

해저평원 지역에서 산출되는 망간단괴의 외형은 구형, 타구형 또는 쟁반형이 많이 산출된다(Fig. 4). 그리고 속성작용의 지시자라 할 수 있는 Mn/Fe 비와 구형, 타구형 및 쟁반형을 합한 산출빈도값은 정의 상관관계를 보여준다(Fig. 10). 속성작용에 의해 퇴적물에 묻혀서 성장한 단괴는 작을 경우(<3 cm) 이동이 쉽고 역전현상도 빈번하여 전체적으로 고르게 철-망간산화물이 흡착되므로서 구형 및 타구형 또는 핵의 모양을 반영하게 되며, 단괴가 커지면(>3 cm) 이동의 효과가 떨어지고 역전되기도 어려워 물질의 공급이 잘 이루어지는 측면부가 상·하부보다 발달하게 된다(Halbach et al., 1988). 따라서 망간단괴의 외형은 구형에서 타구형으로, 타구형에서 쟁반형으로 변모하게 될 것이다. 속성작용의 성장속도는 수성작용에 비해 상당히 빠르므로(3-30배, Raab, 1972; Heye and Marchig, 1977; Bender, 1983), 이러한 효과는 해저평원 지역에서 잘 보여줄 것이다. 연구지역 해저평원 지역에서 구형, 타구형 또는 쟁반형이 많이 산출되고 이들의 산출빈도가 Mn/Fe 비와 정의 상관관계를 갖는 것은 속성작용이 활발하게 이루어진 결과로 생각된다.

해저평원 지역과는 달리 해저산 지역에서는 다단괴형 및 불규칙형이 지배적이다 (Fig. 4). 해저산 지역은 저층해류의 작용으로 단괴의 핵을 이루는 조립질 물질의 공급이 많아 단괴의 산출빈도가 높고(Bonatti and Nayady, 1965), 저층해류의 작

용이 강하여 단괴가 이동되기 쉽다(Glasby et al., 1982). 따라서 높은 산출빈도와 이동의 효과로 단괴가 서로 합칠 수 있는 기회가 높아 다단괴형이 많이 산출된다. 또한 단괴의 성장속도가 늦어 핵의 모양에 따라 불규칙형의 외형을 그대로 유지하게 된다. 즉, 해저산 지역의 다단괴형 및 불규칙형이 많이 산출되는 것은 저층해류 및 느린 성장속도의 영향으로 생각된다.

지역적 환경에 따른 형성기작의 영향에 따라 단괴의 외형이 조절되나, 한 지역 내에서도 여러가지 유형의 단괴가 발견되고, 핵의 모양에 따라 다양한 형태를 갖는 점으로 미루어 외형이 핵의 모양에 의해서도 지배받음을 알 수 있다. 특히, 이러한 현상은 철-망간산화물층의 두께가 얇거나, 또는 핵의 크기가 큰 단괴에서 두드러지게 나타난다. 따라서 망간단괴의 외형은 일반적으로 단괴의 크기가 작을 경우에는(<3 cm) 핵의 모양에 직접 영향을 받는데 비하여, 큰 경우에는(>3 cm) 형성기작에 따라 형태가 유지되는 것으로 생각된다.

V-3. 망간단괴의 분포 특성

동일 조사정점에서 채취된 box core 및 다수의 free-fall grab 시료와 해저면 사진 분석자료에 의하면 망간단괴의 분포밀도는 좁은 지역내에서도 변화가 크다 (Table 1). 특히, 해저산 지역에서의 변화가 크며, 최대 19.9 kg/m^{2}의 분포밀도 차이가 있다. 이러한 현상은 망간단괴가 patch 또는 pavement 상태로 산출됨을 의미하며, 국부적인 지형의 영향에 따른 저층해류의 다양성에 기인된 것으로 생각된다. 따라서 저층해류의 작용이 강한 해저산 지역이 보다 큰 변화를 보인다.

비록 좁은 지역내에서도 분포밀도의 변화가 인지되지만 해저지형의 특성에 따라 상이한 분포밀도를 갖는다. 해저평원 지역의 분포밀도는 평균 3.9 kg/m^{2}로 비교적 낮으며, 해저산 지역은 평균 13.3 kg/m^{2}로 높고, 해저능 지역은 평균 7.2 kg/m^{2}로 중간 값을 나타내나, 지역에 따라 변화가 심하다(Table 1). Horn et al. (1973)은 분포밀도는 철-망간물질이 흡착될 수 있는 유용한 핵의 분포에 의해 조절된다고 하였으며, Bonatti and Nayady(1965)는 해저산 및 volcanic knolls 주변 지역에서는 암석파편의 공급이 많고, palagonite 등이 단괴의 핵으로 흔히 발견되는 점을 근거로 높은 분포밀도를 설명하였다. 또한 저층해류는 주변 해저산 또는 고화된 퇴적결층으로부터 단괴의 핵을 이루는 조립질 물질들을 공급하는데 중요한 역할을 한다(Glasby et al., 1982; von Stackelberg et al., 1987). 그러나 연구지역에서 산출되는 망간단괴는 지역에 관계없이 기존의 단괴파편을 핵으로 재성장한 것이 지배적이며, 해저산 지역 역시 palagonite등의 암석파편을 핵으로 성장한 단괴는 소량만이 인지된다. 따라서 전술한 암석파편 또는 조립질 물질 등을 핵으로 성장하는 씨앗효과(seeding effect)에 의해서만은 해저산 지역의 높은 분포밀

도를 설명하기에는 무리가 있다.

망간단괴는 탈수 및 수축작용에 의해 쉽게 쪼개져 새로운 핵물질로 제공되며, 해저평원 지역에서 산출되는 속성기원의 단괴보다 해저산 지역에서 발견되는 수성기원의 단괴가 쉽게 쪼개진다(Heye, 1975). 또한 기존의 단괴 파편은 철-망간 산화물의 침전을 다른 어떤 물질보다 효과적으로 유도할 수 있다(Halbach et al., 1988). 따라서 해저산 지역이 해저평원 지역보다 분포밀도가 높은 것은 일차적인 단괴의 형성(다른 물질을 핵으로 성장)도 많았지만, 이보다는 이차적인 단괴의 형성(기존의 단괴파편을 핵으로 재성장)을 유도하는 씨앗효과에 의한 결과로 생각된다. 연구지역에서 산출되는 단괴의 크기가 다양한 것은 기존의 단괴가 쪼개질 때는 다양한 크기가 예상되어 이를 핵으로 성장한 단괴 역시 다양한 크기로 산출되는 결과에 기인된 것으로 판단된다.

분포밀도의 변화는 해저지형뿐만 아니라 위도에 따라서도 변화한다. 이러한 변화는 특히 해저평원 지역에서 뚜렷이 인지되는 것으로 북쪽에서 남쪽으로 갈수록 증가한다(Fig. 7). 또한 단괴의 평균적 크기도 위도의 영향을 받아, 고위도에서 저위도 지역으로 갈수록 커진다(Fig. 6). 본 연구지역 지각은 백악기말에 동태평양 해령에서 생성된후, 해저확장에 의해 북 또는 북서 방향으로 이동되어 현재의 위치에 도달하였다(Sclater et al., 1971; Herron, 1972; Berger et al., 1976). 마이오세 시기 이후에 수심이 탄산염보상심도보다 깊어져 규질 퇴적물 및 육원성 점토의 퇴적층이 극히 낮은 퇴적속도(1-3 ㎜/천년)로 발달되었으며(Theyer, 1977; Kennett, 1982), 플라이오세-마이오세 시기는 강한 저층해류의 작용으로 단괴의 핵을 이루는 물질의 공급이 활발하였다(Glasby et al., 1982; Keller and Barron, 1983; von Stackelberg et al., 1987). 따라서 마이오세 시기 이후가 망간단괴

형성의 호시기로 판단되며, 본 연구지역은 적도 고생산대의 북쪽 주변에 위치해 있었다(Francheteau et al., 1979). 수층의 생물생산성은 적도지방에 근접할수록 증가하므로(Romankevich, 1984) 북부 지역보다 남부 지역 퇴적물내에는 유기물 함량이 높다. 따라서 연구지역의 북부에 비해 남부지역이 분포밀도가 높은 점은 일차적으로 남부 지역은 해저산이 많이 분포되어 있어 저층해류의 작용이 강하여 주변 해저산으로부터 핵물질의 공급이 활발한 씨앗효과에 기인된 것이지만, 이차적으로는 남부지역이 적도 고생산대 지역에 근접해 있어 유기물의 공급이 많아 활발한 속성작용을 유도한 결과로 생각된다. 해저평원 지역은 단괴의 형성이 주로 속성작용에 의해 이루어지므로 해저평원 지역에서 위도에 따른 단괴의 크기 및 분포밀도의 변화가 특히 잘 인지된다.

Ⅵ. 결 론

망간단괴의 형성기작은 해저지형에 따라 상이하며, 단괴의 물리·화학적 특성을 조절한다. 해저평원 지역은 주로 속성작용에 의해 망간단괴가 성장하며, 해저산 지역은 저층해류의 작용에 의한 수성작용으로 단괴의 성장이 대표된다. 속성기원의 망간단괴는 전이금속의 함량이 높고, 산화도가 낮은 퇴적물내에서 결정질 망간산화광물이 비교적 빠른 속도로 침전되므로 r-형 표면조직을 갖으며, Mn/Fe 및 토도로카이트/버나다이트 비가 크고, 망간, 구리, 니켈, 아연의 함량이 높으며, 철 및 코발트의 함량이 낮다. 수성기원의 망간단괴는 해수로부터 미정질 산화광물이 매우 느린 속도로 흡착되므로 s-형 표면조직을 갖으며, 속성기원과 상반된 구성광물 및 금속 함량을 갖는다.

망간단괴의 외형은 일반적으로 단괴의 크기가 작을 경우에는(<3 cm) 핵의 모양에 직접 영향을 받으며, 큰 경우에는(>3 cm) 형성기작에 따라 형태가 유지된다. 해저평원 지역에 분포하는 망간단괴는 속성작용에 의해 성장하므로 단괴의 크기가 커짐에 따라 점차적으로 구형, 타구형, 쟁반형의 외형으로 변모한다. 이에 비하여 해저산 지역의 망간단괴는 저층해류의 작용과 느린 성장속도의 영향으로 다단괴형 및 불규칙형의 외형으로 특징된다.

망간단괴의 분포밀도는 일차적으로는 기존의 단괴가 쪼개져 핵물질을 공급하는 씨앗효과에 의해, 이차적으로는 속성작용을 유도하는 유기물의 공급에 의해 조절된다. 해저산 지역은 수성작용에 의한 단괴의 성장으로 기존의 단괴가 잘 쪼개지므로서 씨앗효과가 증대하여 분포밀도가 높다. 해저평원 지역중 남부 지역은 해저산이 많이 분포되어 있어 핵물질의 공급이 용이하며, 이와 더불어 적도 고생산대로부터 원할한 유기물 공급으로 속성작용이 촉진되어 북부 지역에 비해 높은 분포밀도를 갖는다.

VII. 참고문헌

한국해양연구소, 1990. 심해저 광물자원 개발전략연구 (II). BSPG 00094-296-5, 1093pp.

Bender, M.L., 1983. The manganese nodule program: EOS., 64(5): 42-43.

Berger, W.H., C.G. Adeleck, and L.A. Mayer, 1976. Distribution of carbonate in surface sediments of the Pacific Ocean. J. Geophysi. Res. 81(15): 2617-2627.

Bonatti, E. and J.R. Nayudu, 1965. The origin of manganese nodules on the ocean floor. Am. J. Science, 263: 17-39.

Burns, R.G., 1976. The uptake of cobalt into ferromangnaese nodules, soils, and synthetic manganese(IV) oxides. Geochim. Cosmochim. Acta, 40: 95-102.

Burns, R.G. and V.M. Burns, 1977. Mineralogy. In: Marine Manganese Deposites, edited by G.P. Glasby, Elsevier, Amsterdam, 185-248.

Calvert, S.E. and N.B. Price, 1977. Geochemical variation in ferromanganese nodules and associated sediments from the Pacific ocean. Mar. Chem., 5: 3-74.

Cronan, D.S., 1980. Underwater Minerals. Academic Press, Inc., Ltd., London, England, 362pp.

Dymond, J., M. Lyle, B. Finney, D.Z. Piper, K. Murphy, R. Conard and N. Pisias, 1984. Ferromanganese nodules from MANOP site H, S and R.- Control of mineralogical and chemical composition by multiple accretionary processes. Geochim. Cosmochim. Acta, 48: 931-949.

Edmond, J.M., Y.-C. Chung, and J.G. Sclater, 1971. Pacific bottom water: penetration east around Hawaii. J. Geophysi. Res., 76(33): 8089-8097.

Flanagan, F.J. and D. Gottfried, 1980. USGS rock standards, III: Manganese-nodule reference samples USGS-NOD-A-1 and USGS-NOD-P-1. U.S. Government Printing Office, Washington.

Francheteau, J., C.G.A. Harrison, J.G. Sclater, and M.L. Richards, 1979. Magnetization of Pacific seamounts: A preliminary polar curve for the northeastern Pacific: J. Geophys. Res., 75: 2035-2062.

Gardner, W.D., L.G. Sullivan and E.M. Thorndike, 1984. Longterm photographic, current, and nephelometer observations of manganese nodule environments in the Pacific: Earth and Plant. Science Lett., 70: 95-109.

Glasby, G.P., 1977. Why manganese nodules remain at the sediment-water interface. New Zealand Jour. Science. 20:187-190.

Glasby, G.P., P. Stoffers, A. Sioulas, T. Thujssen, and G. Friedrich, 1982. Manganese nodule formation in the Pacific Ocean: a general theory. Geo-Marine Lett., 2: 47-53.

Glover, E.D., 1977. Characterizations of a marine birnessite. Am. Min., 62: 278-285.

Halbach, P. and M. Ozkara, 1979. Morphological and geochemical classification of deep-sea ferromanganese nodules and its genetic interpretation. In Du Centre National De La Recgerche Scientifique, La genese des nodules de manganese: Colloques Internationaux du CNRS, 289, Paris, 77-88.

Halbach, P., G. Friedrich, and U. von Stackelberg, 1988. The Manganese Nodule Belt of the Pacific Ocean. Ferdinand Enke Verag Stuttgart. 254pp.

Halbach, P., U. Hebich, and C. Scherhag, 1981. Geochemical variations of ferromanganese nodules and crust from different provinces of the Pacific ocean and their genetic control. Chemical Geology, 34: 3-17.

Halbach, P., M. Ozkara, and J. Hense, 1975. The influence of metal content on the physical and mineralogical properties of pelagic manganese nodules. Mineral Deposita(Berl), 10: 397-411.

Hayes, J.D., T. Saito, N.D. Opdyke and L.H. Burckle, 1969. Pliocene-Pleistocene sediments of the equatorial Pacific: their paleomagnetic, biostratigraphic, and climatic record. Geol. Soc. Am. Bull., 80: 1481-1514.

Hayes, S.P., 1979. Benthic current observations at DOMES sites A,B, and C in the tropical north Pacific Ocean. In: Marine geology and Oceanography of. the Pacific manganese nodule province, edited by J.L. Bischoff and D.Z. Piper, Marine Science, v.9, Plenum Press, New York, 83-112.

Haynes, B.W., S.L. Law, and D.C. Barron, 1982. Mineralogical and elemental description of Pacific manganese nodules. Bureau of Mines Information circular/8906, U.S. Depart. Interior.

Hein, J.R., F.T. Manheim, W.C. Schwab, and A.S. Davis, 1985. Ferromanganese crusts from Necker Ridge, Horizon Guyot, and S.P. Lee Guyot: Geological considerations. Mar. Geol., 69: 25-54.

Herron, E.M., 1972. Sea-floor spreading and the Cenozoic history of the east-central Pacific: GSA Bulletin, 83: 1671-1692.

Heye, D., 1975. Wachstumsverhaltnisse von Manganknollen. Geol. Jahrbuch, E5: 3-122.

Heye, D. and V. Marchig, 1977. Relationship between growth rate of manganese nodules from the central Pacific and their chemical constitution: Mar. Geol., M19-M25.

Horn, D.R., B.M. Horn, and M.N. Delach, 1973. Copper and Nickel content of ocean ferromanganese deposits and their relation to properties of the substrate. In: Papers on the origin and distribution of manganese nodules in the Pacific and prospects for exploitation, edited by M. Morgenstein, University of Hawaii and IDOE/NSF, Honolulu, 71-76.

Johnson, D.A., 1972. Ocean-floor erosion in the equatorial Pacific. Geol. Soc. Am. Bull., 83: 3121-3144.

Keller G. and J.A. Barron, 1983. Paleoceanographic implications of Miocene deep-sea hiatuses: Geological Society of America Bulletin, 94: 590-613.

Kennett, J., 1982. Marine Geology. Prentice-Hall, Inc., Englewood Cliffs, New Jersey, 813 pp.

Klinkhammer, G.P., D. Heggie, and D. Graham, 1982. Metal diagenesis in oxidative marine sediments. Earth and Planet. Sci. Lett. 61: 211-219.

Ku, T.L. and G.P. Glasby, 1972. Radiometric evidence for the rapid growth rate of shallow-water, continental margin manganese nodules. Geochim. Cosmochim. Acta, 36: 699-703.

Ku, T.L., A. Omura, and P.S. Chen, 1979. Be and U-series isotopes in manganese nodules from the central North Pacific. In: Marine Geology and Oceanography of the Pacific manganese Nodule Province, edited by J.L. Bischoff and D.Z. Piper, Plenum, New York, 791-814.

Mantyla, A.W., 1975, On the potential temperature in the abyssal Pacific Ocean: J. Mar. Res., 33: 341-354.

Mckelvey, V.E., N. A. Wright, and K.W. Bowen, 1983. Analysis of the world distribution of metal-rich subsea manganese nodules., U.S. Geological Survey Circular, 886: 55pp.

Mero, J.L., 1965. The Mineral Resources of the Sea. Elsevier, Amsterdame, 312pp.

Moore, T. C., Jr. and G.R. Heath, 1967. Abyssal hills in the central equatorial Pacific: Detailed structure of the sea floor and sub-bottom reflectors. Mar. Geol., 5: 161-179.

Moore, W.S., T.L. Ku, J.D. Macdougall, V.M. Burns, R.D. Burns, J. Dymond, M.W. Lyle, and D.Z. Piper, 1981. Fluxes of metal to a manganese nodule. Radiochemical, chemical, structural, and mineralogical studies. Earth Planet. Sci. Lett., 52: 151-171.

Moritani, T., S. Maruyama, M. Nohara, K. Matsumoto, T. Ogitsu, and H. Moriwaki, 1977. Description, classification, and distribution of manganese nodules. Cruise Rep. No. 8, Geol. Surv. Japan: 136-158.

Murray, J.W. and J.G. Dillard, 1979. The Oxidation of Cobalt (II) Adsorbed on Manganese Dioxide. Geochim. Cosmochim. Acta, 43: 781-787.

Piper, D.Z. and B. Fowler, 1980. New constraint on the maintenance of Mn nodules at the sediment surface. Nature, 286: 880-883.

Piper, D.Z. and J. R. Blueford, 1982. Distribution, Mineralogy, and texture of manganese nodules and their relation to sedimentation at DOMES Site A in the equatorial North Pacific. Deep-Sea Res., 29(8A): 927-952.

Raab, W., 1972. Physical and chemical features of Pacific deep sea manganese nodules and their implications to the genesis of nodules. In: Papers Conf. Ferromanganese Deposits on the Ocean Floor, edited by D.R. Horn, National Science Foundation, Washington, D.C., 31-49.

Raab, W.J. and M.A. Meylan, 1977. Morphology. In: Marine Manganese Deposits, edited by G.P. Glasby, Elsevier, Amsterdam, 109-146.

Romankevich, E.A., 1984. Geochemistry of organic matter in the ocean. Springer-Verlag, Berlin.

Ryan, W.B.F. and B.C. Heezen, 1976. Smothering of deepsea benthic communities from natural disasters: NOAA Technical Report Contribution No. 03-6-022 -35120, 132p.

Sclater, J.G., R. N. Anderson, and M.L. Bell, 1971. Elevation of ridges and evolution of the central eastern Pacific: J. Geophys. Res. 76(32): 7888- 7915.

Sorem, R.K. and R.H. Fewkes, 1979. Internal characteristics of marine manganese nodules. In: Marine Manganese Deposits, edited by G.P Glasby, Elservier Oceanography Series, No.15, 147-183.

Sorem, R.K., W. R. Reinhart, R.H Fewks, and W.D. McFarland, 1979. Occurrence and character of manganese nodules in Domes sites A, B, and C, East Equatorial Pacific Ocean. In: Marine Geology and Oceanography of the Pacific Manganese Nodule Province, editer by J.L. Bischoff and D.Z. Piper, Plenum, New York, 475-527.

von Stackelberg, U., H. Beiersdorf, and V. Riech, 1987. Relationship between manganese nodule formation and sedimentary processes in the equatorial north Pacific Ocean - a synthesis based on the results of cruise SO25 (1982) with R/V Sonne: Geology Jb., 377-403.

Takematsu, N., Y. Sato and S. Okabe, 1989. Factors controlling the chemical composition of marine manganese nodules and crusts: A review and systhesis. Mar. Chem., 26: 41-56.

Theyer, F., 1977. Micro-paleontological dating of DOMES project box cores from test areas A and B, tropical Pacific, In: Deep ocean mining environmental study: geology and geochemistry of DOMES Sites A, B, and C, equatorial north Pacific, edited by D.Z. Piper, U.S.G.S. Open-File Report, 77-778: 179-194.

Usui, A., 1984. Regional variation of manganese nodule facies on the Wake-Tahiti transect: morphological, chemical and mineralogical study. Mar. Geol., 54: 27-51.

Usui, A., 1979. Minerals, metal contents, and mechanism of formation of manganese nodules from the Central Pacific Basin(GH76-1 and GH77-1 areas). In: Marine Geology and Oceanography of the Pacific Manganese Nodule Province, editer by J.L. Bischoff and D.Z. Piper, Plenum, New York, N.Y., 651-679.

Usui, A., M. Yuasa, S. Yokota, M. Nohara, A. Nishimura and F. Murakami, 1986. Submarine hydrothermal manganese deposits from the Ogasawara(Bonin) Arc, off the Japan islands. Mar. Geol., 73: 311-322.

Volat, J., L. Pastouret and C. Vergnaud-Granzzini, 1980. Dissolution and carbonate fluctuations in Pleistocene deep-sea cores: A review. Marine Geology, 34: 1-28.

Yamashige, T., M. Yamamoto and H. Sunahara, 1989. Comparison of decomposition methods for the analysis of atmospheric particulates by atomic absorption spectrometry. Analyst, 114: 1071-1077.

Table 1. Abundance and morphology of manganese nodules in KODOS-89 area.

Station Number	Location		Water Depth	Abundance (kg/m^2)			Frequency Distribution of Morphology (%)												Sea-bottom Feature
	lati.	long.					External Shape					Surface Texture			Size(long axis,cm)				
	(N)	(W)	(m)	min	max	avg	S	E	D	I	P	r	t	s	<2	2-4	4-6	>6	
1	12° 0'	153° 0'	5,225	0.13	0.44	0.29	22	24	0	25	28	100	0	0	69	31	0	0	Abyssal plain
3	11° 20'	153° 40'	5,220	0.96	1.00	0.98	11	28	50	6	6	100	0	0	23	9	59	9	Abyssal plain
4	11° 20'	152° 45'	5,112	0.00	0.08	0.03	42	33	8	0	17	100	0	0	58	42	0	0	Abyssal plain
5	11° 0'	153° 0'	5,149	0.00	0.03	0.02	50	25	0	25	0	100	0	0	75	25	0	0	Abyssal plain
6	10° 59'	153° 31'	4,935	0.20	2.00	0.70	-	-	-	-	-	-	-	-	-	-	-	-	Abyssal plain
11	10° 0'	153° 41'	5,102	5.68	11.19	8.51	5	30	21	20	24	100	0	0	10	19	69	2	Abyssal plain
12	10° 0'	153° 20'	5,075	5.17	6.62	5.95	15	25	25	12	24	100	0	0	11	47	38	4	Abyssal plain
13	10° 0'	152° 40'	5,276	6.85	8.92	7.80	4	16	23	22	35	35	65	0	0	32	53	15	Abyssal plain
15	9° 20'	152° 40'	5,212	0.90	14.20	6.00	18	32	26	7	17	80	20	0	16	38	38	8	Abyssal plain
16	9° 20'	153° 14'	5,146	6.10	6.10	6.10	0	8	25	17	50	67	33	0	0	42	58	0	Abyssal plain
17	9° 20'	153° 50'	5,070	2.49	5.28	4.23	15	25	28	10	22	100	0	0	12	38	44	6	Abyssal plain
21	10° 10'	153° 30'	5,145	5.83	5.83	5.83	8	33	25	25	8	100	0	0	8	17	58	17	Abyssal plain
2	12° 0'	153° 40'	5,095	6.91	9.20	8.12	7	15	2	17	59	0	0	100	71	27	2	0	Abyssal hill
7	10° 40'	153° 40'	5,210	0.03	1.50	1.00	0	58	25	17	0	100	0	0	50	12	29	8	Abyssal hill
8	10° 40'	152° 40'	5,225	0.23	0.92	0.58	11	31	24	34	0	100	0	0	39	41	10	10	Abyssal hill
14	9° 35'	152° 40'	5,000	13.14	28.86	19.16	0	0	0	22	78	0	9	92	18	50	29	4	Abyssal hill
9	10° 20'	152° 50'	4,894	0.10	17.90	9.40	2	5	0	62	31	5	28	67	46	34	15	5	Seamount
10	10° 20'	153° 50'	4,875	0.13	19.80	7.36	8	5	0	60	28	0	0	100	58	29	9	4	Seamount
18	9° 40'	153° 30'	4,640	20.04	20.04	20.04	0	0	0	20	80	0	55	45	0	65	35	0	Seamount
19	9° 40'	153° 22'	4,800	15.70	21.20	18.40	-	-	-	-	-	-	-	-	-	-	-	-	Seamount
20	9° 40'	153° 14'	5,144	7.97	13.76	11.22	6	11	10	20	52	21	79	0	0	58	42	0	Seamount

Abbreviation ; S=spheroidal, E=ellipsoidal, D=discoidal, I=irregular, P=polynodule,
r=rough type(r-type), t=transitional type(t-type), s=smooth type(s-type),

Table 2. Mineral and metal content of manganese nodules in KODOS-89 area.

Station & Sample No.		Morphology		Size(mm)			Mineral Content (%)					Metal Content (%)						
		Sha	Tex				Ver	Tod	Pla	Qua	T/V	Mn	Fe	Cu	Ni	Co	Zn	Mn/Fe
1	1-B-1	I	r	19	31	35	64	17	9	3	0.27	10.03	6.74	0.40	0.77	0.12	0.05	1.5
	1-F-1	S	r	18	18	21	64	14	19	3	0.22	17.36	8.28	0.69	1.05	0.21	0.07	2.1
2	2-F-1	P	s	11	14	21	79	15	3	2	0.19	25.25	12.11	0.63	1.28	0.39	0.08	2.1
	2-F-2	P	s	12	28	31	86	9	3	2	0.10	23.40	11.95	0.54	1.19	0.35	0.07	2.0
	2-F-3	P	s	17	21	31	84	10	4	1	0.12	19.80	11.81	0.33	0.97	0.29	0.07	1.7
	2-F-4	I	s	27	31	35	84	9	5	2	0.11	21.56	12.18	0.33	0.93	0.28	0.06	1.8
3	3-B-1	D	r	21	47	56	62	30	4	3	0.48	24.21	8.54	0.93	1.23	0.22	0.10	2.8
	3-F-3	I	r	10	14	27	60	29	7	4	0.48	24.14	7.29	1.04	1.29	0.23	0.10	3.3
	3-F-4	E	r	18	26	43	54	39	4	3	0.72	26.44	7.23	1.06	1.32	0.24	0.10	3.7
4	4-F-1	S	r	14	16	18	55	38	4	3	0.69	27.41	5.58	1.36	1.57	0.79	0.13	4.9
	4-F-2	I	r	10	18	24	61	29	6	4	0.48	22.95	6.01	0.94	1.22	0.17	0.10	3.8
	4-F-3	E	r	14	16	17	58	26	13	3	0.45	21.81	4.77	1.01	1.22	0.15	0.09	4.6
5	5-F-2	S	r	<5, 3 ea.			60	31	6	3	0.52	24.55	4.49	1.10	1.37	0.14	0.12	5.5
7	7-B-1	E	r	11	12	20	62	26	6	4	0.42	21.56	4.83	1.09	1.37	0.16	0.11	4.5
	7-F-4	E	r	14	17	26	61	31	5	3	0.51	24.49	5.20	1.17	1.33	0.19	0.12	4.7
	7-F-6	P	r	30	49	60	58	37	3	2	0.64	23.78	6.23	0.78	1.26	0.20	0.11	3.8
8	8-B-1	I	r	6	30	73	60	32	5	3	0.53	24.57	5.75	1.05	1.35	0.21	0.11	4.3
	8-B-3	P	r	12	20	21	58	31	5	2	0.53	24.00	5.26	1.09	1.32	0.16	0.11	4.6
	8-B-5	I	r	13	14	36	55	34	8	3	0.62	28.16	5.88	1.15	1.40	0.16	0.14	4.8
9	9-B-1	I	s	8	21	26	75	20	3	2	0.27	18.77	11.90	0.62	1.11	0.53	0.09	1.6
	9-B-4	I	r	10	15	25	64	33	2	1	0.52	22.55	4.95	0.82	0.89	0.49	0.07	4.6
10	10-B-1	I	s	<5, 4 ea.			91	7	1	1	0.08	20.35	18.71	0.21	0.63	0.30	0.06	1.1
	10-F-3	P	t	15	20	29	77	19	3	1	0.25	24.97	9.43	0.76	1.32	0.31	0.10	2.6
11	11-B-1	D	r	23	42	47	67	28	3	2	0.42	23.94	7.79	0.86	1.37	0.24	0.11	3.1
	11-B-2	E	r	22	24	40	64	33	2	1	0.52	25.84	6.71	1.08	1.38	0.24	0.12	3.9
	11-B-4	E	r	19	23	31	57	27	9	3	0.47	22.38	8.59	0.80	1.24	0.24	0.09	2.6
12	12-B-1	D	r	25	45	47	63	33	1	3	0.52	26.15	7.16	1.10	1.40	0.23	0.12	3.7
	12-B-5	S	r	17	19	20	65	28	5	2	0.43	24.00	6.20	1.18	1.42	0.23	0.11	3.9
	12-B-6	D	r	25	34	37	63	31	4	2	0.49	27.87	6.35	1.19	1.36	0.20	0.11	4.4
	12-B-7	P	r	22	32	37	68	27	3	2	0.40	24.66	7.45	1.01	1.36	0.21	0.11	3.3
	12-B-8	S	r	10	11	13	67	25	5	3	0.37	22.80	5.94	1.02	1.39	0.23	0.12	3.8

Table 2. (continued)

Station & Sample No.		Morphology		Size(mm)			Mineral Content (%)					Metal Content (%)						
		Sha	Tex				Ver	Tod	Pla	Qua	T/V	Mn	Fe	Cu	Ni	Co	Zn	Mn/Fe
13	13-B-2	D	r	15	24	33	76	20	2	2	0.26	23.69	9.88	0.77	1.25	0.30	0.10	2.4
	13-B-3	P	t	27	37	44	75	20	3	2	0.27	23.84	9.44	0.71	1.26	0.26	0.09	2.5
	13-B-4	I	r	13	31	49	79	18	1	2	0.23	23.26	9.09	0.72	1.23	0.26	0.09	2.6
14	14-B-1	I	t	27	31	39	86	11	-	3	0.13	20.15	16.11	0.37	0.87	0.19	0.09	1.3
	14-B-2	P	t	27	29	46	84	11	3	2	0.13	24.45	13.38	0.52	1.03	0.30	0.08	1.8
	14-B-4	P	s	16	18	25	86	11	1	2	0.13	20.80	13.92	0.36	0.92	0.30	0.08	1.5
15	15-B-1	P	r	29	32	42	65	29	4	1	0.45	23.22	7.19	0.95	1.32	0.14	0.11	3.2
16	16-B-1	E	t	25	32	59	65	29	4	2	0.45	22.29	7.69	0.90	1.35	0.24	0.11	2.9
	16-B-5	D	r	26	36	41	62	32	4	2	0.52	26.48	8.48	0.94	1.33	0.23	0.11	3.1
	16-B-6	I	r	24	27	37	75	18	5	2	0.24	27.41	7.27	0.94	1.33	0.20	0.11	3.8
17	17-B-1	P	r	24	30	55	64	30	4	2	0.47	25.97	7.34	1.02	1.35	0.17	0.12	3.5
	17-B-3	S	r	22	26	29	62	29	6	3	0.47	24.80	6.95	0.98	1.27	0.18	0.11	3.6
	17-B-4	D	r	28	41	54	63	33	3	1	0.52	25.99	6.75	1.02	1.31	0.18	0.11	3.9
18	18-B-2	P	t	24	41	42	84	11	3	2	0.13	22.78	12.18	0.52	1.06	0.29	0.09	1.9
	18-B-3	P	s	19	27	35	85	11	3	1	0.13	24.29	11.90	0.51	1.08	0.33	0.09	2.0
	18-B-4	P	s	18	34	38	87	12	-	1	0.14	23.32	12.34	0.45	1.02	0.30	0.08	1.9
19	19-D-5	I	s	12	31	33	92	6	-	-	0.07	22.51	17.81	0.11	0.50	0.28	0.06	1.3
	19-D-6	P	s	34	35	42	87	12	-	1	0.14	23.69	13.33	0.47	1.03	0.32	0.08	1.8
	19-D-7	P	s	28	31	52	82	16	1	1	0.20	23.60	13.66	0.48	1.03	0.32	0.08	1.7
20	20-B-2	E	r	12	21	26	69	25	4	2	0.36	23.01	9.94	0.70	1.21	0.30	0.09	2.3
	20-B-3	P	r	27	38	44	73	21	4	2	0.29	22.50	10.53	0.63	1.28	0.25	0.09	2.1
	20-B-4	E	t	19	28	45	76	19	3	2	0.25	24.54	10.60	0.76	1.34	0.26	0.10	2.3
	20-B-5	D	r	16	36	41	80	15	3	2	0.19	22.39	10.71	0.68	1.33	0.26	0.09	2.1
	20-B-6	D	t	19	22	30	74	20	4	2	0.27	24.70	9.33	0.81	1.37	0.26	0.10	2.6
21	21-B-1	D	r	30	45	60	63	32	3	2	0.51	27.76	8.44	1.00	1.42	0.24	0.13	3.3
	21-B-3	E	r	11	28	43	69	26	3	2	0.38	24.41	8.23	0.94	1.44	0.23	0.12	3.0
	21-B-4	E	r	18	19	26	56	35	6	3	0.63	22.87	8.40	0.95	1.38	0.18	0.11	2.7
	21-B-5	P	r	21	27	42	63	32	3	2	0.51	25.41	8.66	0.98	1.44	0.23	0.12	2.9

Abbreviation ; Sha = external shape, S = spheroidal, E = ellipsoidal, D = discoidal, I = irregular, P = polynodule,
Tex = surface texture, r = rough type(r-type), t = transitional type(t-type), s = smooth type(s-type),
Ver = vernadite, Tod = todorokite, Pla = plagioclase, Qua = quartz, T/V = todorokite/vernadite

Figure Captions

Fig. 1. Bathymetry and sample locations in KODOS-89 area. ----------115

Fig. 2. Photographs showing occurrence of manganese nodules in KODOS-89 area. a: Top of box core (20x30 cm), b: Nodules from box core (grid scale: 2 cm). abbreviation: E=ellipsoidal, D=discoidal, P=polynodule, I=irregula, r=r-type, s=s-type, t=t-type. ----------116

Fig. 3. Photographs showing internal texture of manganese nodules in KODOS-89 area. a: r-type, b: s-type c: t-type. Scale bar: 1 cm. ----117

Fig. 4. Frequency distribution of external shape of manganese nodules in KODOS-89 area. ----------118

Fig. 5. Frequency distribution of surface texture of manganese nodules in KODOS-89 area. ----------119

Fig. 6. Relationship between latitude and size frequency of manganese nodules in KODOS-89 area. ----------120

Fig. 7. Relationship between latitude and abundance of manganese nodules in KODOS-89 area. ----------121

Fig. 8. Relationship between todorokite/vernadite and Mn/Fe ratios of manganese nodules in KODOS-89 area. ----------122

Fig. 9. Relationship between todorokite/vernadite ratio and metal content of manganese nodules in KODOS-89 area. ----------123

Fig.10. Relationship between shape frequency(spheroidal+ellipsoidal+ discoidal) and Mn/Fe ratio of manganese nodules in KODOS-89 area.---124

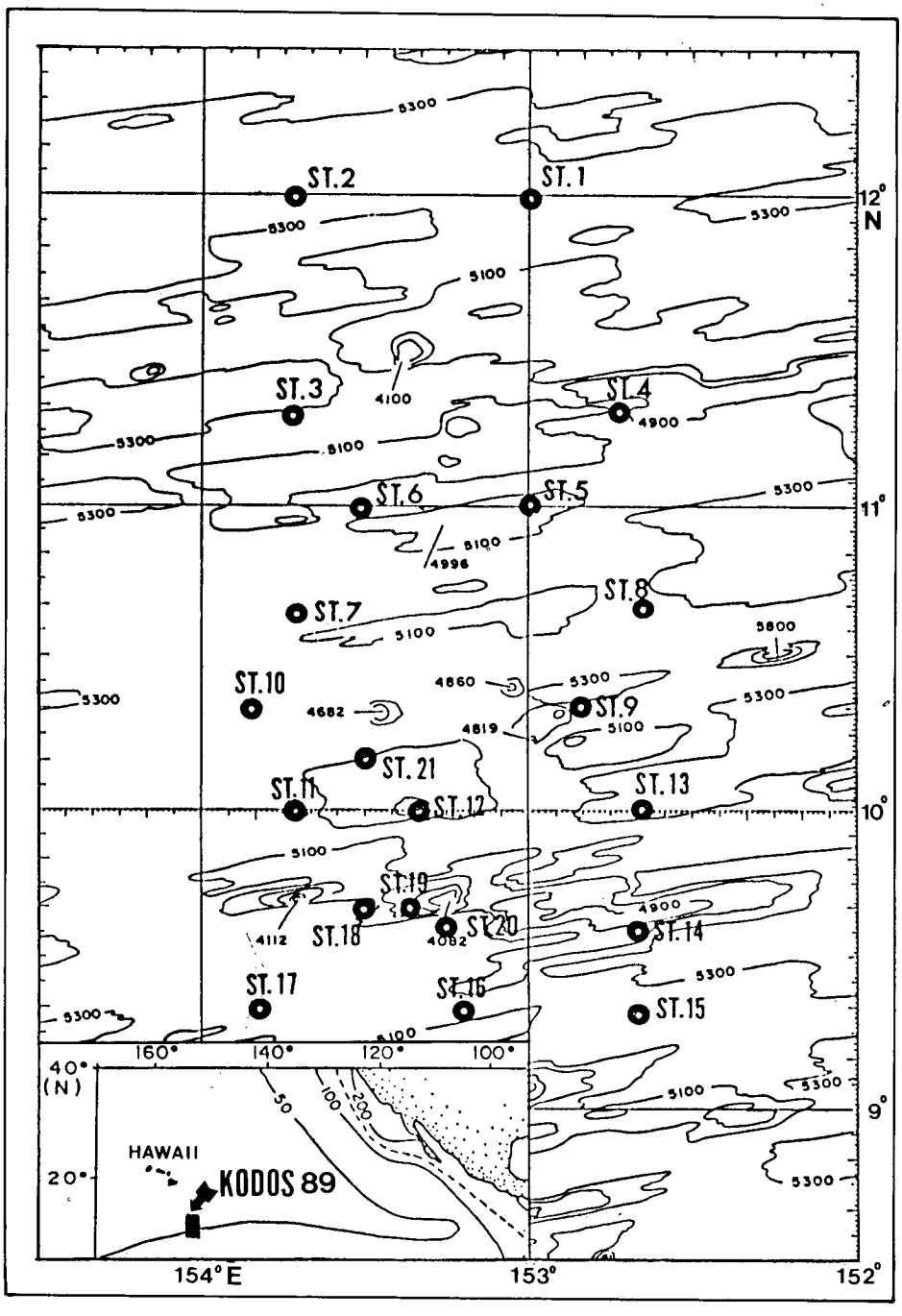
ST.1
ST.2
ST.3
ST.4
ST.5
ST.6
ST.7
ST.8
ST.9
ST.10
ST.11
ST.12
ST.13
ST.14
ST.15
ST.16
ST.17
ST.18
ST.19
ST.20
ST.21
5300
5100
4900
4860
4819
4682
4112
4082
4100
4996
5800
12° N
11°
10°
9°
160°
140°
120°
100°
40° (N)
20°
HAWAII
KODOS 89
50
100
200
154° E
153°
152°

E , Dr (5.8 kg/m^2)

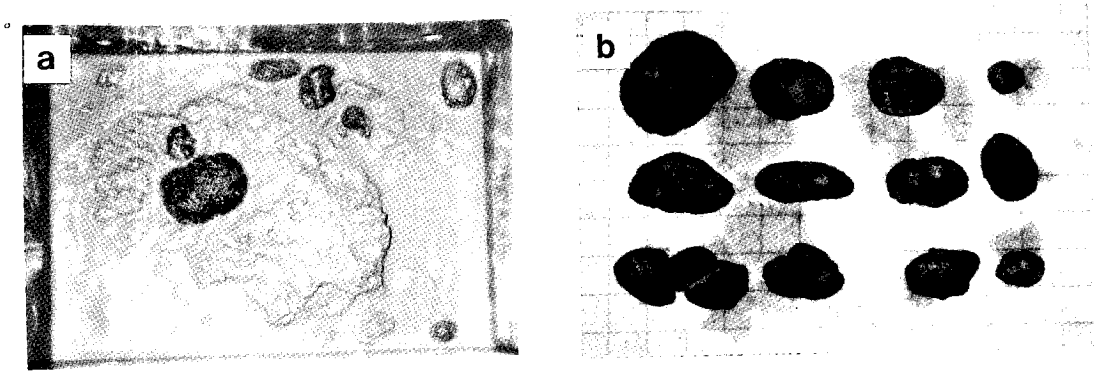

Abyssal plain (st.21)

P , Is , t (20.0 kg/m^2)

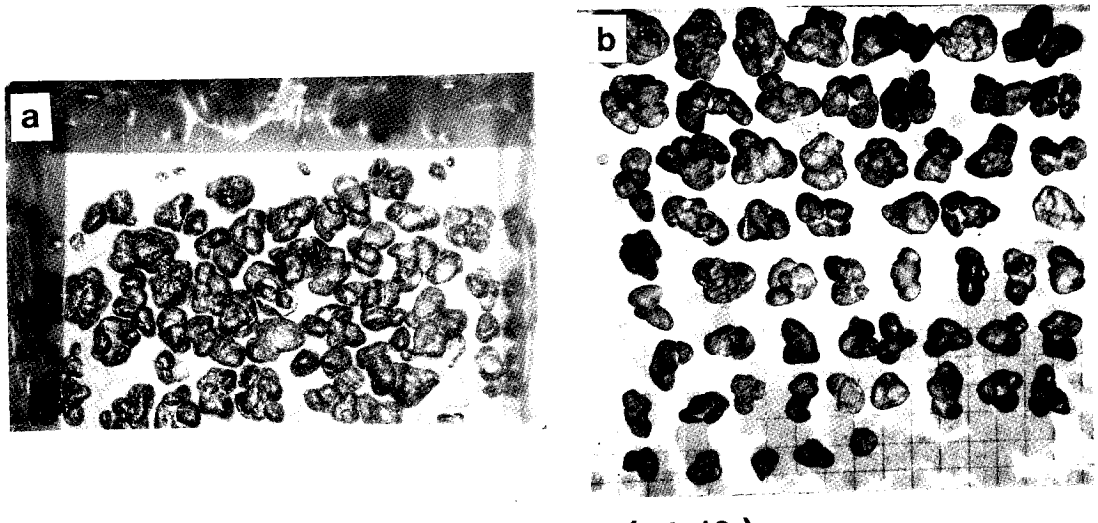

Seamount (st.18)

a
b
c
Top
Bottom

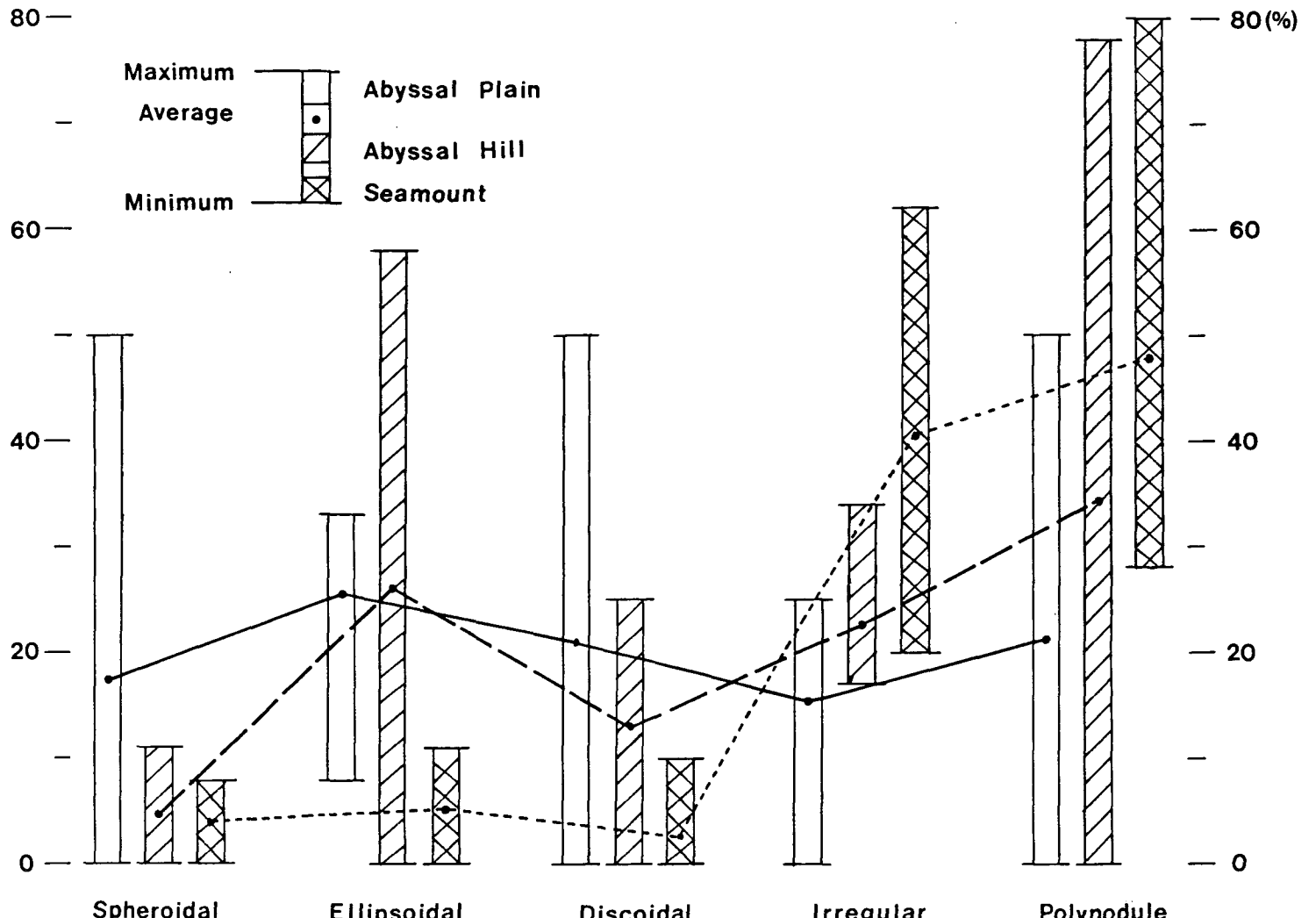
80
60
40
20
0
80(%)
60
40
20
0
Maximum
Average
Minimum
Abyssal Plain
Abyssal Hill
Seamount
Spheroidal
Ellipsoidal
Discoidal
Irregular
Polynodule

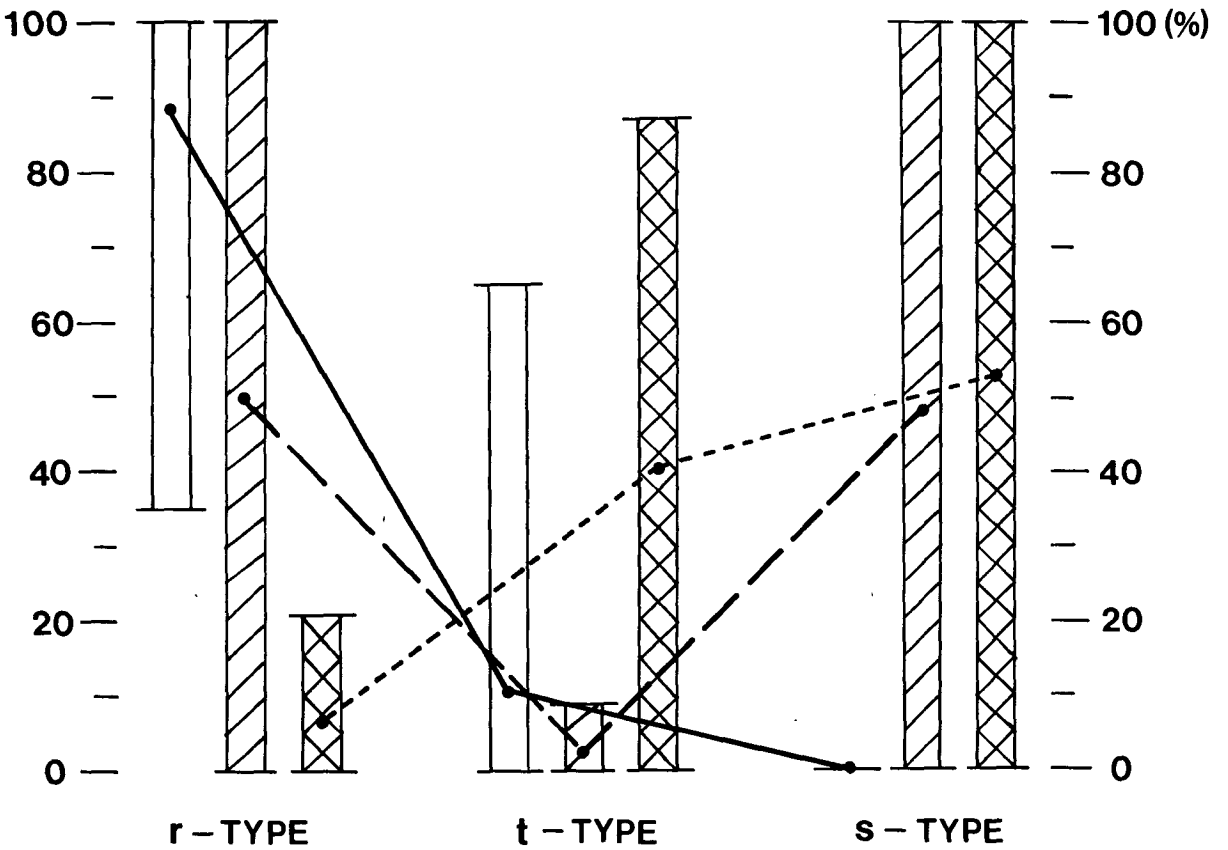
100
80
60
40
20
0
100 (%)
80
60
40
20
0
r – TYPE
t – TYPE
s – TYPE

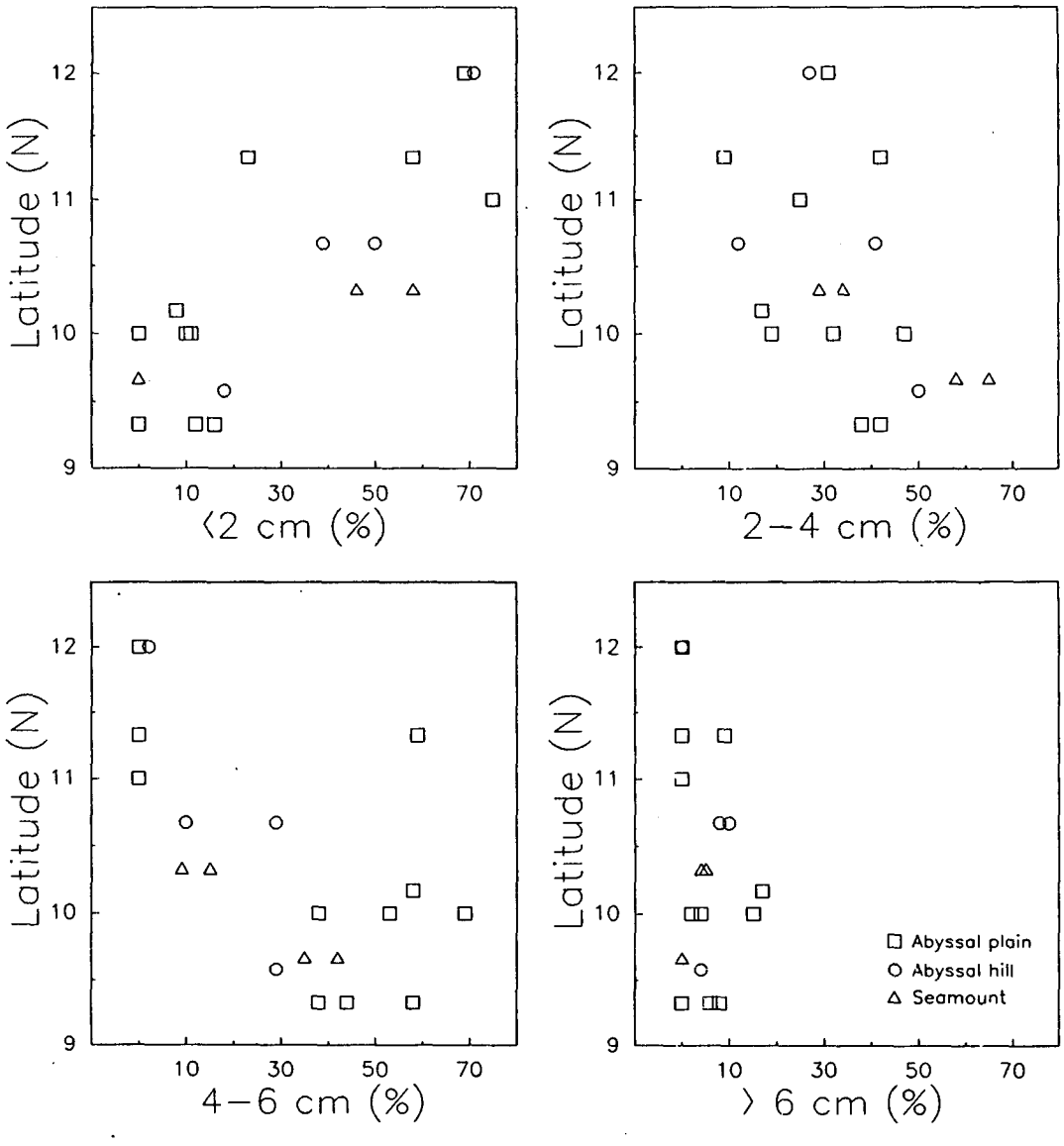
Latitude (N)
12
11
10
9
10
30
50
70
〈2 cm (%)
2−4 cm (%)
4−6 cm (%)
〉6 cm (%)
Abyssal plain
Abyssal hill
Seamount

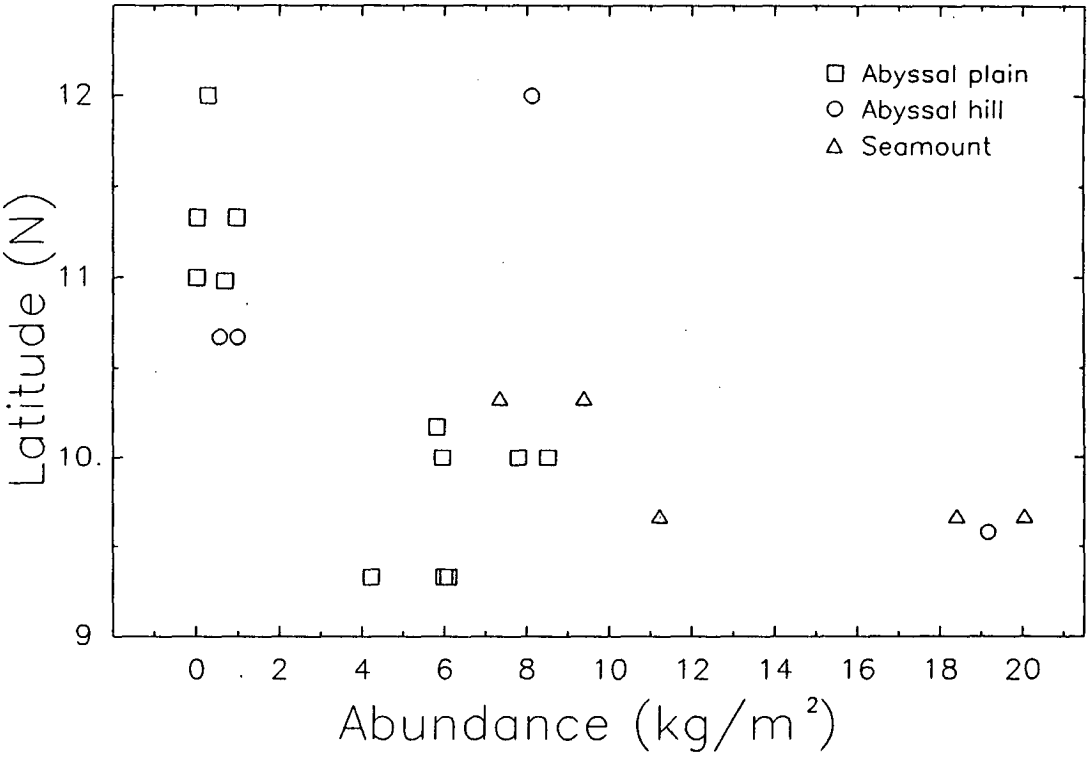
Abyssal plain
Abyssal hill
Seamount
Latitude (N)
12
11
10.
9
0
2
4
6
8
10
12
14
16
18
20
Abundance (kg/m²)

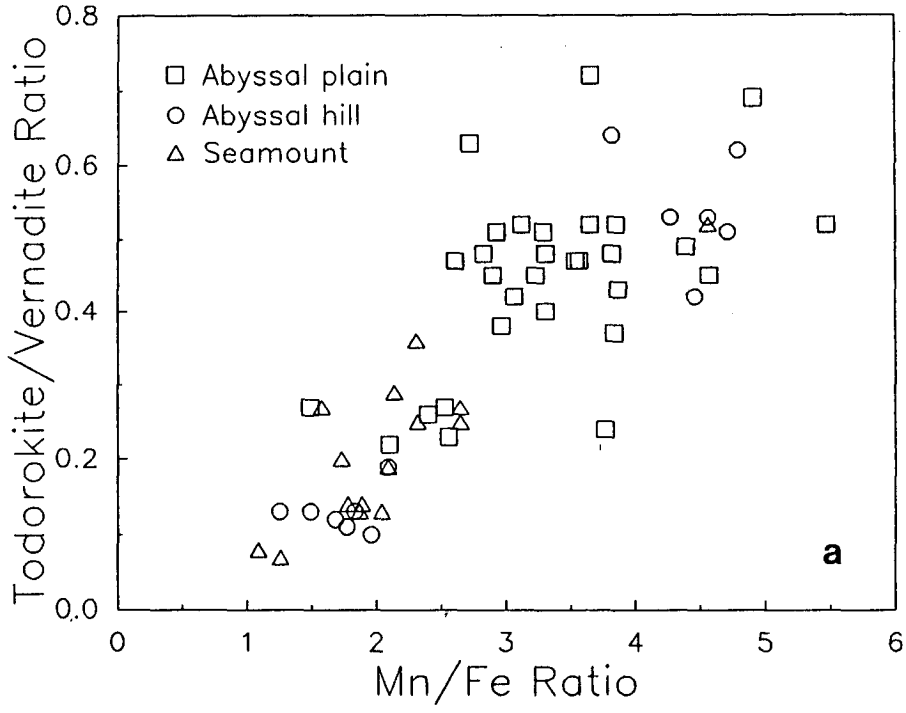
Abyssal plain
Abyssal hill
Seamount
a
Todorokite/Vernadite Ratio
Mn/Fe Ratio
0.0
0.2
0.4
0.6
0.8
0
1
2
3
4
5
6

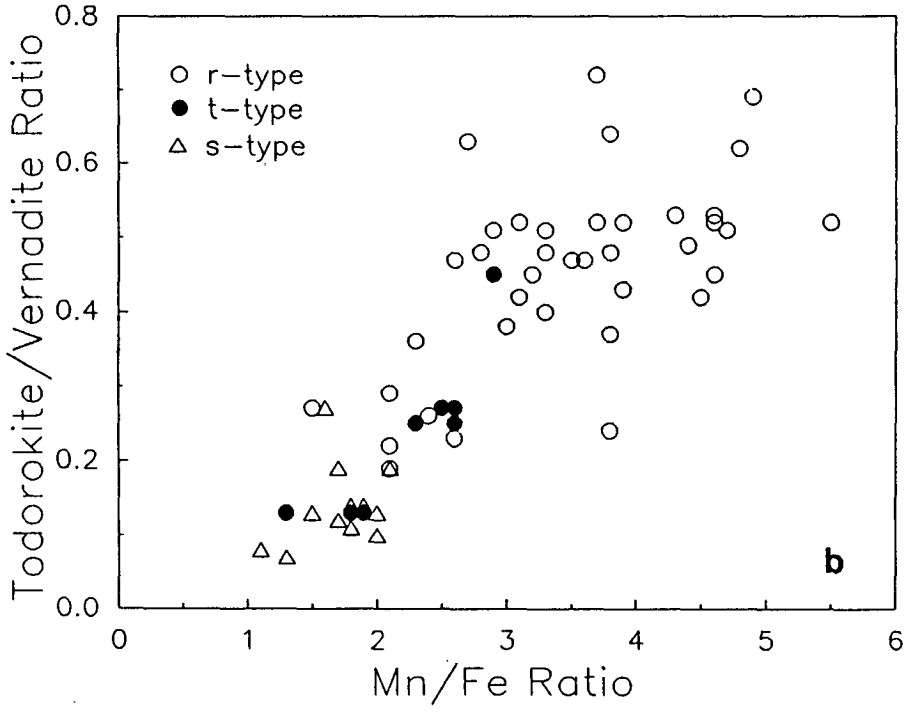
r-type
t-type
s-type
b
Todorokite/Vernadite Ratio
Mn/Fe Ratio
0.0
0.2
0.4
0.6
0.8
0
1
2
3
4
5
6

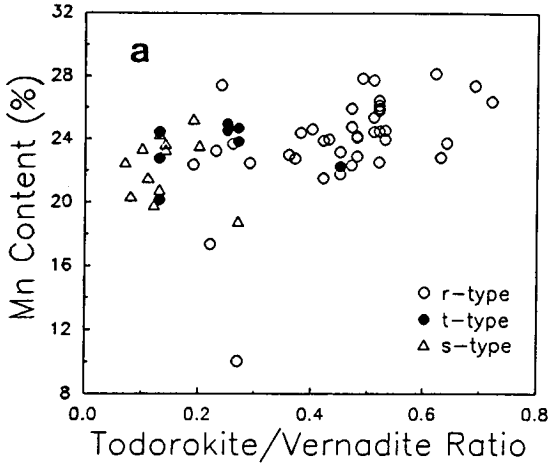
a
Mn Content (%)
Todorokite/Vernadite Ratio
r-type
t-type
s-type

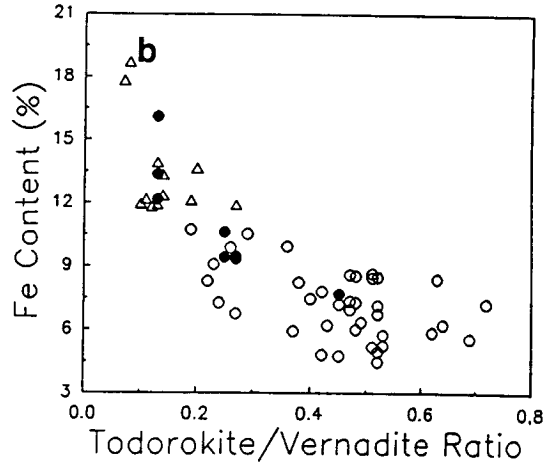
b
Fe Content (%)
Todorokite/Vernadite Ratio

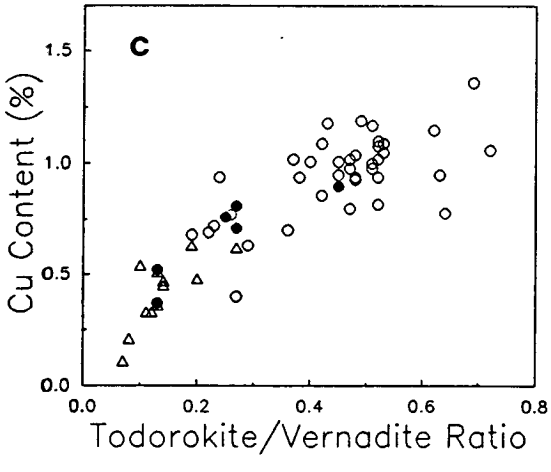
c
Cu Content (%)
Todorokite/Vernadite Ratio

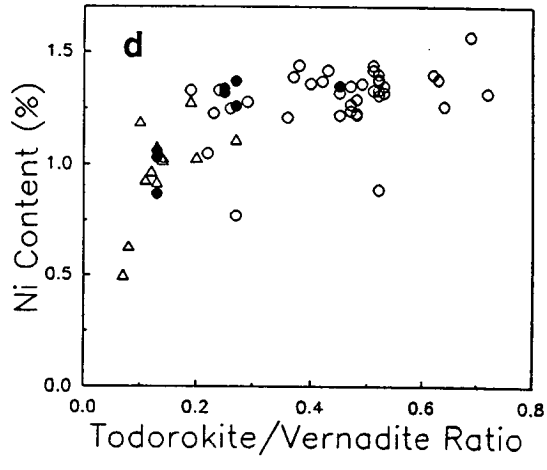
d
Ni Content (%)
Todorokite/Vernadite Ratio

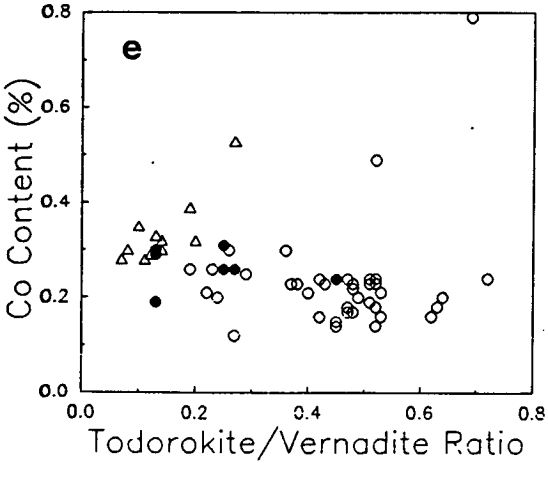
e
Co Content (%)
Todorokite/Vernadite Ratio

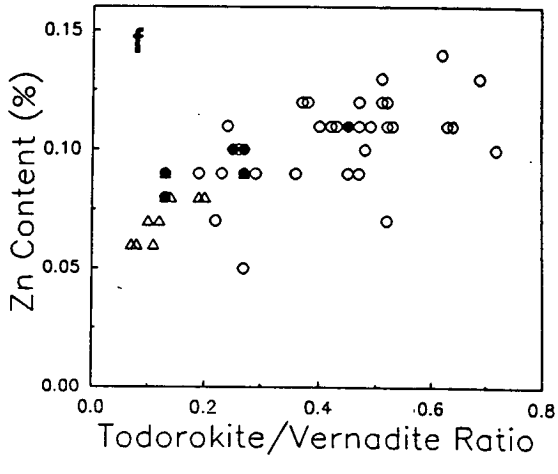
f
Zn Content (%)
Todorokite/Vernadite Ratio

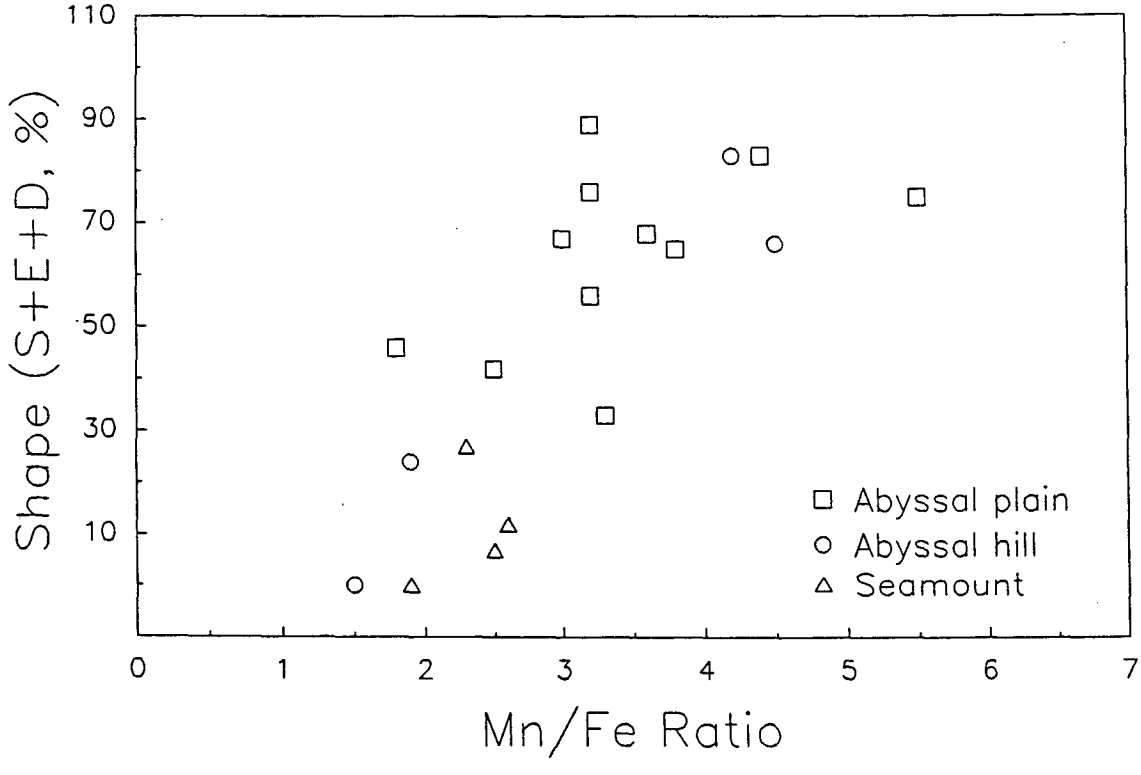
110
90
70
50
30
10
Shape (S+E+D, %)
0
1
2
3
4
5
6
7
Mn/Fe Ratio
Abyssal plain
Abyssal hill
Seamount